Femtosecond Fiber Lasers

by

Katherine J. Bock

Thesis submitted to the Faculty of Graduate and Postdoctoral Studies
in partial fulfillment of the requirements for the degree of
Master of Applied Science in Biomedical Engineering

School of Electrical Engineering and Computer Science
University of Ottawa
The Ottawa-Carleton Institute for Biomedical Engineering

Abstract

This thesis focuses on research I have done on ytterbium-doped femtosecond fiber lasers. These lasers operate in the near infrared region, lasing at 1030 nm. This wavelength is particularly important in biomedical applications, which includes but is not limited to confocal microscopy and ablation for surgical incisions. Furthermore, fiber lasers are advantageous compared to solid state lasers in terms of their cost, form factor, and ease of use. Solid state lasers still dominate the market due to their comparatively high energy pulses.

High energy pulse generation in fiber lasers is hindered by either optical wave breaking or by multipulsing. One of the main challenges for fiber lasers is to overcome these limitations to achieve high energy pulses. The motivation for the work done in this thesis is increasing the output pulse peak power and energy. The main idea of the work is that decreasing the nonlinearity that acts on the pulse inside the cavity will prevent optical wave breaking, and thus will generate higher energy pulses. By increasing the output energy, ytterbium-doped femtosecond fiber lasers can be competitive with solid state lasers which are used commonly in research. Although fiber lasers tend to lack the wavelength tuning ability of solid state lasers, many biomedical applications take advantage of the 1030 μm central wavelength of ytterbium-doped fiber lasers, so the major limiting factor of fiber lasers in this field is simply the output power. By increasing the output energy without resorting to external amplification, the cavity is optimized and cost can remain low and economical.

During verification of the main idea, the cavity was examined for possible back-reflections and for components with narrow spectral bandwidths which may have contributed to the presence of multipulsing. Distinct cases of multipulsing, bound pulse and harmonic mode-locking, were observed and recorded as they may be of more interest in the future.

The third-order dispersion contribution from the diffraction gratings inside the laser cavity was studied, as it was also considered to be an energy-limiting factor. No significant effect was found as a result of third-order dispersion; however, a region of operation was observed where two different pulse regimes were found at the same values of net cavity group velocity dispersion.

Results verify the main idea and indicate that a long length of low-doped gain fiber is preferable to a shorter, more highly doped one. The low-doped fiber in an otherwise equivalent cavity allows the nonlinear phase shift to grow at a slower rate, which results in the pulse achieving a higher peak power before reaching the nonlinear phase shift threshold at which optical wave breaking occurs. For a range of net cavity group velocity dispersion values, the final result is that the low doped fiber generates pulses of approximately twice the value of energy of the highly-doped gain fiber. Two techniques of mode-locking cavities were investigated to achieve this result. The first cavity used NPE mode-locking which masked the results, and the second used a SESAM for mode-locking which gave clear results supporting the hypothesis.

Statement of Originality

The author declares that the results presented in this thesis were obtained during the course of her M.A.Sc. research under Dr. Hanan Anis, and that this is to the best of her knowledge original work.

The following academic contribution was made from some of the work presented in this thesis:

1. Bock, K. J., Kotb, H. E., Abdelalim, M. A., and Anis, H., “Increasing energy in an ytterbium femtosecond fiber laser with a longer gain medium and lower doping”, Proc. SPIE 8237, 823721 (2012).

Acknowledgements

I would like to express my gratitude to my supervisor and mentor, Dr. Hanan Anis, who welcomed me into her research group in 2009. She has taught me to have confidence in my research and work, and has supported my participation in activities such as workshops, conferences, and courses to expand the breadth and depth of my knowledge. Dr. Anis has helped me to always see the big picture and keep my goals in mind while focusing on trying to solve specific problems. I would also like to thank my examiners, Dr. John Armitage and Dr. Paul Corkum, for their time and evaluations.

I must extend my thanks to my colleagues at the Innovation Lab of Photonics at the University of Ottawa. First and foremost, Hussein Kotb for spending many days with me in the lab helping with measurements, for running simulations in OptiSystem and VPI software, and for deriving a calculation for the nonlinear phase shift. I also thank Mohammed Abdelalim for his work training me on the femtosecond project when I started on it and for his advice and discussions when I had questions. I also want to thank the other students and researchers I have worked along-side in the lab over the past years who have encouraged me and created an enthusiastic work environment.

Finally, I must thank my friends and family, especially my mother, father, and brother, who have encouraged me, supported me, and counseled me throughout my degree.

Table of Contents

List of Figures

List of Tables

Glossary

AC	Autocorrelator
ANDi	All-normal dispersion
BW	Bandwidth
CPA	Chirped pulse amplification
CW	Continuous wave
DM	Dispersion management
GVD	Group velocity dispersion
HWP	Half-wave plate
NA	Numerical aperture
NIR	Near infrared
NPE	Nonlinear polarization evolution
OSA	Optical spectrum analyzer
PBS	Polarization beam splitter
PM	Polarization maintaining
PMT	Photomultiplier tube
QWP	Quarter-wave plate
SA	Saturable absorber
SESAM	Semi-conductor saturable absorber mirror
SMF	Single mode fiber
SPM	Self-phase modulation
Ti:sapphire	Titanium-doped sapphire
TOD	Third order dispersion
WDM	Wavelength division multiplexor

Symbols

β_2	Second order dispersion parameter (fs^2/mm)
β_3	Third order dispersion parameter (fs^3/mm)
γ	Nonlinear coefficient (W^{-1} m^{-1})
g	Gain parameter
g_o	Small gain parameters
λ	Wavelength
τ	Pulse width (s^{-1})
E	Pulse energy
P_{ave}	Pulse average power
P_{peak}	Pulse peak power
T	Intensity dependent SA transmission
Φ_{NL}	Nonlinear phase shift
c	Speed of light
d	Grooves per unit length on the surface of a diffraction grating
m	Order of grating diffraction
I	Normal length between a pair of diffraction gratings
B	Slant length between a pair of diffraction gratings
ψ	Angle of incidence onto the surface of a diffraction grating
θ	Angle of diffraction off a diffraction grating for a specific frequency component
$Sech^2$	Squared hyperbolic secant function pulse shape

Chapter 1 - Introduction

1.1 Lasers in medicine

Ytterbium-doped femtosecond fiber lasers are commonly regarded as biomedical lasers because they operate at a wavelength of 1030 nm, which is particularly well-suited to biomedical applications. Lasers that operate at this range are ideal for these applications due to what is called the "water window" which is a range of wavelengths near 1 μm that have a maximal penetration depth in biological tissues due to their low absorption in water. Since water is the primary component of all biological tissues, it is useful to have a range of wavelengths that provide long penetration depths for various applications. Furthermore, the 1030 nm wavelength produced by ytterbium-doped lasers is immune to absorption in melanin, hemoglobin, collagen, and proteins making it ideal for probing biological tissues [1].

Lasers have become a common tool in a variety of medical fields, such as dermatology, ophthalmology, dentistry, neurosurgery, cardiology, otolaryngology, gastroenterology, etc. Some medical lasers are used in place of surgical knives thanks to their precision and ability to cauterize the tissues while performing cuts, while others are used for their ability to vaporize surfaces of biological tissues. Furthermore, some lasers are used for observing biological functions (i.e. microscopy, endoscopy) instead of modifying tissues [2].

Pulsed lasers are critical for taking advantage of nonlinear optical processes, such as two-photon absorption, second harmonic generation, coherent anti-Stokes Raman scattering (CARS), etc. which can be used in nonlinear confocal microscopy. These processes only occur in high intensity focal points, which are created by using short pulses to generate high peak powers with low average power to prevent damaging the samples [3]. This allows for precise localization of nonlinear signals produced in the sample, ideal for confocal microscopy.

In research, the Titanium-sapphire solid state laser (Ti:sapphire) is a tremendously popular mode-locked laser which produces pulses centered at 690 - 1000 nm in the femtosecond temporal regime. The Ti:sapphire laser is popular due to its broad tuning range, variable pulse widths, and high average power in the hundreds of milliwatts. Its applications span from multiphoton microscopy and photodynamic therapy to ablation [4]. The major downfall of the Ti:sapphire is the cost as it is a bulky laser with a cooling system and a pump laser (typically an argon laser or a frequency doubled Nd:Yag laser). The specifications and tunability of the Ti:sapphire have secured its place as the laser of choice when researching nonlinear biomedical phenomena; however, its cost, form factor, need for water cooling and large power supplies prevent it from being used in the field and at the bedside [5].

Mode-locked fiber lasers solve many of the problems that solid-state lasers suffer from. Fiber lasers are smaller and less expensive than solid state lasers, and therefore can be more easily integrated into portable devices with the potential for use in bed-side biomedical applications. They also have the advantage of being self-cooled due to the large surface area to volume ratio that is inherent in fiber optics. Furthermore, mode-locked fiber lasers are very stable and have excellent beam quality, and as a result are truly becoming highly-performing and practical laser sources [6].

1.2 Possible applications

There are numerous biomedical areas that could benefit from the development and commercialization of oscillator-only femtosecond fiber lasers. The primary field motivating this work is that of confocal and multiphoton microscopy. Imaging cells and thick tissues in three dimensions at high resolution is made possible in this field with the use of ultrafast pulses of light. Fiber lasers are advantageous in this field particularly due to their cost since solid state lasers make up a significant portion of the cost of confocal microscope systems.

Another possible application is that of dentistry, where lasers are already becoming commonplace tools. The most common lasers used in offices today are diode lasers which are only capable of cutting soft tissues (i.e. gums). More expensive solid state lasers (i.e. Nd:Yag) are capable of cutting soft and hard tissue, making them a tool that can replace a common dental drill [7]. The Nd:Yag laser, much like the Yb-doped fiber laser, operates in the water-window, at 1064 nm. Yb-doped fiber lasers will also be capable of hard and soft tissue ablation if the energy can be increased sufficiently.

Furthermore, ophthalmology and dermatology also are fields that can benefit greatly from Yb-doped femtosecond fiber lasers for a variety of reasons. In ophthalmology, the primary use for fiber lasers would be for corrective eye surgeries. Currently, excimer lasers are commonly used for ablation as a replacement for traditional surgical knives in corrective eye surgeries. By making a precise cut across the cornea, a flap is created allowing the surgeon to change the shape of the corneal stroma to correct vision [8]. In dermatology, femtosecond lasers are used for a multitude of applications including tattoo removal, and treatments of birthmarks, *nevus flammeus* (commonly called port wine stains), and spider veins [9].

The limiting factor preventing Yb-doped fiber lasers from becoming competitive in any of these biomedical fields is simply the pulse energy. By increasing the pulse energy, these types of lasers could become a viable option for biomedical applications as they are significantly less expensive than their solid state laser counterparts.

1.3 Objectives

Biomedical applications are a focus of interest for the research of ytterbium fiber lasers due to the exceptionally useful wavelength at which ytterbium-doped gain media generate light. Fiber lasers themselves have many advantages over the Ti:sapphire used so commonly in research, but are limited in pulse energy [5]. Laser sources need high peak powers and low average powers to take advantage of nonlinear processes in biological tissues while avoiding unintentionally damaging them by means of burning them, causing necrosis of the tissues [10]. Optimizing the parameters of fiber lasers is important for making them competitive with solid state alternatives in research and for bringing them to the bedside and making fiber lasers a more common medical tool.

The main objective of this work was to improve the available energy per pulse output of a prototype of a femtosecond fiber laser, which is partially built from free-space optics. Another objective is to keep the cost of the laser low and retain simplicity of the design. Optimizing the energy out of the laser helps keep the cost low by removing the need for traditional external amplification. Ease of use is also an important consideration in working with the laser in hope of making it a viable and preferred source.

The major result of the work in this thesis was that it showed that increasing the length of the gain fiber and simultaneously lowering the doping improves the energy that pulses can carry in the cavity before collapsing due to optical wave-breaking. The lower doped gain fiber slows the rate of accumulation of nonlinear phase shift, allowing the pulse to reach a higher peak power before the maximum nonlinear phase shift at which wave-breaking occurs. The primary issue in getting to this result was overcoming multipulsing in the cavity, which reduced the energy per pulse as well as the ability to compare two different cavity arrangements. When the laser is mode-locked after changing a parameter, the cavity must remain otherwise unchanged to make a fair comparison of the independent variable; if multipulsing is present, there is no way to know if the pulse shapes are the same in both scenarios, so it is possible the two cases are not comparable at all. Single pulse operation was a necessity to investigate the gain fiber length and doping. Another investigation that was done was on determining the effect of the third order dispersion (resulting from the diffraction gratings) on the type of mode-locking and the resulting energy.

The overlying goal of the femtosecond fiber laser project is to move towards designing a laser cavity that generates high energy pulses. Theoretically, this could be done using the gain bandwidth of the ytterbium-doped fiber itself as a filter to initiate mode-locking. A long, low-doped piece of ytterbium-doped gain fiber would be used in place of all the single mode fiber (SMF) in the cavity. This is what motivated the work I did towards displaying the advantages of using a long, low-doped gain fiber compared directly to a short gain fiber under the same cavity conditions.

1.4 Thesis outline

Having in mind the main objectives listed above, the thesis is structured as follows: Chapter 2 discusses the background theory of femtosecond fiber lasers, including various pulse modes and problems that can be encountered. Chapter 3 discusses the problem of multipulsing that was encountered throughout the research. Certain cavity parameters thought to contribute to multipulsing were investigated. Two special cases of multipulsing were observed and are presented. Chapter 4 discusses the investigation done regarding the effect of third-order dispersion (TOD) on the cavity's ability to mode-lock. Chapter 5 discusses the work done regarding showing that lower doped gain fiber in the cavity can delay the onset of the wave-breaking of optical pulses. Chapter 6 summarizes the results and discusses some future work that can be done in this direction.

Chapter 2 - Background

2.1 Mode-locking principles

Lasers can vary tremendously in terms of how they operate and for what purpose. Pulsed lasers differ from continuous wave (CW) lasers due to their cavities being biased towards operating in a manner that generates pulses of light as opposed to constant amplitude CW light. Lasers can be pulsed using various methods, such as Q-switching or cavity dumping; however, the most popular technique is referred to as mode-locking [4].

Mode-locking refers to the process of locking together multiple longitudinal modes inside a laser cavity. This generates pulsed radiation when the phases of the modes are forced to be 'locked' to one another generating coherence, which can be achieved through various techniques [11]. Fixing the phase relationship of multiple longitudinal modes in the cavity causes pulsing simply through the periodic constructive interference lined up by the locking of the modes and the destructive interference at all other points in time. When the phase relationships are fixed together, they can be interpreted as the Fourier components of a periodic function (i.e. the periodic pulse train) [4]. The case in which the phases of all the modes oscillating in the laser are locked together produces the narrowest pulse [12]. When a single pulse is circulating a ring cavity, the period, T, is $T = L/c$ where L is the length of the cavity and c is the speed of light [4].

Fiber laser cavities typically take on one of a few basic shapes, as shown in Figure 2-1. The most common laser cavity configuration is the Fabry-Perot cavity, which is used in Ti:sapphire and other solid state lasers. It consists of two mirrors and a gain medium in the region between the mirrors. This method can be applied to fiber lasers, but to maintain an all-fiber set-up dielectric mirrors would have to be deposited on the ends of the fiber. One problem is that this type of mirror is very sensitive to imperfections on the ends of the fiber. Another problem is that the high-power pump light that would have to pass though these mirrors, possibly causing damage to them. As a result there was a move towards the development of ring cavities [13]. The ring cavity's most basic form consists of a length of gain fiber in a circular geometry, as well as an isolator to force unidirectional operation and an output coupler. The figure-8 laser is a more complicated ring cavity which uses a second coupler to split light from the main ring to counter-propagate around the adjacent ring before recombining with the light in the main ring. This is fundamentally a Sagnac interferometer [14].

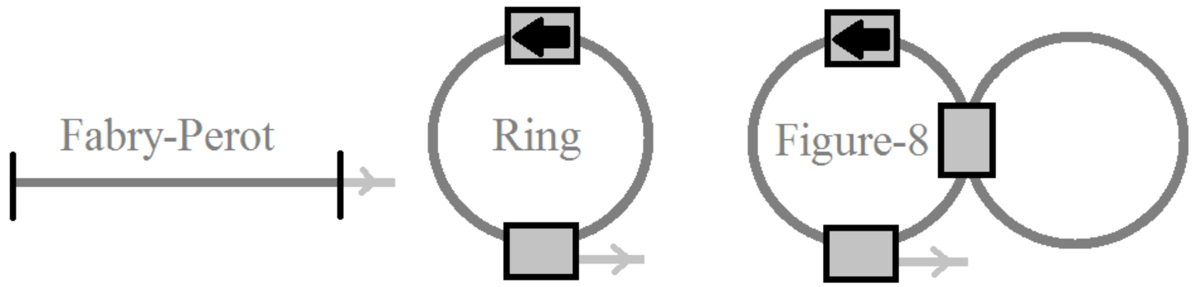

Figure 2-1: Basic fiber laser cavity configurations [11]

Fiber lasers cannot generate mode-locked pulses in the same way as a solid state Ti:sapphire laser. Kerr lens mode-locking used in Ti:sapphire lasers relies on the nonlinear self-amplitude modulation that results from the self-focusing of a beam. A hard (i.e. physical) or soft (i.e. induced) aperture can be used to change the beam profile to control the losses and gain in the laser cavity. All-fiber lasers have no equivalent aperture to control since the beam profile is determined by the fiber waveguide itself. Thus, there are two vastly different categories, active and passive, of mode-locking for fiber lasers.

Amplitude modulation and phase modulation are the main techniques to achieve active mode-locking [14]. Active mode-locking is not good for generating pulses less than 1 ps because of mechanical limitations resulting from using an active modulator [13]. These relatively long pulse durations arise from periodically modulating resonator losses or round-trip phase changes at the laser cavity frequency; some commonly used modulators include acousto-optic, electro-optic, Mach-Zehnder integrated-optic, semiconductor electroabsorption modulators [3]. The frequency of the modulator has to be matched to the cavity's repetition rate to achieve the pulse formation.

Passive mode-locking has been used to produce the shortest pulses from fiber-lasers, and typically relies on semiconductor saturable absorbers to create pulse-shaping action [14]. Passive mode-locking is different from active in that it does not rely on a physical modulator changing cavity parameters. Passive techniques are faster as they bias the cavity towards forming pulses as a steady state solution of the cavity [3]. The cavity is designed to favour the pulse solution over the continuous wave solution [12]. Some techniques for passive mode-locking include additive pulse mode-locking and semiconductor saturable absorbers.

Mode-locking has been done with saturable absorbers since the 1970s [13]. Since the saturable absorber's transmission curve preferentially transmits high intensity light with less attenuation than lower intensities, as shown in Figure 2-2, they are commonly used in mode-locked laser cavities to initiate pulse-shaping out of a noise spike in CW operation [4]. By transmitting a pulse through a saturable absorber material, the central part of the pulse will saturate the absorber, while the wings (i.e. low-intensity edges) of the pulse will undergo losses, resulting in the narrowing of the peak. Real saturable absorber materials do not typically respond faster than a fraction of a 1ps. This is a problem when trying to generate ultrafast pulses [13].

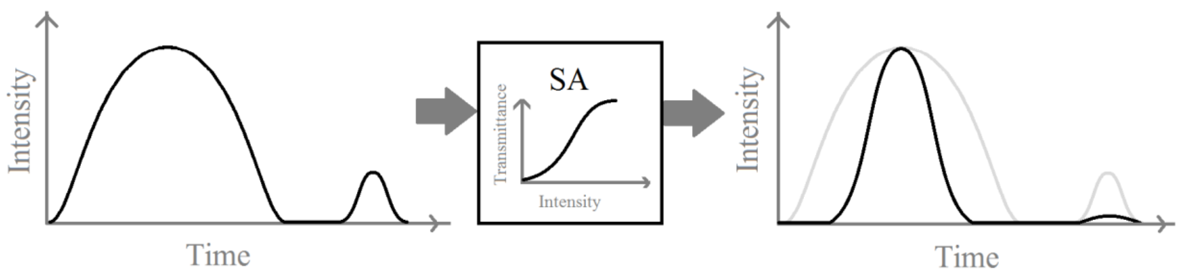

Figure 2-2: Saturable absorber transmission [6]

Artificial saturable absorber techniques were developed for ultrafast pulse generation. One such technique is Kerr lens mode-locking (used in Ti:sapphire lasers) since the laser can be aligned such that the high-intensity part that will experience the most self-focusing overlaps best with the gain medium [15].

2.1.1 Nonlinear polarization evolution

In fiber lasers, nonlinear polarization evolution (NPE) is a technique commonly used as an artificial saturable absorber. This technique is based on the fact that the nonlinear medium rotates the azimuth of the elliptically polarized light in proportion to the light intensity. The high and low intensity parts of the pulse experience different angles of rotation after the nonlinear optical fiber. There is an intensity dependent polarization across the pulse, and the polarizer changes this into an intensity dependent transmission. This method can be adjusted to select the high intensity parts of the pulse while suppressing the weaker wings. In 2003, this method was used to achieve 36 fs pulses with an ytterbium doped gain fiber [5].

Figure 2-3 shows the dependence of the transmittance vs. intensity curve for NPE mode-locking. It differs from a saturable absorber material since high intensities can "overdrive" the transmittance, causing the negative slope regions in Figure 2-3 [6]. At high energies, the NPE the transmission function becomes periodic because of the dependence on the angle of rotation of the elliptically polarized light [16]. This over-driving of the mode-locking creates limitations in the attainable pulse energy [17]. Despite limitations, NPE is still a tremendously useful and broadly used technique for mode-locking.

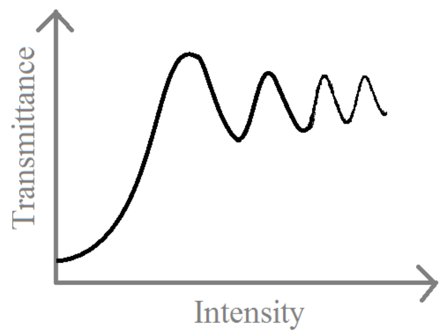

Figure 2-3: Artificial saturable absorber transmittance vs. intensity [6]

NPE is fundamentally rooted in the principle of the intensity-dependent nonlinear refractive index (i.e. Kerr effect) which causes a rotation of the polarization of the pulses. The amount of rotation is nonlinear in that it depends on the index of refraction, which itself depends on the intensity [6]. Figure 2-4 shows a simplified NPE laser cavity and the evolution of the polarization rotation within it. The basic components required (here, shown in free space) are two quarter-wave plates (QWP1, QWP2), a half-wave plate (HWP), a polarizer (which in the case of this thesis is a polarization beam splitter, PBS), and a fiber with collimated ends.

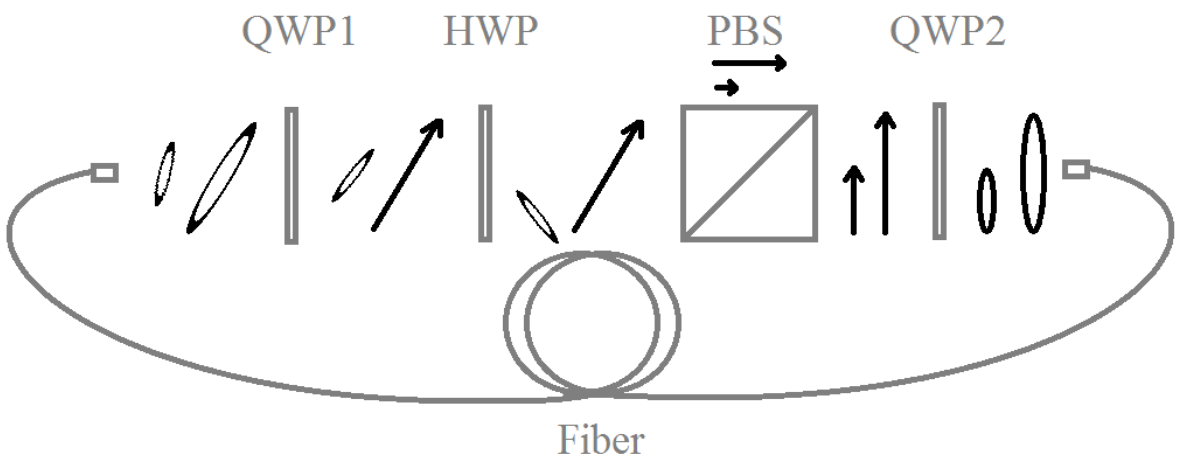

Figure 2-4: Evolution of the polarizations of high and low intensity light inside a simplified cavity [6] [18]

Between each component, a low and a high intensity pulse's polarizations are depicted respectively with a small and a large oval or arrow (depending on the state of polarization being elliptical or linear). The PBS splits the light into two orthogonal polarizations. Light after the polarizer (PBS) is linear and then transformed into elliptical by QWP2. At this point, the low and high intensities of a pulse have the same angle of rotation. By injecting the pulse into the gain fiber, nonlinear effects become significant and the high intensity part of the pulse undergoes more rotation than the low intensity parts; this happens mostly in the length of nonlinearly-acting SMF (i.e. the Kerr medium) after the gain fiber. QWP1 then can be tuned to turn the high-intensity light back to linear. The HWP then simply turns the orientation of the linearly polarized light entering the output coupling polarizer, which acts as a polarization filter [18]. Arranging the orientations of the wave plates causes the NPE to act like an artificial saturable absorber [6]. Although NPE is the most important method of mode-locking for this thesis as it is the primary technique used, other methods such as using a semiconductor saturable absorber mirror (SESAM) do exist and are commonly used.

In an NPE ring fiber cavity such as the one used in bulk of this thesis, there are also other components required besides the basic components shown in Figure 2-4. Firstly, a laser pump is coupled into the ring cavity. In this work, two 980 nm laser diode pump lasers are passed through a combiner and a fiber isolator to prevent damage to the sources before being coupled into the cavity through a wavelength division multiplexer (WDM). Appendix A describes how the laser sources which are controlled with current are converted to power values. The purpose of the pump lasers is to cause population inversion which leads to lasing in the gain medium. The ytterbium-doped fiber (see Appendix B for specifications of the two types of gain fiber used) serves as the gain medium in this work and is pumped by 980 nm light, and emits 1030 nm continuous wave (CW) light. After the gain fiber, there is a section of SMF referred to in this work as the nonlinearly-acting SMF which contributes to the NPE-action. If this length is too short, NPE becomes unachievable, and if it is too long the attainable pulse energy level decreases [6]. In a cavity such as the one studied in this thesis, there is a free-space region with bulk optical components. As discussed, the quarter-wave plates and half-wave plate, in combination with a polarizer, are used for achieving NPE. In this case, the PBS is used for both as a polarizer and as an output coupler. A pair of diffraction gratings in the cavity is used to control with precision the total group velocity dispersion (GVD) in the cavity since the SMF and gain fiber both provide normal dispersion and the diffraction grating set adds anomalous dispersion, discussed in Appendix C. The net amount of GVD is a large factor in determining what pulse shape will be generated in the cavity, which will be seen in section 2.2 . An isolator inside the cavity ensures unidirectional operation. Then the light is collected through a tilted-end collimator with antireflective coating and an angle-polished internal fiber to prevent back-reflections in the cavity (50 dB return loss). Next, the light passes through another length of SMF which is referred to as the linearly-acting SMF since it is placed before the gain fiber and therefore receives relatively low powered light. This SMF rejoins the gain fiber, completing the ring cavity.

2.1.2 SESAM mode-locking

One major short-coming of NPE mode-locking is that it is difficult experimentally to avoid falling into the overdriven regions in the transmission curve from Figure 2-3. One of the most recent techniques for avoiding this is a move towards using semi-conductor saturable absorber mirrors (SESAM) instead of, or in combination with, NPE for mode-locking. A SESAM does not typically have an over-driven region and its transmission curve saturates monotonically, making it a more reliable technique for mode-locking.

A SESAM is typically produced on a substrate, such as a GaAs semi-conductor wafer, and has two distinct layers on it. The first is the saturable absorber material layer, which can be designed with a certain absorption curve. The second is a Bragg mirror, which reflects the light back through the saturable absorber layer [19].

SESAMs are advantageous because they can be designed with particular saturation intensity, recovery time, reflection bandwidth, and so on, entirely in a small package [19] [20]. However, SESAMs still are not ideal solutions for femtosecond fiber lasers. They are limited in how short they can shape pulses due to their nature as semi-conductor materials. Furthermore, SESAMs are easily damaged when used in high power lasers [21].

2.2 Regimes of operation

Mode-locked fiber lasers can operate in a variety of regimes, depending on their cavity parameters. The main regimes of operation are solitonic, stretched-pulse, self-similar, and dissipative soliton regimes [12]. These regimes are determined by the total GVD of the laser cavity and different regimes generate different pulse shapes. This also depends on the type of laser cavity, since different types of cavities operate at different values of GVD. All-negative GVD cavities support solitons. Dispersion managed (DM) lasers can sustain stretched-pulse, self-similar, and also dissipative solitons. All-normal dispersion (ANDi) cavities typically support dissipative solitons, although they have recently generated self-similar pulses as well [22]. Figure 2-5 shows a simplified map of where the regimes lie for various regions of GVD: soliton pulses occur when the cavity dispersion is anomalous ($\beta_2 <0$), stretched-pulses can occur for normal or anomalous dispersion, self-similar pulses occur at slightly-normal dispersion ($\beta_2 >0$), and dissipative solitons appear at very high net normal dispersion [12] [3].

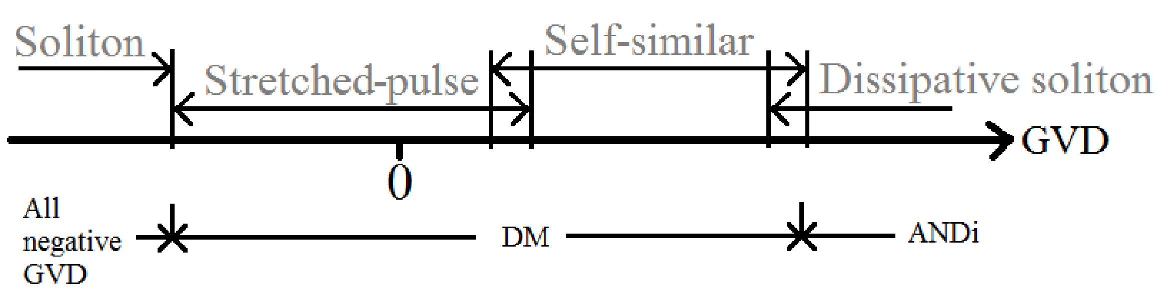

Figure 2-5: Simplified distribution of pulse regimes depending on net GVD of the laser oscillator

It should be noted that the two most significant problems in designing fiber lasers are dispersion and nonlinearity. Nonlinearity causes wave-breaking and instability in the pulse when it is excessive. Dispersion within the cavity results in inevitable chirping of the pulse. Anomalous dispersion causes a down-chirp of the frequency components, while normal dispersion results in an up-chirp. Higher order dispersive effects cause additional changes to the pulse shape. GVD (β_2) broadens the pulse in time, and TOD (β_3) causes asymmetric ripples in the tail end of the pulse [12].

Looking only at the cavity GVD gives only a simplified perspective of how pulses are shaped in different regimes. The nonlinear pulse propagation in gain fibers is described with the nonlinear Schrödinger equation. When a parabolic gain profile of the fiber is considered, the resulting equation that describes the evolution of a pulse envelop described by A, is:

$$\frac{\partial A}{\partial z} = -\frac{i}{2}\left(\beta_2 + i\frac{g}{\Omega_g^2}\right)\frac{\partial^2 A}{\partial t^2} + i\gamma|A|^2 A + \frac{1}{2}(g-l)A$$

Eq. 1

In this equation, z is the direction of propagation, β_2 is the second order dispersion (s^2/m) parameter, Ω_g is the gain bandwidth, g is the gain per unit length, and l is the loss per unit length. The term γ is the nonlinear coefficient which is equal to $2\pi n_2/\lambda F$. Here n_2 is the nonlinear refractive index, λ is the wavelength and F is the core area of the fiber. The nonlinear coefficient controls the self-phase modulation.

Following the Schrödinger equation, many different pulse shapes can arise depending on the conditions in the cavity. Sech^2 pulses, or solitons, occur when there is both a negative dispersion and when there are no gains or losses in the fiber, which results from the balance of nonlinearity and anomalous dispersion. Other pulse shapes that can satisfy the Schrödinger equation include chirped sech^2 pulses, Gaussian shaped pulses, and parabolic pulses.

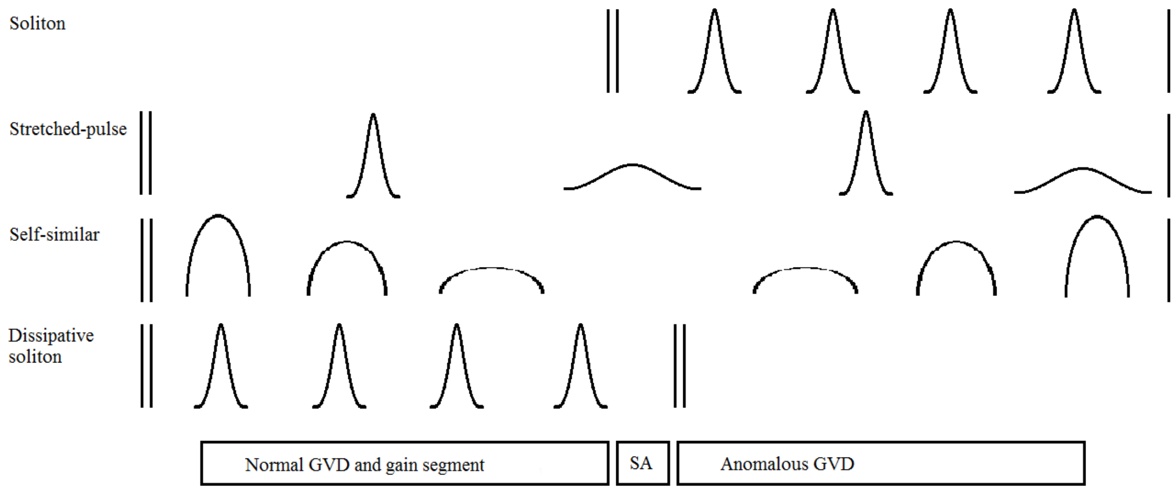

Figure 2-6: Simplified pulse evolution in basic laser cavities for soliton, stretched-pulse, self-similar and dissipative soliton operation. Note: The soliton cavity does not include the normal GVD region. The dissipative soliton does not include anomalous GVD. The double bars denote the beginning and end of a single pass of the cavity. [6]

Figure 2-6 shows a simplified diagram of the pulse evolution in several different regimes: soliton, stretched-pulse, self-similar, and dissipative soliton. The bar along the bottom of the figure illustrates the basic components of the cavity. Gain and loss, as well as the pulse shaping effects of the saturable absorber are not shown here. This simply illustrates the basic pulse propagation differences for the different regimes. For example, the soliton keeps the same shape and amplitude throughout the cavity, which does not contain a normal dispersion segment. Self-similar pulses have two locations of minimum pulse width, and self-similar pulses have their minimum pulse width after the anomalous dispersion. Dissipative solitons are typically produced in all-normal dispersion cavities with no anomalous dispersion segment and maintain their size and shape. These various regimes will be discussed in the subsequent sections.

2.2.1 Solitonic pulses

Solitonic pulses occur under highly negative cavity GVD. The anomalous GVD contribution comes from a component with a positive nonlinearity [6]. Solitons occur when the dispersion in the cavity and the self-phase modulation are balanced [23]. This generates a transform-limited soliton with a $sech^2$ pulse shape [24]. Solitonic pulses have no chirp and have unchanging pulse energies within the cavity [3].

Soliton lasers were introduced in the 1980's [25]. This early on, soliton pulses were only produced with erbium-doped gain fibers. The regular step-index fibers that were used provided anomalous dispersion at the telecom lasing wavelength of 1550 nm, which was needed to form a solitonic pulse [23]. Because of the long fiber lengths, dispersion and nonlinearities both make significant contributions to the pulse shape in each pass through the cavity and can cancel each other out to form solitons in negative dispersion fibers [26].

Real fiber cavities however have fluctuations in loss and gain. Typically, true solitons cannot exist [27]. Strictly speaking, perfect solitons cannot be produced when the pulse undergoes perturbations due to gain and loss. These perturbations cause the soliton to lose energy in the form of dispersive waves which resonate in the laser cavity at certain frequencies causing spectral side bands, called Kelly side-bands. Soliton sidebands occur because part of the soliton energy is removed at the output coupler. The soliton then has to build back up its energy over the course of the pulse's next pass through the cavity. Since the peak power varies throughout the cavity, a nonlinear index grating is formed, which changes the soliton's properties as it propagates. The soliton adjusts to these changes by depositing energy into dispersive waves, which appear as soliton sidebands [13]. The sidebands are narrow peaks that occur in the spectral domain of the pulse and have lower intensities further away from the central wavelength [28].

The dispersive waves are simply the non-soliton parts of the pulse that propagate in the cavity and accumulate phase shifts. Each time passing through the cavity, the soliton will generate dispersive waves which interfere with previous ones. Only constructively interfering dispersive waves that have phase shifts equal to multiples of 2π will survive [14]. Dispersive waves propagate according to linear dispersion and therefore have a different dispersion coefficient (β_D) than the nonlinear soliton pulse (β_S). The 2π dependence for constructive interference comes out of the fact that the strongest dispersive waves are generated when they are phase matched with the soliton. This can be expressed with the equation,

$$\beta_S(\tilde{\omega}_m)L = \beta_D(\tilde{\omega}_m)L + 2m\pi$$

Eq. 2

Here, ω_m is the difference between the *m*th sideband frequency and the central frequency, *m* is an integer, and L is the cavity length [26]. By substituting the Taylor expansions [14] for $\beta_S(\omega)$ and $\beta_D(\omega)$ into this equation, the positions of the soliton sidebands can be predicted by the equation

$$m = \frac{\beta_2 L}{4\pi}\left[T_0^{-2} - \tilde{\omega}_m\right] - \frac{\beta_3 L}{12\pi}\tilde{\omega}_m$$

Eq. 3

In equation (3), T_0 is the soliton pulse width parameter, and β_2 and β_3 are the 2nd and 3rd order dispersion coefficients [26]. This equation can be used to predict the locations of the theoretical sidebands.

The transfer of energy into the sidebands is the major limitation to the minimum pulse width achievable with soliton lasers. The energy and pulse width in soliton lasers are inversely proportional, and as a result soliton lasers are optimal in the picosecond regime where they can generate up to 10 nJ of energy [23]. In contrast, dispersion managed cavities which produced stretched-pulses are not limited by Kelly side-bands [12].

2.2.2 Stretched pulses

Stretched pulses are formed using dispersion management (DM) and have advantages over soliton lasers. DM allows the pulse to avoid nonlinearity by using lengths of fiber with opposite signs of dispersion, allowing the pulse to breathe [6]. Alternating positive and negative dispersion fibers increases the average pulse width and allows higher energy, and it permits shorter pulses to be generated [23]. Higher energies are tolerable since the broadening of the pulse reduces the peak power and in turn the nonlinear effects that can limit the pulse energy. Gaussian pulses occur when the spectral broadening is equal to the spectral compression (both of which are induced by SPM) in a pass through the cavity [23]. The pulses are generated by creating cavities that manage the dispersion within them by using both positive (normal) and negative (anomalous) dispersion fibers, as seen in Figure 2-6 [27]. Soliton lasers cannot generate pulse widths as short as one can with DM fiber laser systems. Gaussian pulses are generated from DM lasers and do not suffer from soliton sidebands in the wings due to the pulse breathing while propagating within the cavity. A characteristic of a stretched-pulse is that it changes the sign of its chirp while propagating through the cavity.

DM lasers are constructed differently for ytterbium-doped gain fiber than for erbium-doped gain fibers. Telecom fiber lasers using erbium-doped gain fiber lase at 1550 nm. At this wavelength, standard SMF provides anomalous dispersion in the cavity, which compensates for the stretching of the pulse in the erbium-doped fiber. A crucial difference between ytterbium-doped fiber lasers and erbium-doped is that the latter lase at 1550 nm compared to 1030 nm for the former. Since 1550 nm undergoes anomalous GVD in the SMF and normal GVD in the gain fiber, erbium-doped fiber lasers can be made entirely from fiber. On the contrary, 1030 nm suffers from normal dispersion in the gain fiber as well as in the SMF, meaning that dispersion compensation is usually needed in the form of bulk elements such as prisms or diffraction gratings. The method of dispersion compensation influences the types of pulses attainable [3]. Some fiber-based methods of controlling dispersion include chirped fiber gratings, microstructured fibers for anomalous dispersion, highly nonlinear fibers, photonic bandgap fibers [23], and also photonic crystal fibers [29].

Stretched pulses breathe in the cavity, stretching in the normal dispersion regions and compressing again under the influence of anomalous dispersion. The pulse width can change by up to an order of magnitude inside the cavity, which as mentioned previously is advantageous as it reduces unwanted nonlinear effects [30]. Due to the breathing of the pulse, these are sometimes called ‘average soliton’ pulses [24]. Typically, the pulse-width is minimal and bandwidth-limited at two positions within the cavity [23]. As a result, these lasers can generate more energy and shorter pulses than soliton lasers can by exactly compensating the spectral broadening with spectral compression, both resulting from the SPM [26]. Practically, stretched pulses occur in the near-zero net-cavity dispersion regime.

When the pulse is stretched, the effect of SPM is reduced; higher pulse energies can be used since a given energy will have less unwanted nonlinearities than in a soliton laser of the same energy [27]. When there is a slight net positive dispersion, the soliton sidebands are suppressed, and under these conditions the smallest stretched-pulse widths are generated [26]. The most important aspect of dispersion control is that it allows for pulses to have energies higher than is otherwise possible in soliton lasers [27].

2.2.3 Self-similar (similariton, parabolic) pulses

The self-similar pulse regime exists in a net normal GVD laser cavity with no nonlinearity in the anomalous dispersion component [6]. The chirp of the similariton is always positive inside the cavity. Recalling from Figure 2-5, it requires more net positive dispersion than the stretched-pulse regime; however, the same cavity conditions might generate both the stretched-pulse and self-similar pulses [6]. Increasing the positive net-cavity dispersion decreases the breathing range and drives the ratio of widest to narrowest pulse width (breathing ratio) to unity. The pulse is chirped positively in the normal dispersion region of the cavity. Since there is more normal dispersion than anomalous, only some of this chirp is countered by the negative chirp of the anomalous region resulting in a positively chirped pulse. The self-similar pulse regime is a special case of the wave-breaking free regime where self-similar pulses are positively linearly chirped and have parabolic spectral and temporal profiles [24]. Wave-breaking free pulses accumulate positive frequency chirp inside the cavity which is partially compensated with segments of anomalous GVD [31]. Pulse energies in fiber lasers are typically limited by wave breaking resulting from high levels of nonlinearity; however, self-similar pulses in similariton lasers are able to undergo higher levels of nonlinearity than other regimes without experiencing wave-breaking [17].

Wave breaking of optical pulses is aptly named as it is analogous to breaking of waves in water. It is the distortion of the temporal shape of the pulse resulting from self-phase modulation. The SPM induced frequency chirp causes the red-shifted light at the front of the pulse to speed up and the blue-shifted tail to slow down; however, the center of the pulse is unaffected due to the linear frequency shift, and the low-intensity leading and trailing tails of the pulse are also unaffected since they do not undergo nonlinear effects. The aforementioned red and blue-shift overlap the low intensity pulse tails. This results in two frequencies in these regions, generating new frequencies [32]. Wave breaking results in fine structures in the edges of the pulse [33]. This can occur in a NPE cavity that is overdriven [34].

A major problem with the stretched pulse regime is its susceptibility to wave-breaking for a high intensity pulse. Wave-breaking free pulses have been known since the 1980's [33]. Only in the 2000's have self-similar pulses been achieved, first by simulations and later by experiments [17]. The first observed self-similar pulses relied on a short length of ytterbium-doped gain fiber to compensate for losses in the cavity, while only negligibly contributing to the dispersion and nonlinearity [17]. The spectral filtering of the gain fiber due to the amplifier transition bandwidth must be wider than the input spectrum for stable pulse propagation; unstable operation occurs when the bandwidth of the input pulse is comparable to the gain bandwidth [35]. However, because of the decoupling of the gain-bandwidth from the nonlinear effects due to the use of a short gain fiber, the gain-bandwidth is able to filter the nonlinearly-generated bandwidth from the SMF to create a periodic, self-consistent pulse [36].

Self-similar pulses can exist under stronger SPM (>π) compared to both stretched-pulse (Gaussian) and solitonic ($Sech^2$) pulses [23], and as a result have exceeded the wave-breaking energy limits of stretched pulse lasers [34]. Self-similar pulses also have been found to become unstable and lose out to the CW steady-state below a threshold value of net cavity dispersion [37].

Self-similar pulses are distinct due to their parabolic shape in both the time and frequency domains which aids in resisting optical wave-breaking. The pulse shape is parabolic throughout the cavity, including at the output [23]. Ideal self-similar pulses also have a linear frequency chirp throughout the cavity making pulse compression to the transform-limit relatively simple [17]. Unlike soliton or DM lasers, there is one location of minimum pulse width in the cavity, which naturally occurs after compression of the pulse by the diffraction gratings, however this minimum is not transform-limited [36].

The most important distinction, however, is that the magnitude of anomalous dispersion required to compress the pulse after it has exited the cavity is always more than the magnitude of anomalous dispersion applied within the cavity (i.e. the “intra-cavity” anomalous dispersion). This is a useful experimental means of distinguishing between self-similar and stretched pulses, which is employed in this thesis. Since the stretched-pulse regime has two pulse width minima in the cavity, less dispersion compensation is needed outside the cavity to reach the transform-limit [17] [38] [39]. It is not enough to judge the regime simply by the pulse shape because stretched-pulses can appear parabolic-looking and can be easily confused with self-similar pulses [36] [40] [41].

Despite the self-similar pulse regime's tolerance of optical wave breaking, this pulse regime is still susceptible to multiple pulsing and bound pulses. Typically, multiple pulses that occur when the pump power crosses a threshold value are randomly spaced in the cavity; however under some conditions bound states of closely-spaced pulses can exist [40].

Multi-pulsing is an issue that has been found across different kinds of mode-locked lasers and seems independent of the mode-locking technique. By increasing the pump power delivered to the gain medium, the number of pulses in the cavity increases. This is a result of the peak power and spectral bandwidth increasing with the energy circulating in the cavity. When the spectral bandwidth becomes larger than the gain bandwidth, the pulse in the cavity splits into lower energy pulses, which in turn have smaller spectral bandwidths [16].

Self-similar pulses are the focus of this work. One major reason for this is their linear frequency chirp which causes them to have a high immunity against wave breaking and ease of compression outside the cavity [31], and the robustness against optical wave-breaking allows them to carry a high energy [17].

2.2.4 Dissipative solitons

Dissipative solitons occur in high net normal GVD cavities. They undergo loss and gain in the cavity, unlike conservative solitons, and produce hyperbolic secant pulse shapes [42]. They are also characterized by a small spectral breathing ratio (<5) [22], and are strongly chirped due to the high GVD in the cavity [43]. Dissipative solitons have been seen in some DM laser cavities, such as in this thesis, but are more commonly seen in all normal dispersion (ANDi) lasers, which have changed the direction of fiber laser research.

Prior to 2006, all femtosecond fiber lasers required the implementation of anomalous dispersion to operate [44]. Increasing the positive net cavity GVD allows the pulse to be able to carry higher energies without optical wave breaking. At certain values of high GVD, stable pulses cannot be achieved without the additional use of spectral filtering. This concept led to the generation of stable-mode-locked dissipative soliton pulses with only spectral filtering and no dispersion compensation [44]. As a result of the lack of dispersion compensation, the ANDi laser cavity is also capable of generating higher-energy pulses, making it an important advancement in fiber laser technology. Initially, in [44], NPE was used in combination with a spectral filter, which enhanced the self-amplitude modulation under higher nonlinearities. Pulses generated in the all-normal dispersion regime are typically dissipative solitons. The GVD broadens the pulse, and the saturable absorber in combination with the spectral filter shorten the pulse [45].

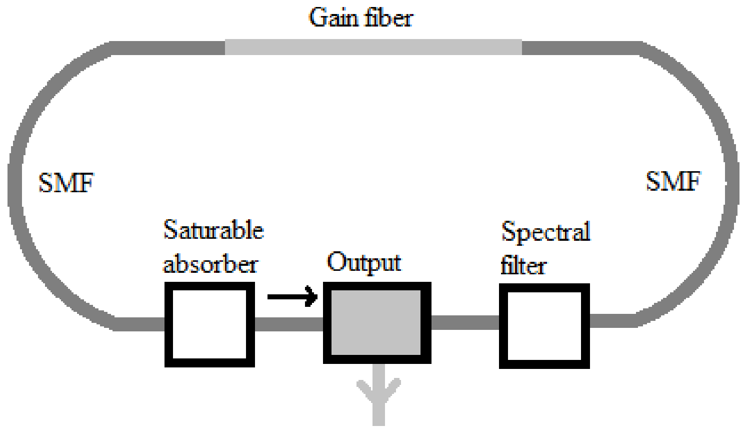

Figure 2-7: ANDi fiber laser cavity for generating dissipative solitons

More recently, self-similar pulses have also been achieved in an ANDi laser [22]. This work relies on the long length of ytterbium-gain fiber acting as a local attractor, forcing pulses of any shape to become parabolic. The narrow band filter of 4 nm acts to make the pulse self-consistent, cutting the pulse's duration drastically after monotonically increasing in the gain fiber [22]. However, the highest energy pulses made to date with an ANDi laser have been dissipative solitons pulses, not self-similar. Pulse characteristics comparable to solid-state femtosecond fiber lasers have been achieved in a dissipative soliton fiber laser, generating 80 fs pulses with over 1 W of average power and 200 kW of peak power [46].

The ANDi laser cavity is advantageous not only due to its improved output pulse power, but also due to the simplicity of its design. Removing anomalous dispersion components makes it easier to develop an all-fiber laser cavity. ANDi lasers and their high-energy dissipative soliton pulses are an important development in the field of femtosecond fiber lasers. Studying this type of laser cavity will be considered as a future prospect on the femtosecond fiber laser project, continuing where this thesis leaves off.

2.3 Improving power

It is difficult to generate high peak powers and pulse energies due to nonlinearity deteriorating the pulse, and this concept applies also to amplification. The classic approach has been to use an oscillator in combination with an amplifier such as in [47], which is shown in

Figure 2-8. In this example, an approach similar to chirped pulse amplification (CPA) is demonstrated.

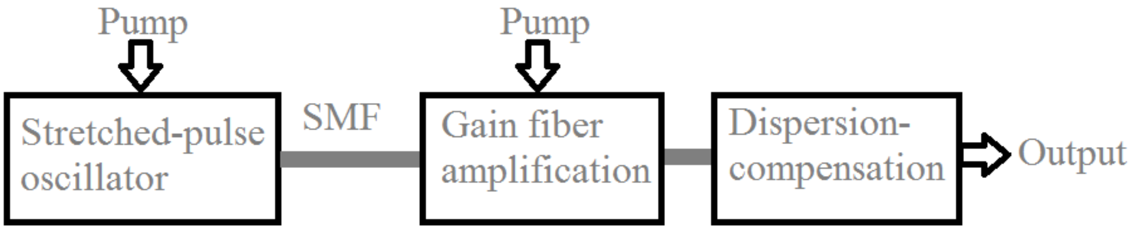

Figure 2-8: Classic oscillator with amplifier fiber laser approach [38]

CPA is a technique for minimizing unwanted nonlinearities during amplification, commonly used in solid-state lasers. Strickland and Mourou introduced this technique for laser amplification in 1985 [48]. CPA works simply by amplifying a pulse after chirping and stretching it. By reducing the peak power with chirp-induced broadening, it is possible to amplify the pulse significantly and to transfer large amounts of energy to the pulse before saturating the available gain [13]. Pulses are stretched, amplified and then compressed; temporal scaling increases the pulse energies that can be generated [27]. For all-fiber systems, chirped fiber Bragg gratings can be used for pulse stretching and compression done through CPA [23]. Conventional bulk gratings, however, provide better saturation-fluence-limited energies [27].

In Figure 2-8, the pulse exiting the oscillator is stretched having to pass a long length of SMF before the amplifier stage to increase the chirp. After amplification, the pulse is compressed (in this case, with diffraction gratings). The disadvantages of this scheme include additional complexity and also the additional amplification of noise. However most commercially available fiber laser devices are based on this technique.

Another method used to increase the energy capacity of a fiber laser is to use fiber with a larger core diameter which effectively reduces the intensity of the pulse [27]. The maximum femtosecond pulse energies that have been generated in fiber lasers used chirped pulse amplification (CPA) and large core fibers. The highest energies that can be generated are limited by self-phase modulation, self-focusing, and damage that the pulses cause to the fiber [23].

The work in this thesis is towards obtaining a laser cavity with optimized parameters that would generate high-energy pulses that do not need traditional external amplification. This approach has advantages in terms of simplicity and in cost. Improving the output energy at the oscillator stage also allows for the possibility of greater benefits from external amplification, which can be added on later.

Chapter 3 - Multipulsing

3.1 Introduction

The objective of this thesis is primarily to increase energy in an ytterbium-doped femtosecond fiber laser by means of varying the doping parameter of the gain fiber. The major obstacle in progressing with this work has been that multiple pulsing (multipulsing) in the cavity would occur for unknown reasons. When multiple pulses are circulating inside the laser cavity they must share the available energy. Consequently, this means that a cavity with multipulsing will have lower energy per pulse than a laser cavity functioning optimally with a single pulse per cavity period. Multipulsing prevented studying single-pulse dynamics and was an issue that obstructed observing true single pulses for quite some time in this experiment. Moreover, multipulsing is typically unstable and not a useful mode of operation for fiber lasers.

Many problems were faced over the course of making the final experimental set-up robust, as it is today. After determining that the laser cavity was not producing single pulses of high enough energy compared to similar laser cavities in the literature [6], it was concluded that despite the maximum pump power in this experiment being smaller than those used in literature, the pump power was not the limiting factor in the low energy pulses observed. Instead, the low threshold of multipulsing in the cavity limits the energy. However, increasing the pump power past the threshold at which multipulsing occurs does not improve the energy per pulse in a meaningful way, but increasing the energy threshold at which multipulsing manifests would allow for more of the available pump power to be used effectively.

General multipulsing is unstable and hinders the generation of usable single pulses. However, occasionally bound multiple pulses are observed, which maintain their temporal separation throughout the round trip of the cavity and are generally very stable. Furthermore, bound pulses can in some special cases become equidistantly spaced and generate harmonic mode-locking which could be used to control repetition rate for a constant cavity length.

This chapter presents the experimental set-up used in most of this thesis. Then it examines possible causes for the seemingly low threshold for multipulsing observed in this experimental set-up. The latter part of the chapter focuses on multipulsing bound states that were observed and are described qualitatively as they have stable operation and could be useful in the future.

3.2 General experimental set-up

In general for conducting these experiments, the femtosecond fiber laser cavity was arranged as shown in Figure 3-1 with some variations. Two 980 nm pumps were combined and injected into the cavity via a wavelength division multiplexer (WDM). The fiber portion of the cavity consists of a linear, low power region of SMF before the gain fiber and another nonlinear, high power region of SMF after the ytterbium gain fiber. The free-space region contains two quarter-wave plates and a half-wave plate for mode-locking by means of nonlinear polarization evolution (NPE). A polarizing beam-splitter (PBS) cube was used as both the output rejection port and as a polarizer necessary for NPE action. A pair of diffraction gratings was used for anomalous dispersion compensation inside the ring cavity. A Faraday isolator was used to ensure unidirectional operation in the ring cavity. Mode-locking was therefore achieved by nonlinear polarization evolution in a cavity using a combination of fiber and bulk optical components.

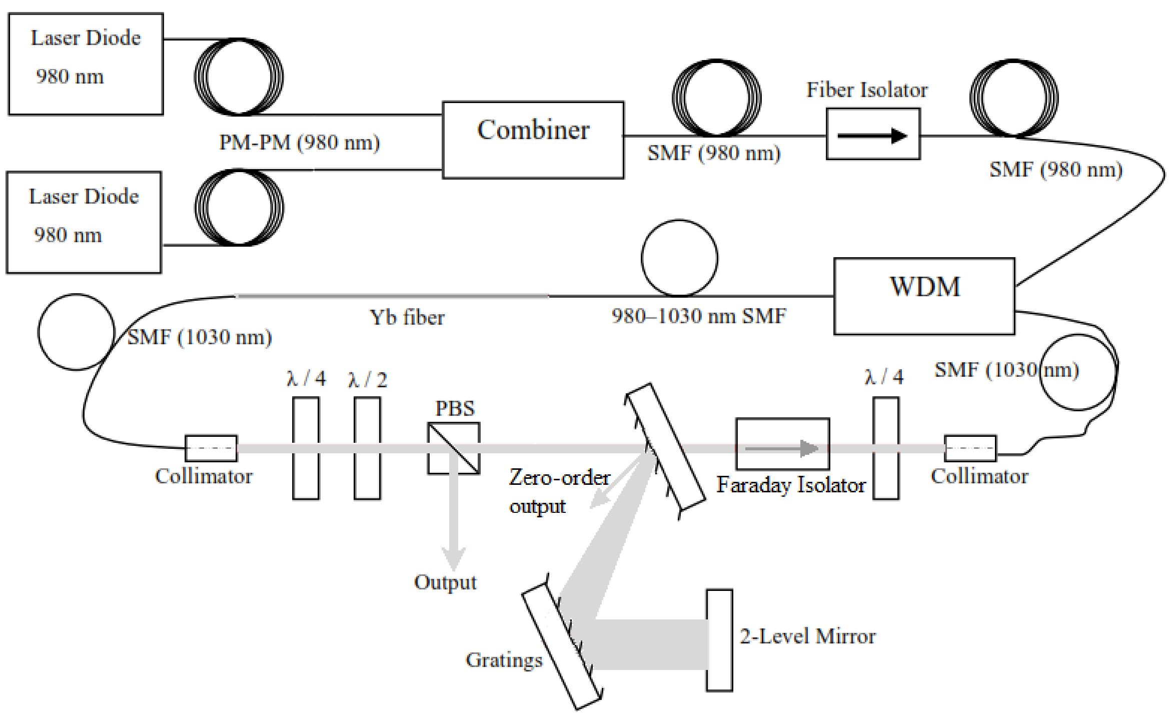

Figure 3-1 Experimental set-up

The output from the PBS is typically put through a 50/50 beamsplitter, where the output is split between an optical spectrum analyzer (OSA) and an autocorrelator to measure the pulse width. A small amount (~1 mW) of light escapes through the 4th interface of the beamsplitter, and this is used as an input to a photo-detector input to a high-speed oscilloscope. The high-speed oscilloscope displays pulses that are broadly spaced (>0.8 ns) in time as the resolution is limited to that of the photodetector (1.2 GHz).

3.3 Investigating causes of multipulsing

This section discusses some parameters that were investigated to determine their effect on pulse energy over a long period of time during which the laser cavity was changed frequently, thus from experiment to experiment some parameters vary. It should be noted that this was not a methodical study of multipulsing, but an investigation of the experimental apparatus at the time and the problem of why the pulse energy was low compared to what was expected based on the literature.

It was observed early on in encountering undesirable multipulsing in the cavity that the pump power had an effect on the amount of multipulsing. Increasing the pump power increases the amount of gain, which in turn increases the nonlinearity, leading to wave-breaking. Multipulsing could be observed on the high-speed oscilloscope or on the autocorrelator depending on the separation of the pulses. It was noticed that multipulsing manifests itself on the oscilloscope as a small pulse following the primary triggering pulse into the detector; however, because the resolution is so low, it is not useful to use only this method as the pulse separation may be lower than the detector resolution, making the pulses indistinguishable from one another.

Turning down the pump power of the 980 nm laser diode pump lasers decreased the temporal separation of the secondary pulse from the primary pulse on the oscilloscope until they were irresolvable. Upon turning down the pump power further, the multiple pulses would appear in better resolution on the autocorrelator. This indicates that the multiple pulses got more closely spaced in time with lower pumping power, or conversely that higher pumping breaks the pulse into multiple pulses that spread apart in the cavity.

The pump power was reduced to get single pulses in experimental work in this thesis. It should be noted that after doing this, the pump power could be increased again before hitting the threshold for multipulsing again; however, this was not performed experimentally because there is no warning before the onset of multipulsing when increasing the pump power. This hysteresis is commonly observed [49] [50]. As the pump power decreases, the intensity of all pulses will decrease until a pulse crosses below the threshold of a certain peak intensity. Then the number of pulses will decrease one by one. At this point the energy per pulse for the remaining pulses increases due to the energy balance, and then the peak powers decrease again with the pump power until another pulse vanishes. This continues until the laser is operating in CW mode after the final pulse crosses below the mode-locking threshold [49].

Turning down the pump power to remove multipulsing is not a true solution to the problem because in the literature higher pump powers are commonly used to achieve highly energetic single pulsing, thus is it only a technique for circumventing multipulsing. Because the threshold power of multipulsing is determined by the cavity design parameters, two possible causes for the low threshold of multipulsing, filtering and back-reflections, are investigated to determine their influence on increasing this threshold value.

3.3.1 Filtering effect

Initial work with the fiber laser was done in effort to compare the available output energy to similar work done in the literature as a baseline for ensuring that the laser cavity was operating at an acceptable level. Komarov et al. noted that multiple pulsing could result from spectrally selective losses in the cavity [49]. This indicated that there may have been elements in the cavity with bandwidths that were attenuating part of the circulating spectrum, causing multipulsing.

After investigating the spectral bandwidth values of the components used in the free space part of the cavity, it was determined that the isolator was the likeliest component that could be causing multipulsing, if the multipulsing was in fact the fault of spectral losses. The isolator, which is used inside the cavity to ensure unidirectional circulation of the light, is placed in the cavity after the PBS and the intracavity diffraction gratings where the light is linearly polarized. The isolator is a Faraday rotator which requires a linear polarization at its input. The central wavelength of the isolator (EOT 1030 – 1080 nm Faraday isolator) could be changed by tuning the transmission axis; tuning the central wavelength shifts the 3 dB bandwidth of 26 nm, effectively changing the allowable bandwidth inside the cavity.

To determine if the spectral bandwidth of the isolator was causing some of the multipulsing problems, the total pulse energy per period vs. GVD was measured for two cases where the isolator was tuned to two settings; setting A has a center wavelength of 1030 nm and setting B has a center wavelength at 1060 nm. The other pertinent laser cavity parameters for this work are that there are 373 cm of linearly acting SMF, 61 cm of the ytterbium-doped gain fiber (*CorActive* Yb214), and 118 cm of the nonlinearly acting SMF. The repetition rate is 30.3 MHz.

The average power at the output port was measured, along with the repetition rate, spectral bandwidth, and dechirped pulse width and the value of anomalous dispersion required to dechirp the pulse. The maximum available pump power of 540 mW was used in all of these measurements; however, multipulsing occurs so the energy calculated is total energy of all pulses in a period, not the energy for a single pulse. The energy is plotted against the GVD below in Figure 3-2; the GVD is tuned by adjusting the separation of the diffraction gratings inside the laser cavity. What can be seen from this is that the isolator with the incorrect central wavelength of 1060 nm, which limits the spectral bandwidth inside the cavity, attenuates the total energy circulating inside the cavity as expected. However, the operation was stable in the 1060 nm case and 1030 nm case, and multipulsing was observed in both cases. The filtering of the spectrum attenuates the average power output by the laser. The cavity is still favouring multipulsing during the process of mode-locking and single pulses are not attainable. The comparison between the two cases is not fair because the number of pulses could not be determined due to the lack of instrumentation. However, it is expected that the number of pulses obtained in the 1030 nm case is lower than that of the 1060 nm case. In this case, the single pulse operation can be tuned by selecting the proper filter.

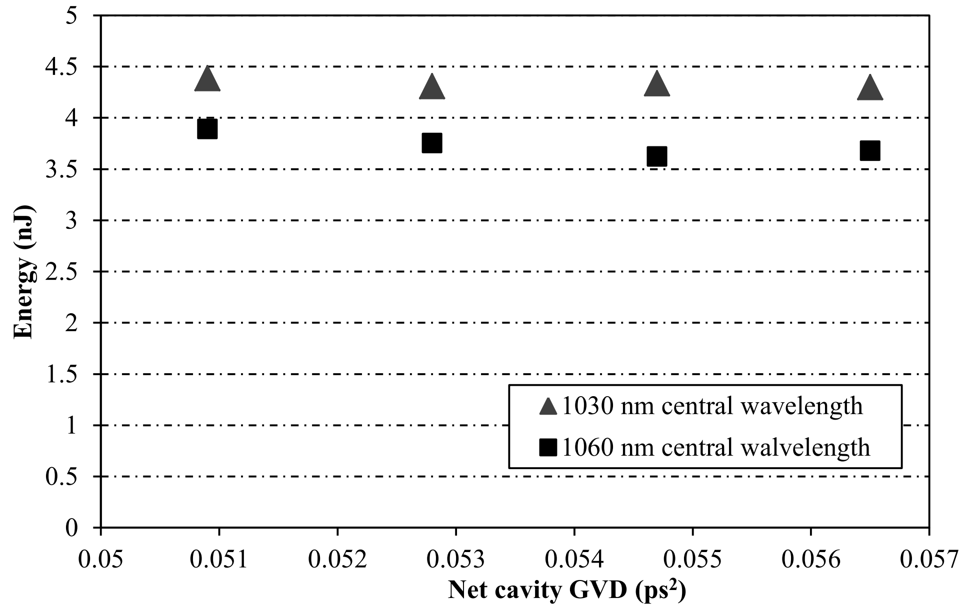

Figure 3-2: Energy vs. GVD with isolator in two different settings

This isolator was compared with a broader bandwidth isolator (IO5-1030HP from OFR with ± 40 nm), both with 1030 nm central wavelengths. These measurements are shown in Figure 3-3. In this case, the length of nonlinear SMF is increased to 135 cm, the linear SMF is 719 cm, and the length of Yb214 is 49 cm. For the results reported in subsequent chapters in this document, the wideband isolator was used inside the cavity since Figure 3-3 shows that causes less attenuation. The EOT 1030 – 1080 nm Faraday isolator is used in the output port to prevent possible back-reflections from destabilizing the pulse.

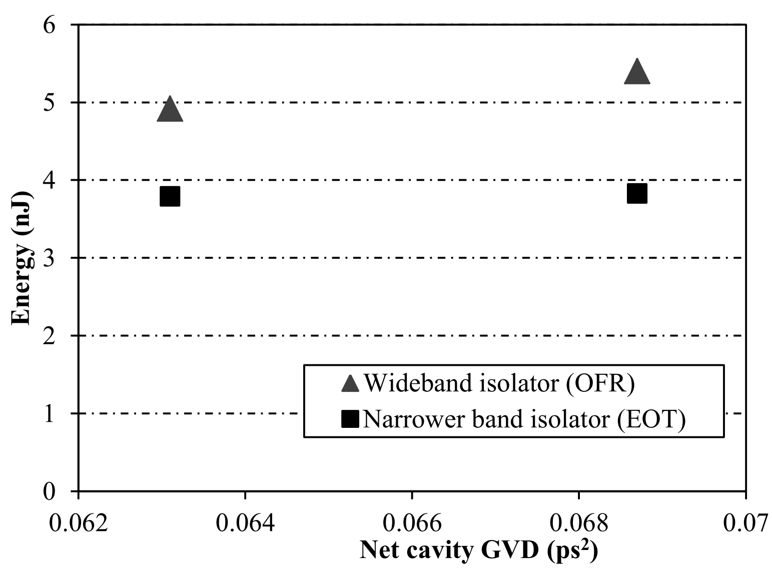

Figure 3-3: Energy vs. GVD for two isolators

3.3.2 Reflections

Reflections in the cavity were investigated as a potential reason for some of the multipulsing observed in the laser. Elements in the cavity (i.e. wave plates) were adjusted at slightly off-normal incident angles to see if their small amount of back-reflection was responsible for causing secondary pulses; however, this exploration did not eliminate any of the multipulsing. Reflections from inside the cavity were not found to contribute to the generation of secondary pulses; however, reflections from the output beam path were responsible for causing some problems to stabilizing the mode-locking.

The tilt of the collimator placed in the output beam path outside the ring cavity to collect light into the spectrum analyzer was found to have an effect on the stability of the mode-locking. Back-reflections into the cavity from this collimator were found to cause occasional disruptions that could collapse the pulses and revert the operating point of the laser to the CW state. Furthermore, the autocorrelator in the output beam path was found to occasionally disturb mode-locking while fine-tuning the mirrors inside of it. While attempting to take measurements of the pulse shape, the process of aligning the autocorrelator would disturb the mode-locking and cause the loss of the desired pulse mode. To combat this, another isolator was put in the output beam path. This isolator was found to improve stability of the mode-locked laser operation but not to reduce any form of multipulsing.

3.4 Special cases of multipulsing: bound and harmonic pulses

One reason for the formation of multiple pulses that has been discussed is that of gain filtering, where a narrow spectrum in the cavity causes multipulsing to be the favoured mode of operation [50]. Another well-known reason that limits the generation of single pulses is that the saturation of the NPE transmission curve [40]. The periodic saturation curve can lead to the break-up of pulses with high pumping power. When the pulse intensity is too high, the threshold of single pulse operation may be crossed, leading to multiple pulses. When there is a constant phase relationship between the pulses, they become bounded and have a fixed temporal spacing in the cavity. In general, commonly observed multiple pulses are randomly spaced in a cavity [40]. In lasers mode-locked with NPE, bound states can be generated by rotating the waveplates used for controlling the polarization [49]. In soliton lasers, the multiple pulses are usually too far apart to interact with one another and become bound, unless the waveplates are adjusted to lock their phases [51]. In solitons these bound pulses result from the interactions between the soliton and the resonant dispersive waves; in stretched pulse lasers, the bound pulses directly overlap when they are stretched in the normal dispersion part of the cavity [40]. In the self-similar regime, the existence of bound pulses has been explained by the existence of a non-vanishing pulse tail that allows for stable binding of highly chirped pulses [41].

Under the right cavity conditions, single pulses can break apart into bound pulses with nearly equidistant spacing in the temporal domain. This type of mode-locking is called harmonic mode-locking and is typically quite stable [40]. The first published harmonic mode-locking in a passively mode-locked ytterbium-doped femtosecond fiber laser was in 2004 [52], but it has not been observed in a similariton laser with self-similar pulses to my knowledge. Changing the orientation of the waveplates can generate harmonic mode-locking by changing the characteristics of the saturable absorber [52], and this technique is what was used to find harmonic mode-locking in this section.

3.4.1 Bound state pulses

Self-similar bound pulses were observed with the experimental set-up in Figure 3-1; bound pulses in this regime have been documented before [41] [40]. In this section, experimentally measured bound pulses are presented as a confirmation that this could be achieved; bound states were rarely observed in mode-locking and two such examples are presented here.

The cavity was set as in Figure 3-1, with 19 cm of ytterbium-doped gain fiber (*Coractive* Yb214), 134 cm of nonlinearly acting SMF, and 387 cm of linear SMF. Bound states in the form of triplet pulses were observed at two values of net cavity GVD in this arrangement (0.0325 ps^2 and 0.0390 ps^2). At maximum pump power, the mode-locking was fairly unstable at most values of GVD and was reduced; for these two values of GVD, bound pulses were found after reducing the pump power. For the first case (0.0325 ps^2) the first laser source was set to its maximum value and the second source was reduced to 383 mA, making the pump power 335 mW (see Appendix A). For the second case (0.0390 ps^2), the second laser source was only reduced to 933 mA, resulting in 498 mW.

The autocorrelation trace of both cases of observed chirped bound pulses are shown in Figure 3-4. Both of these cases show triplet pulses, since the autocorrelation of three pulses results in a pattern of five pulses on the oscilloscope. If the pulses are of equal magnitude, they ratio of magnitudes of the five detected pulses is 1/3:2/3:1:2/3:1/3. In both Figure 3-4 (A) and (B) this ratio is not held, and this indicates that the pulses do not have the same amplitudes.

Using the autocorrelation traces in Figure 3-4 (A) and (B), the separation between adjacent pulses can be gathered from the measured separation of the main autocorrelator peak to both the peaks to one side of the main peak; the distance to either side of the main peak is symmetric due to the nature of the autocorrelation function. From Figure 3-4 (A) the time separation between the adjacent pulses was found to be 35.38 ps and 67.98 ps, and from Figure 3-4 (B), the time between pulses in the triplet is found to be 35.64 ps and 68.51 ps. The separation between the pulses results in interference causing spectral modulation [40]. The spectra for both cases are shown in Figure 3-5 (15.28 nm in (A) and 19.36 nm in (B)), but only in Figure 3-6 which shows the zoomed-in region of the spectral bandwidth is there some evidence of this spectral modulation.

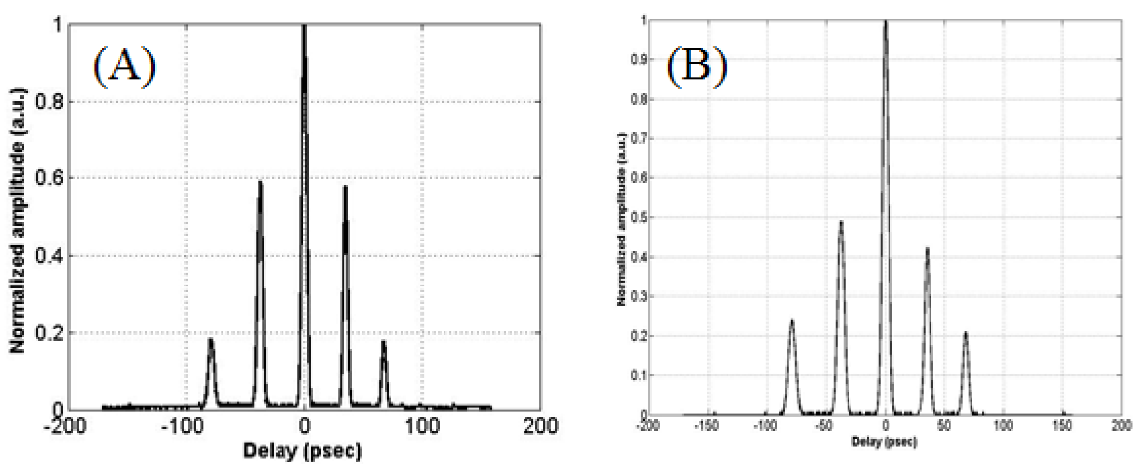

Figure 3-4: Autocorrelation trace of the chirped pulse out of the cavity via the zero order reflection of the intracavity diffraction grating with a net cavity GVD of (A) 0.0325 ps^2, and (B) 0.0390 ps^2

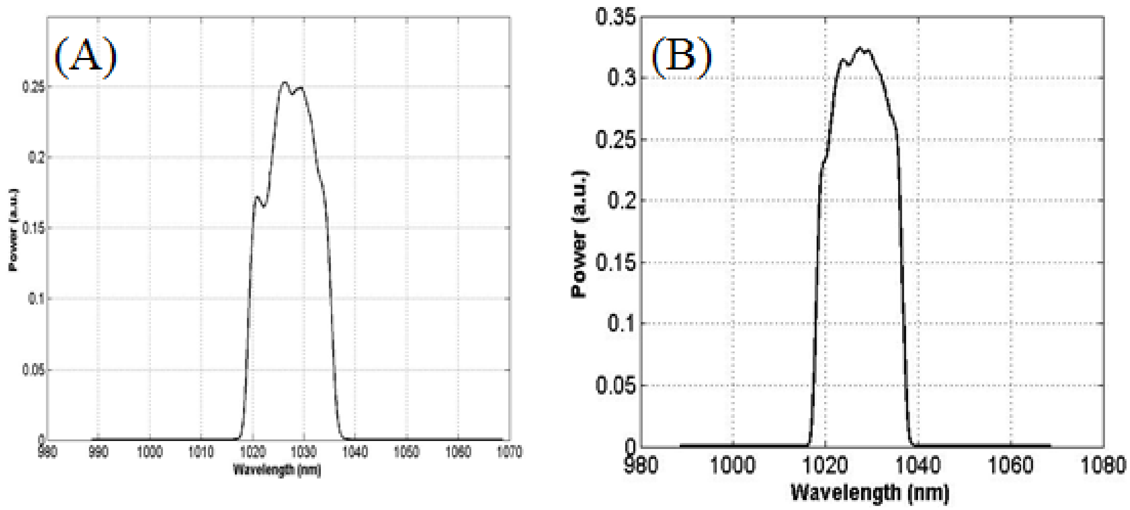

Figure 3-5: Measured bound state output spectrum in arbitrary units at a net cavity GVD of (A) 0.0325 ps^2, and (B) 0.0390 ps^2

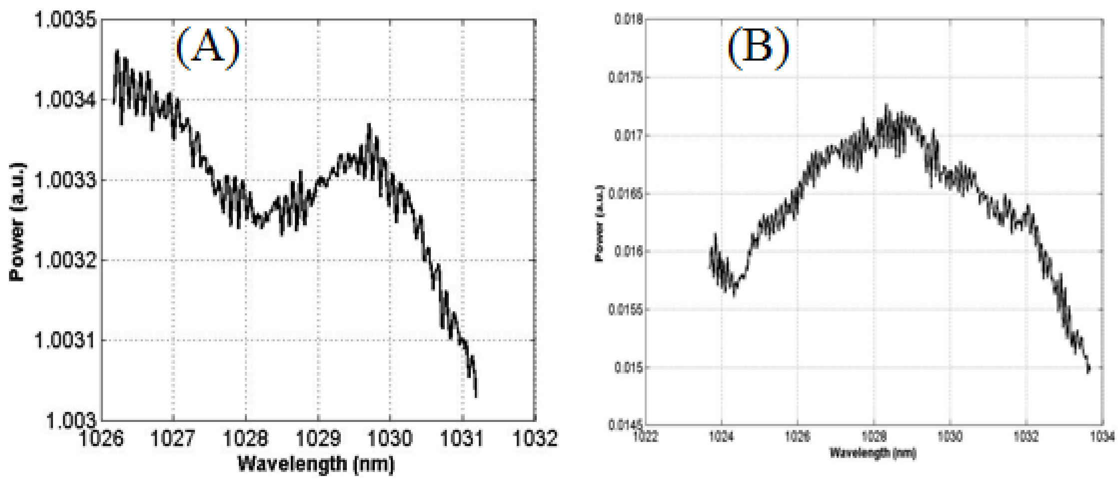

Figure 3-6: Zoomed-in view of bound pulse spectrum at a net cavity GVD of (A) 0.0325 ps^2, and (B) 0.0390 ps^2

The expected interference pattern should have peaks in the range of 0.05 – 0.1 nm; this is found by converting the bandwidth from a time interval (i.e. the pulse separation, or period $\Delta\tau$) to a measure of length using the wavelength λ and the speed of light *c*:

$$\Delta\lambda = \frac{\lambda^2}{c}\frac{1}{\Delta\tau}$$

Eq. 4

Figure 3-6 (A) shows a bit more clearly the alternating of higher and lower intensity fringes that is commonly seen in the spectral domain of triplet pulses [40]. However, since the resolution of the spectrum analyzer is only 0.05 nm, the interference pattern is not sampled enough to be used to interpret anything about the pulses, but instead is simply qualitative confirmation of the expected fringes seen in a bound triplet pulse.

The dechirped pulses after being passed through the compression gratings are shown in Figure 3-7 for both values of GVD, 0.0325 ps^2 for (A) and 0.0390 ps^2 for (B). The dechirped pulse widths for (A) and (B) respectively are 187 fs and 165 fs. The anomalous dispersion values used for compressing the pulses to these minimal pulse widths for both cases were larger in magnitude than the anomalous dispersion values inside the cavity, which is the main identifying factor of a self-similar pulse [40].

Figure 3-8 shows the pulse train of the chirped output pulses (i.e. not compressed pulse train). This trace is done on a high-speed oscilloscope (40 GHz) using a photodetector (1.2 GHz). This was done to ensure there are no other pulses in the period of the laser cavity with separations outside the range of the autocorrelator. This trace confirms that the repetition rate is 30.54 MHz, and that no other pulses are circulating. Figure **3-9** shows a zoomed in version of the impulse from Figure 3-8 for both cases. This was always checked because closely spaced pulses could appear as one in the wider view but upon closer inspection could be resolved.

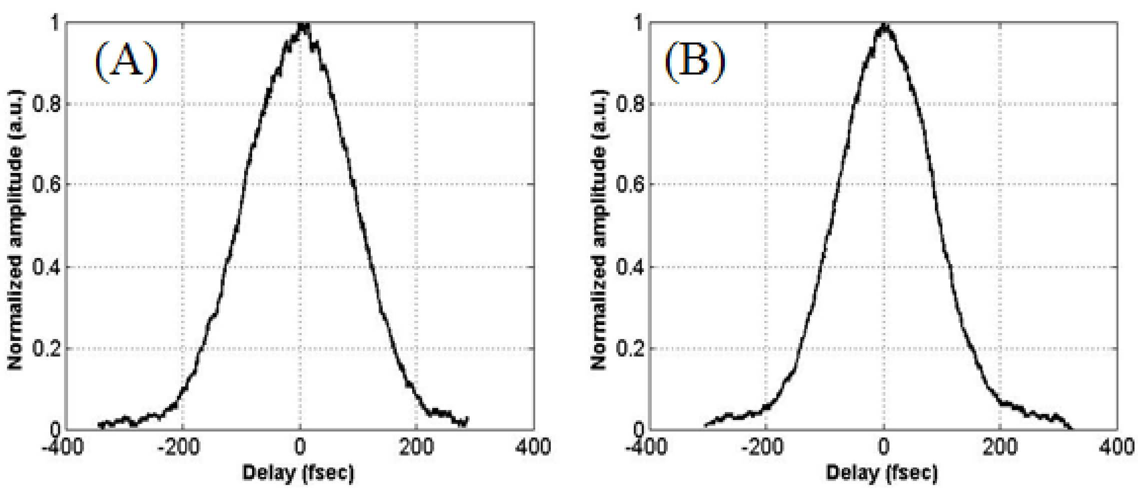

Figure 3-7: Autocorrelator trace of the dechirped pulse exiting the cavity at a net cavity GVD of (A) 0.0325 ps^2, and (B) 0.0390 ps^2

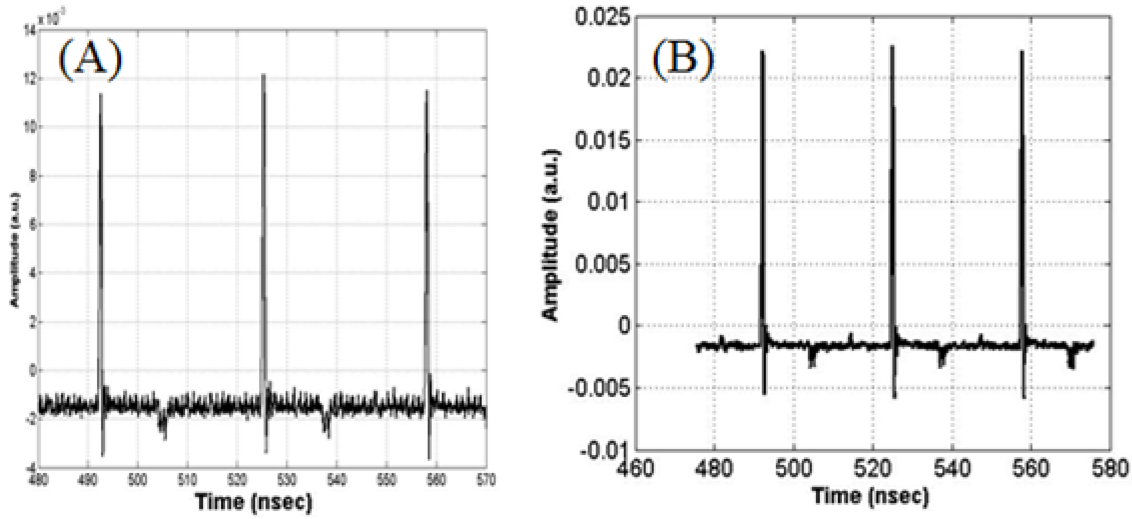

Figure 3-8: Zoomed-out view of pulse waveform to measure the repetition rate for a net cavity GVD of (A) 0.0325 ps^2, and (B) 0.0390 ps^2

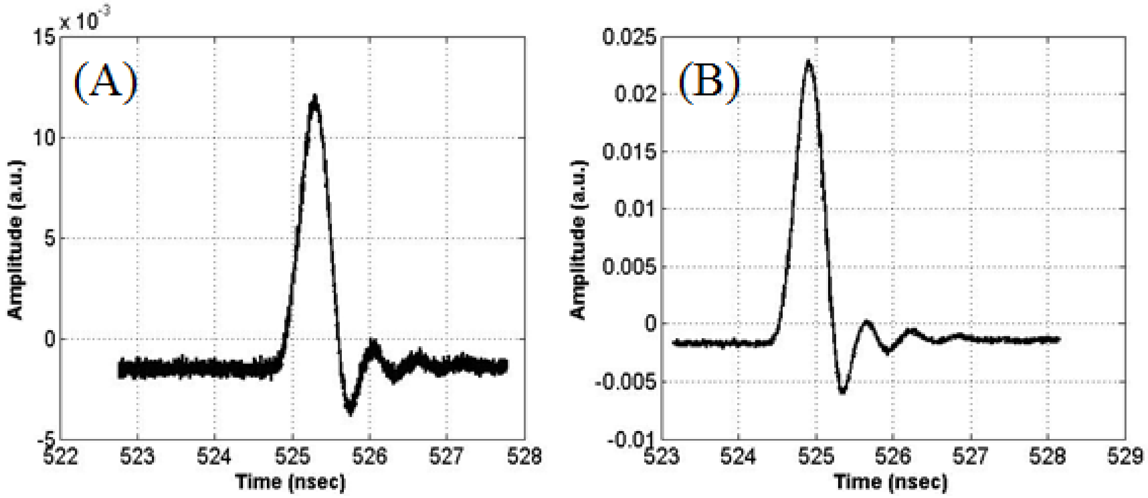

Figure 3-9**: Zoomed-in view of pulse waveform at a net cavity GVD of (A) 0.0325 ps^2, and (B) 0.0390 ps^2**

3.4.2 Harmonic mode-locking

Harmonic bound pulses in a self-similar fiber laser have not been represented in the literature, to the best of my knowledge prior to this work. Herein, a harmonic mode-locking was observed in the self-similar regime. The detected repetition rate in Figure **3-10** (A) was 61.5 MHz measured with the high-speed oscilloscope, which is twice the fundamental frequency for this cavity arrangement of 30.76 MHz. This indicates that this is the second harmonic. The laser cavity included 17.5 cm of Yb214, 385 cm of linear SMF and 134 cm of nonlinearly-acting SMF after the gain segment. The value of net cavity GVD upon observing this rare mode-locking was 0.0316 ps^2. Figure **3-10** (B) shows no secondary pulses in the range of a few ns from the peak. Figure 3-11 shows the radiofrequency spectrum which more clearly shows the frequency detected to be near 60 MHz, and not near the fundamental frequency. The RF spectrum was also used to ensure that of the harmonic mode-locking at the second harmonic frequency was stable.

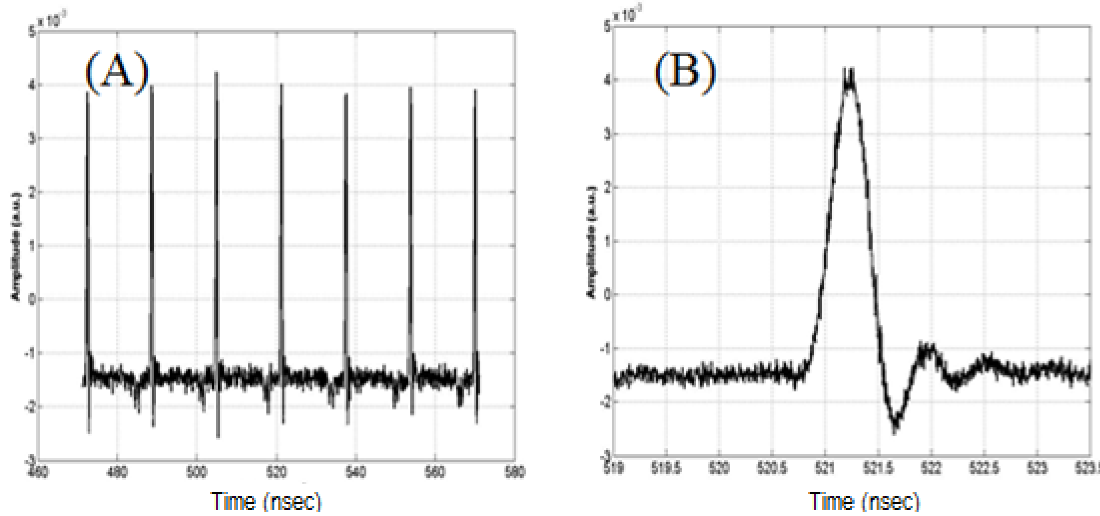

Figure 3-10: Harmonic mode-locked waveform (A) zoomed out and (B) zoomed-in

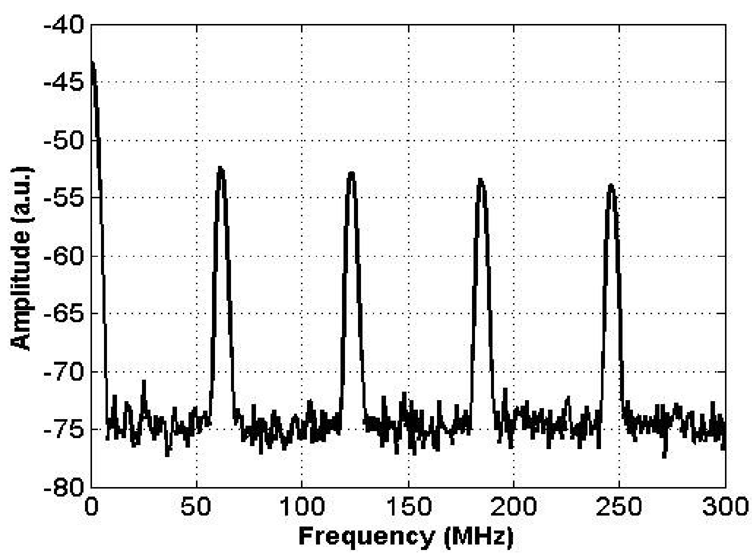

Figure 3-11: Radiofrequency (RF) spectrum of the pulse train

The chirped pulse out of the cavity was measured using an autocorrelator (200 ps scanning range) which produced the intensity profile shown in Figure 3-12 (A). The chirped pulse width was found to be 4.50 ps. Figure 3-12 (B) shows the intensity profile of the compressed pulse after dechirping with diffraction gratings outside the cavity, which has a pulse width of 147 fs. The magnitude of anomalous dispersion from the compression gratings (-0.1702 ps^2) is larger than the anomalous dispersion contribution from the diffraction gratings inside the cavity (-0.1008 ps^2). In combination with the parabolic pulse shape and spectral shape (21.12 nm bandwidth) shown in Figure 3-13, this is a confirmed example of self-similar second harmonic mode-locking.

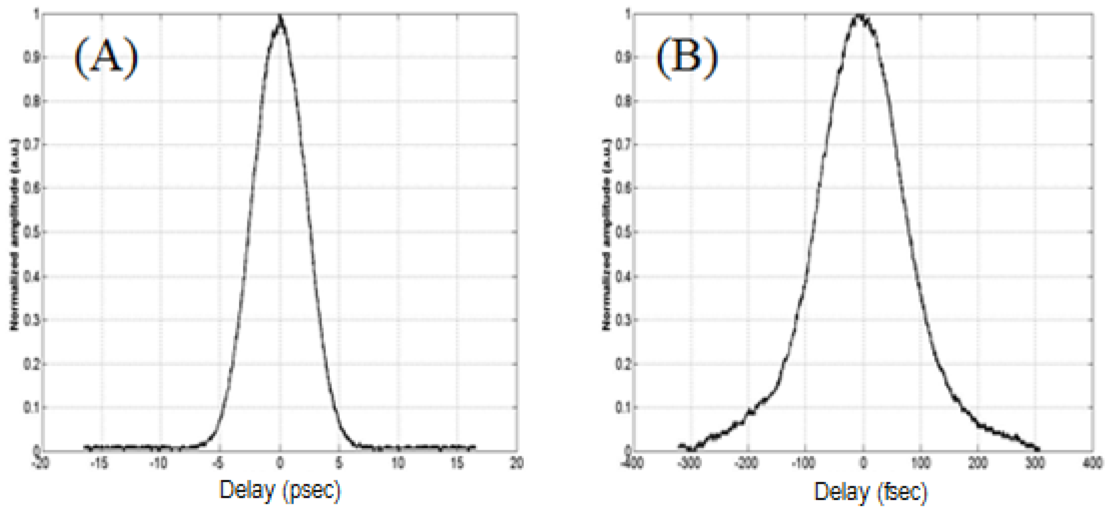

Figure 3-12: Autocorrelation trace of (A) chirped and (B) dechirped pulses out of the cavity

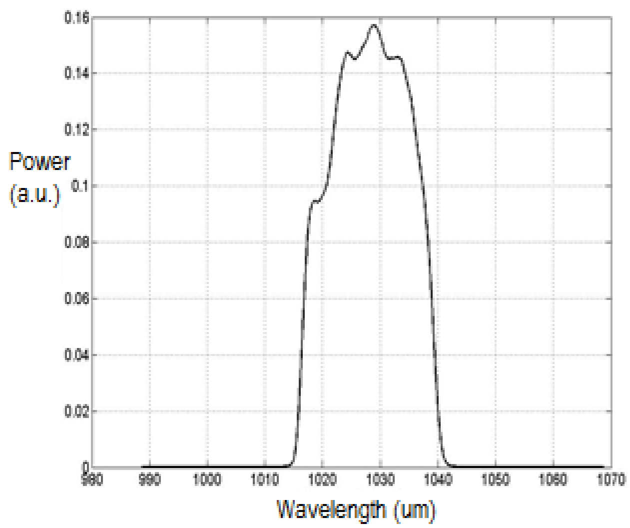

Figure 3-13: Spectrum of harmonically mode-locked pulses

3.5 Conclusion

Multipulsing is an energy-limiting effect that the fiber laser in this experiment suffers from. The threshold power of multipulsing is determined by the parameters of the cavity components. So by the proper engineering of the laser cavity, the multipulsing threshold power can be moved up, as seen in the filtering effect. Multipulsing is an issue that requires further study to be avoided in the fiber laser.

Bound pulses and harmonic mode-locking were observed in the cavity; these are special cases of multipulsing and may be studied further in the future as there is interest in the literature focusing on bound pulses in fiber lasers. Bound pulses benefit from stability but lack the possibility of the high peak powers of single pulse operation. Studying harmonic mode-locking in particular, with more control over the amount of pulses and their separation, can be used to control the repetition rate of the laser, while maintaining the size of the cavity.

Chapter 4 - Dispersion

The initial objective of the work presented in this chapter was to investigate the third order dispersion (TOD) inside the cavity and how it affects the energy and mode-locking in terms of pulse stability. This avenue of exploration was inspired by some early work described in section 4.1 The rest of the work done in this chapter provided interesting and unexpected results related more to the net cavity group velocity dispersion (GVD) than to TOD contributed from the diffraction gratings, which will be pursued further by others in the future. The main finding is that there are two stable pulse regimes of operation for some values of dispersion, an original discovery about which there is little information in the current literature.

Although the second order dispersion term typically dominates dispersion-induced pulse broadening, it is well-known that as it approaches zero, TOD effects become more apparent. Moreover, in pulses of less than 1 ps in duration, TOD cannot be ignored. For example, when it becomes dominant factor, it causes distortions that appear as oscillations in the pulse shape, either in the tail if the TOD parameter β_3 is positive or in the leading edge of the pulse if it is negative [53]. In addition to temporal asymmetry, TOD also causes asymmetry in the spectral profile of the generated pulse [37]. Although TOD is commonly associated with negative effects in solitons, less is known about its effects in stretched-pulse and similariton (self-similar pulse) lasers. For example, it was shown recently that contrary to common belief, TOD could be used to shorten pulse durations in the stretched-pulse regime [54]. Since relatively little is known about TOD effects in passively mode-locked fiber lasers, especially for self-similar pulses, this was the motivation for this investigation, which led to unexpected results.

4.1 Motivation for dispersion investigation

After observing and working with self-similar pulses with Yb214 fiber experimentally in the laser cavity, the next stage was to move toward studying the Yb501 fiber, which has a lower doping, in preparation for comparing the two fibers (shown in Chapter 5). The laser cavity was set up as shown previously in Figure 3-1. The two diffraction gratings inside the cavity with 900 lines/mm were set up parallel to each other such that the light would hit the first one with a 20° incident angle (see Appendix C for the diffraction grating geometry for anomalous dispersion). A long length of Yb501 was spliced into the cavity for the purpose of investigating the effect of the length gain fiber on the pulse energy (as done in Chapter 5). The length of linear SMF in the cavity was 381 cm (SMF1) and the gain fiber was 66.5 cm (Yb501). Initially, self-similar operation could not be found with this cavity arrangement and the length of nonlinear SMF had to be increased from 83 cm to 110 cm (SMF2) to achieve it. When SMF2 is too short, there is an insufficient amount of nonlinear action to get mode-locking with nonlinear polarization evolution (NPE). With the longer length of SMF2, self-similar pulses were achieved, but they suffered from multipulsing. There is typically a compromise between increasing the NPE action to facilitate mode-locking and accumulating excess nonlinear phase-shift causing optical wave-breaking, when playing with SMF2. Some references such as [6] have noted that a minimum of 1 m of SMF after the gain fiber was required for NPE action for their cavity parameters.

With 110 cm of SMF2 and 66.5 cm of Yb501, self-similar pulses were found. The pump power was reduced until a single pulse was observed on the autocorrelator trace of the output pulse (120 ps resolution) and on a high speed oscilloscope (1.2GHz), circulating at the expected repetition rate defined by cavity length. Lowering the pump power shows the maximum energy that a pulse can carry without breaking up into multiple pulses for particular cavity conditions. For example, at one particular value of net cavity GVD that was investigated, the effective energy during multipulsing was 6.8 nJ split up over several pulses in a period; reducing the pump power reduced the energy to 4.8 nJ for a single pulse per period.

High values of net cavity GVD were quite stable for the cavity conditions described; however, lower values of GVD suffered from poor stability and severe multipulsing, causing the energy to drop significantly for single-pulses. This result suggested that the TOD was causing problems at low GVD since it is well known that as GVD approaches zero, higher order dispersion becomes more apparent [54]. I decided to try reducing the TOD by replacing the diffraction gratings inside the cavity from 900 lines/mm to 600 lines/mm (also at a 20° incident angle), knowing that the 600 line/mm gratings have a smaller TOD from equation [26]:

$$\left.\frac{\partial^{3}\phi(\omega)}{\partial\,\omega^{3}}\right|_{\omega=\omega_0}=\left.\frac{\partial^{2}\phi(\omega)}{\partial\,\omega^{2}}\right|_{\omega=\omega_0}\frac{3}{2\pi c}\left[1+\frac{m\lambda_0}{d}\frac{\sin\theta}{(\cos\theta)^2}\right]$$

Eq. 5

In Eq. 5, the third derivative of the frequency-dependent phase-shift represents the TOD, the second order derivative is the GVD, d is the line spacing of the diffraction gratings, m is the diffracted order, λ_0 is the central wavelength and θ is the angle of incidence.

Several data points were measured for the two cases. The 900 line/mm gratings inside the cavity generate a high TOD (β_3=14233 fs^3/mm) and the 600 line/mm case demonstrates a lower TOD (β_3=2925 fs^3/mm). The GVD parameter of the 600 line/mm gratings is -1506 fs^2/mm and requires a larger spacing than the 900 line/mm gratings (β_2 = -4759 fs^2/mm) to achieve the same values of net cavity dispersion. Despite this, the TOD value (i.e. β_3 multiplied by the grating separation) of the 900 line/mm gratings is still larger than for the 600 line/mm gratings when their spacing gives the same net cavity GVD value. It should be noted that the TOD contributed from the fiber is positive, and constant between both cases, so it is not considered in the comparisons of TOD of the diffraction gratings.

The results for the single pulse energy vs. GVD for both of these cases are in Figure 4-1, denoted by the line density of the gratings. There is still another difference between the pairs of diffraction gratings, which is that their efficiency is not the same. The 600 line/mm gratings have more loss and the 900 line/mm gratings are more efficient. The light passes twice through the pair of gratings due to the retroreflector mirror (see Appendix C), so the efficiency of the sets of gratings is the individual grating efficiency to the power of 4. The 600 line/mm set of gratings has a measured efficiency of 23.5%, and the 900 line/mm set of gratings has 29.9% efficiency, which are in the same region and are not expected to influence the results greatly. In fact, contrary to expectations, the lower efficiency (lower TOD) gratings produced higher energy single pulses.

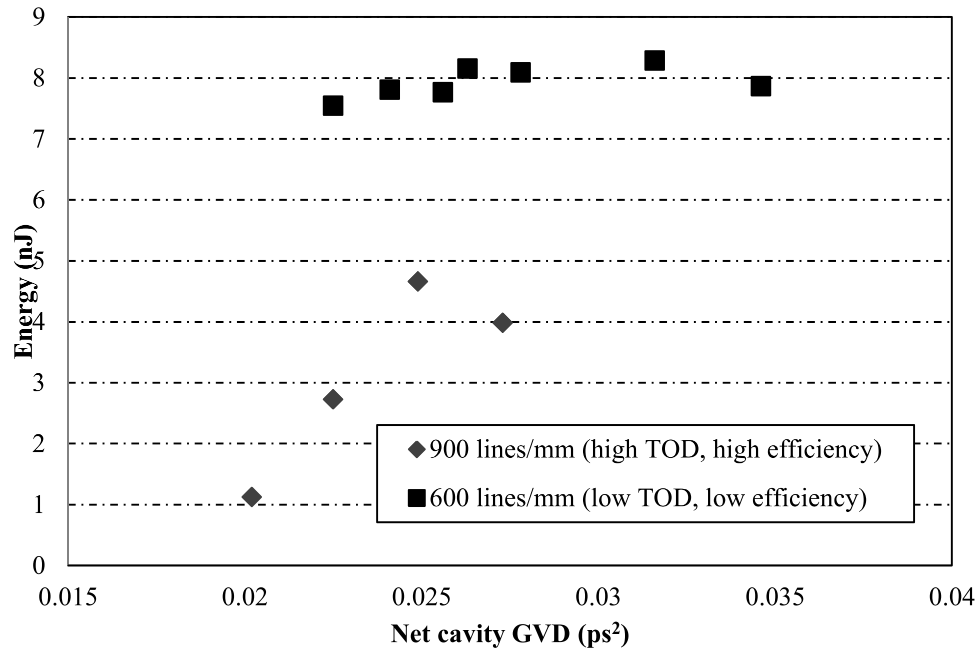

Figure 4-1: Single pulse output energy for two different pairs of gratings in the cavity vs. net cavity GVD

It can be seen in Figure 4-1 that the 600 line/mm (lower efficiency, low TOD) diffraction gratings have a much higher single pulse energy output. The energy was measured for a series of net cavity GVD value, controlled by changing the separation of the anomalous diffraction gratings within the laser cavity. It is important to note that the pump power was maximal for the entire 600 line/mm data set in Figure 4-1, indicating that there was good stability and multipulsing was not a limiting problem; on the contrary for the 900 line/mm case, multipulsing was an issue and for all the data points in Figure 4-1 and the pump power had to be lowered for each to achieve single pulsing. In addition, fewer ripples were observed on the high speed oscilloscope waveform with the low TOD diffraction gratings.

The subsequent measurements were taken with the 600 line/mm gratings tilted so that the incident angle was reduced to 5° degrees from 20°. Decreasing the incident angle to 5° translates to increasing the TOD to β_3= 5343 fs^3/mm. This change results in lowering the net cavity GVD region of stable mode-locking as shown in Figure 4-2. However, multipulsing in the pulses at 2° is observed, so the pump power is lowered to get single pulse results, which are shown alongside the results for the same gratings at 20° in Figure 4-2.

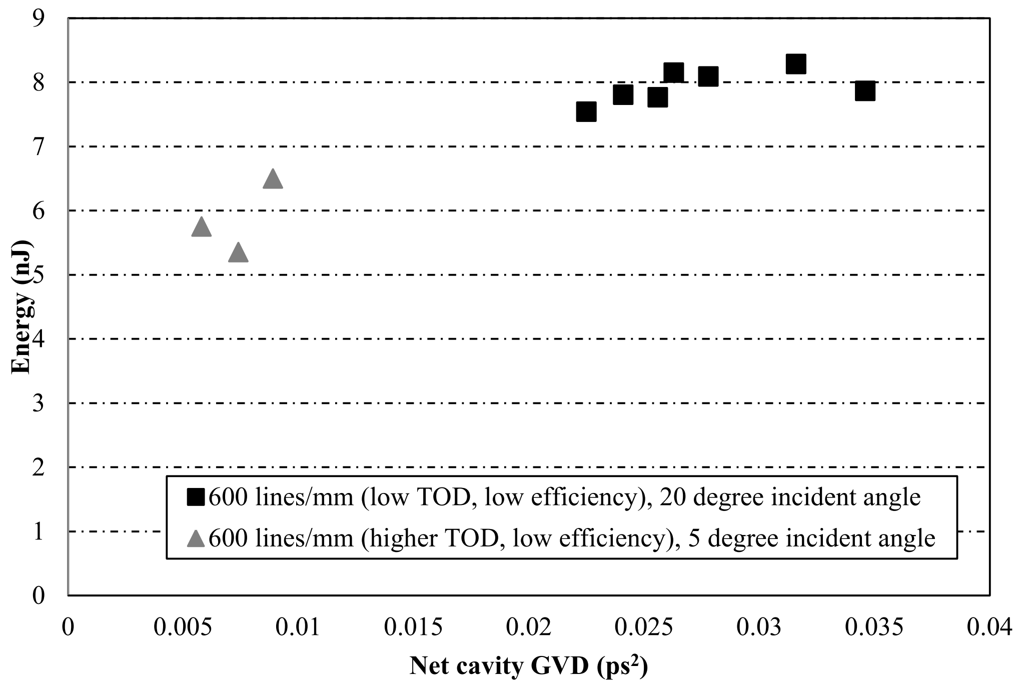

Figure 4-2: Single pulse energy for varying GVD for two different incident angles of the diffraction gratings (note: the 20 degree points are at maximum pump power, and the 5 degree points are at lower pump powers to achieve single pulsing)

It is well-documented that high TOD causes asymmetry in the frequency domain. Experimentally, TOD effects were evident immediately in the spectral shape, agreeing with the sense that it cannot be ignored in this case.

The results in Figure 4-1 and Figure 4-2 suggested that studying the TOD in the cavity would be an interesting route to explore further as the only differences between the various cases investigated are TOD and losses. Intuitively, it does not make sense that a laser with higher losses should have a higher output power, and in this case the losses are reasonably the same, so it is TOD that is the most interesting thing to pursue.

It should be noted that much of this work was preliminary and was done before having access to a high-speed photodetector. It is very likely, in hindsight, that there is multipulsing in the 600 line/mm, 20° angle of incidence case in the ‘dead zone’; extra pulses may not have been visible if their separation was above the resolution of the autocorrelator and below the resolution of the photodetector.

4.2 Experimental design and set-up

Based on the inspiration from the work in section 4.1 it is hypothesized that diffraction gratings used for anomalous dispersion inside the laser cavity with low TOD can give higher energy self-similar single pulses than more power efficient, higher TOD diffraction gratings. Furthermore, it is expected that the TOD will have an effect on the mode-locking ability of the laser because from the preliminary work, the high TOD case had difficulties generating single pulse, resulting in lower pulse energy due to the occurrence of multi-pulsing. This can be interpreted as the low TOD case increasing the threshold at which multipulsing occurs, resulting in higher energy single pulses.

The experiment is designed to compare two identical laser cavities, with the exception of the arrangement of the diffraction gratings used for dispersion compensation, to investigate differences in the pulse characteristics that depend on the diffraction gratings. By taking one set of gratings and changing the angle of incidence, the TOD contribution is effectively changed with negligible change to anything else. The laser is set-up with 16 cm of Yb214, 349 cm of linear SMF and 132 cm of nonlinearly-acting SMF. One set of diffraction gratings with 600 lines/mm is used for both cases studied and only the angle of incidence and separation is changed.

For the first case investigated, the angle of incidence is 20°, resulting in the m = -1 order diffracted beam at 16.02° using the grating equation in Appendix C. This causes the GVD parameter of the gratings to be β_2 = -1506 fs^2/mm and the TOD parameter to be β_3 = 2924.574 fs^3/mm. For the second case, the diffraction gratings were tilted such that the angle of incidence was only 2°, and the m = -1 order diffracted beam is found at 35.67°, generating β_2 = -2108 fs^2/mm and β_3 = 5343 fs^3/mm.

4.3 Yb214 Results

For each case investigated (20° and 2° incident angles), several data points were taken for the fiber lengths used. The grating separation was changed to adjust the net cavity GVD, and the energy recorded is plotted against this cavity parameter. Changing the separation of the diffraction gratings does have an effect on the total TOD contribution of the gratings, so some comparisons between the two cases are done in the TOD domain.

4.3.1 Incident angle of 20°

For each consecutive step of changing the separation of the diffraction gratings set to a 20° incident angle, the waveplates were tuned to try to attain self-similar pulses. At lower GVD values (~10,000 – 25,000 fs^2) self-similar pulses were found. These pulses suffered from multipulsing and required a reduction in pump power to become single pulses. At higher GVD values, a dissipative soliton mode was observed. This is a highly chirped pulse mode [6]. These pulses were high-energy, single pulses which did not require lowering of the pump power. Of most interesting note, as seen in Figure 4-3, there is an overlap in the net cavity GVD region where both of these modes exist, based only on the tuning of the waveplates (i.e. tuning the NPE mode-locking).

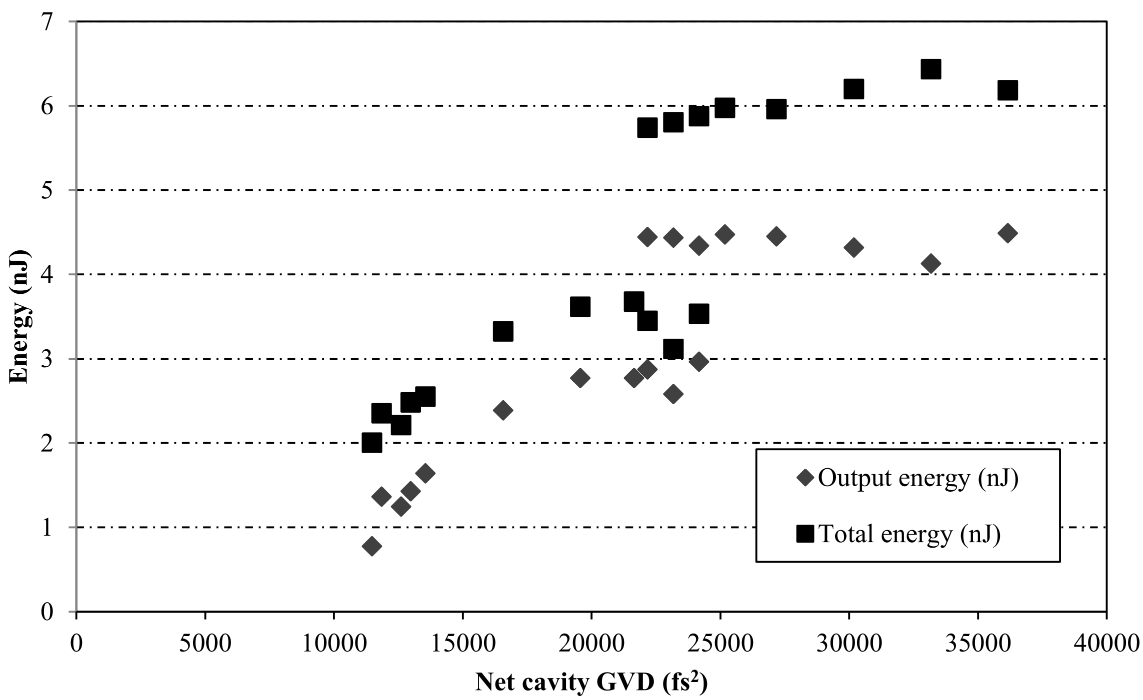

Figure 4-3: Energy for single pulses vs. net cavity GVD

For each value of GVD, the pulse spectrum, the chirped and dechirped (compressed) pulse, the pulse train, the power out of the cavity, the power reflected in the 0^{th}-order beam off the first diffraction gratings, and the repetition rate were recorded. Figure 4-3 shows the output single-pulse energy as well as the total energy of the same pulse circulating inside the cavity against the variable values of net cavity GVD. The increase in self-similar pulse power was expected [17]; however, the observation of a region of overlap with the dissipative soliton mode was not.

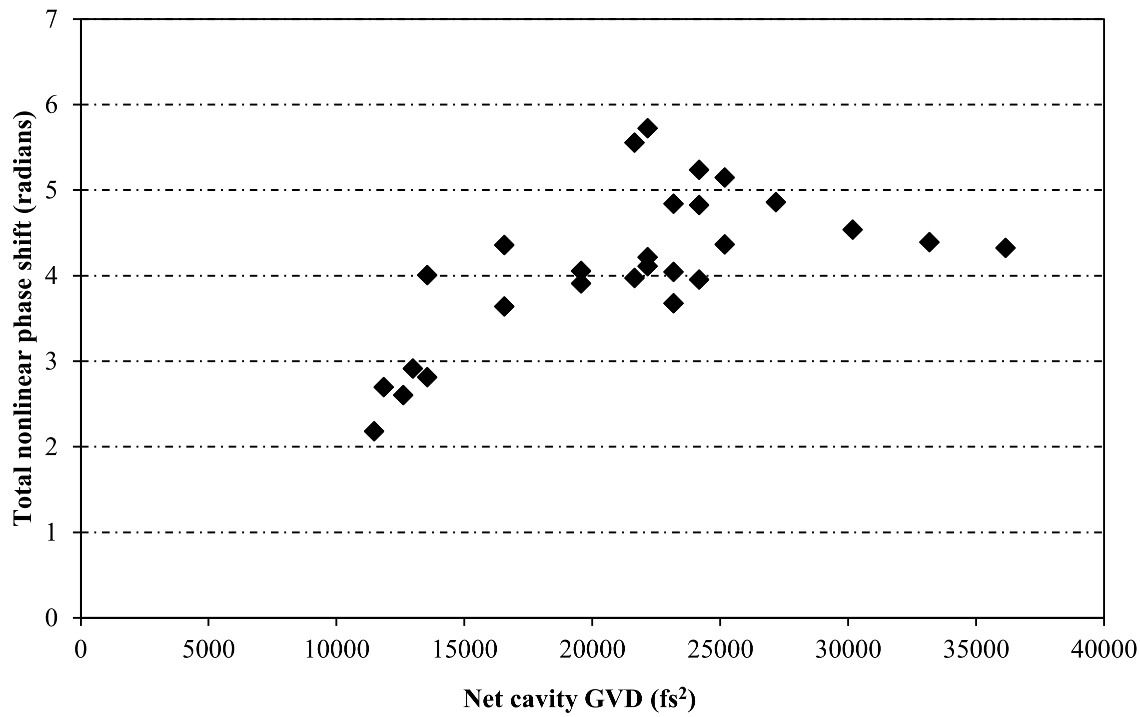

Figure 4-4: Total calculated nonlinear phase shift for each mode-locking

Figure 4-4 shows that as the GVD increases in the region of 10,000 – 25,000 fs^2 responsible for the self-similar pulses, the nonlinear phase shift limit before wave-breaking (and the loss of single pulsing) increases. Conversely, as the net GVD increases in the higher region of the dissipative soliton mode, the nonlinear phase shift decreases (however, it should be noted that this is no longer the limiting nonlinear phase shift since the pulses in the dissipative soliton mode were not limited by pump power).

As mentioned, many of the points in Figure 4-3, and Figure 4-4 were not taken at maximum pump power so as to achieve single pulsing. Only eight points were not limited by pumping power, and those were for the dissipative soliton mode. Another evident difference between the two modes appears in a plot of the anomalous dispersion of the gratings inside the cavity and of the dechirping (compression) gratings outside the cavity versus the total net cavity dispersion as shown in Figure 4-5. The dechirping gratings are set up similarly to the ones inside the cavity; the laser's output beam path enters the set of gratings, and the separation is tuned to achieve the shortest pulse. In Figure 4-5 is the anomalous dispersion needed to generate the shortest pulse plotted against the net GVD of the cavity which generated the pulse is shown. The other set of data in this figure is simply the linear contribution of anomalous dispersion inside the cavity for each GVD value for generating the pulse. It is clear to see that the relationship between the two sets of data changes drastically in the region of the two overlapped pulse modes. For the low-GVD self-similar pulses, the magnitude of the dispersion needed to dechirp the pulse is larger than the contribution from the gratings inside the cavity. The slope then radically steepens in the GVD region responsible for the dissipative soliton mode. This further indicates that this is in fact the highly chirped dissipative soliton regime, as it requires a much larger amount of dechirping to compress the pulse.

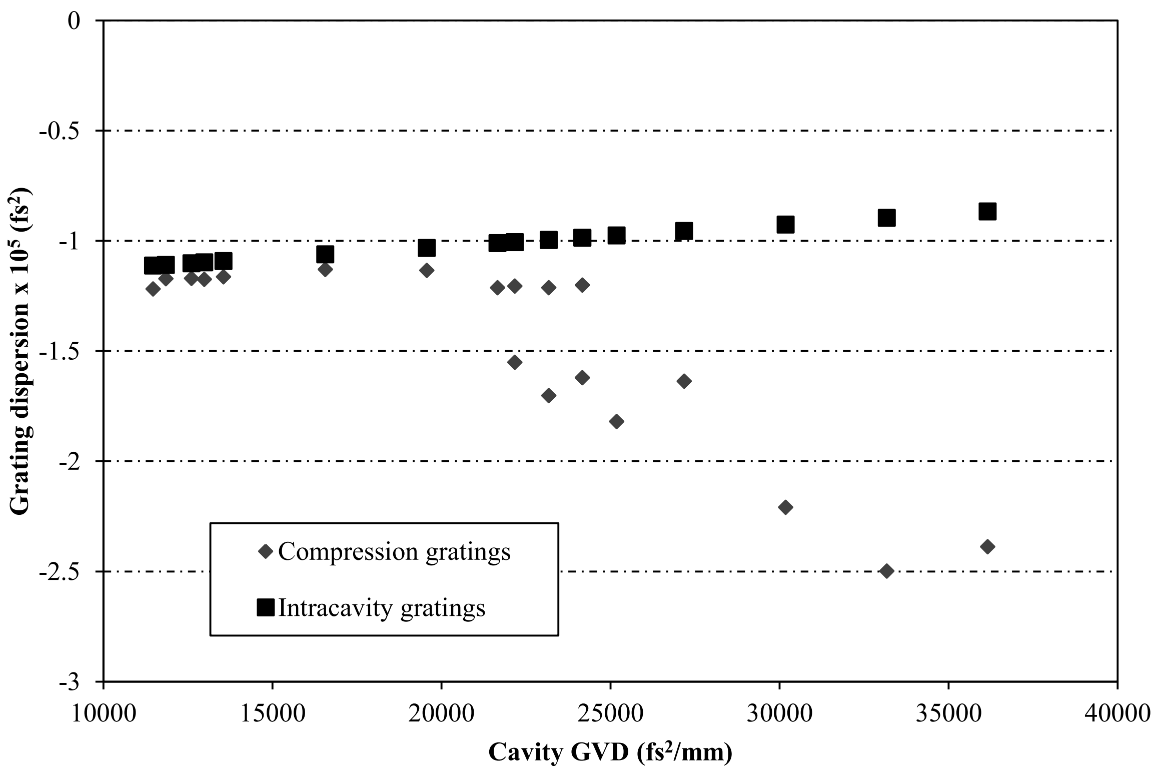

Figure 4-5: Comparison of dispersion contributed from intracavity gratings and dechirping gratings

Furthermore, the difference in pulse modes is evident for each data point taken, not just from the general trend in energy and chirp. The spectral bandwidth for both observed modes is very different. The self-similar pulse is known to have a parabolic pulse shape as seen on the linear scale in Figure 4-6. At the same value of GVD, under the same cavity conditions, except for the bias point of the NPE determined by the angle of the waveplates, the spectrum in Figure 4-7 is found. This spectrum is notably less parabolic and curved in the center.

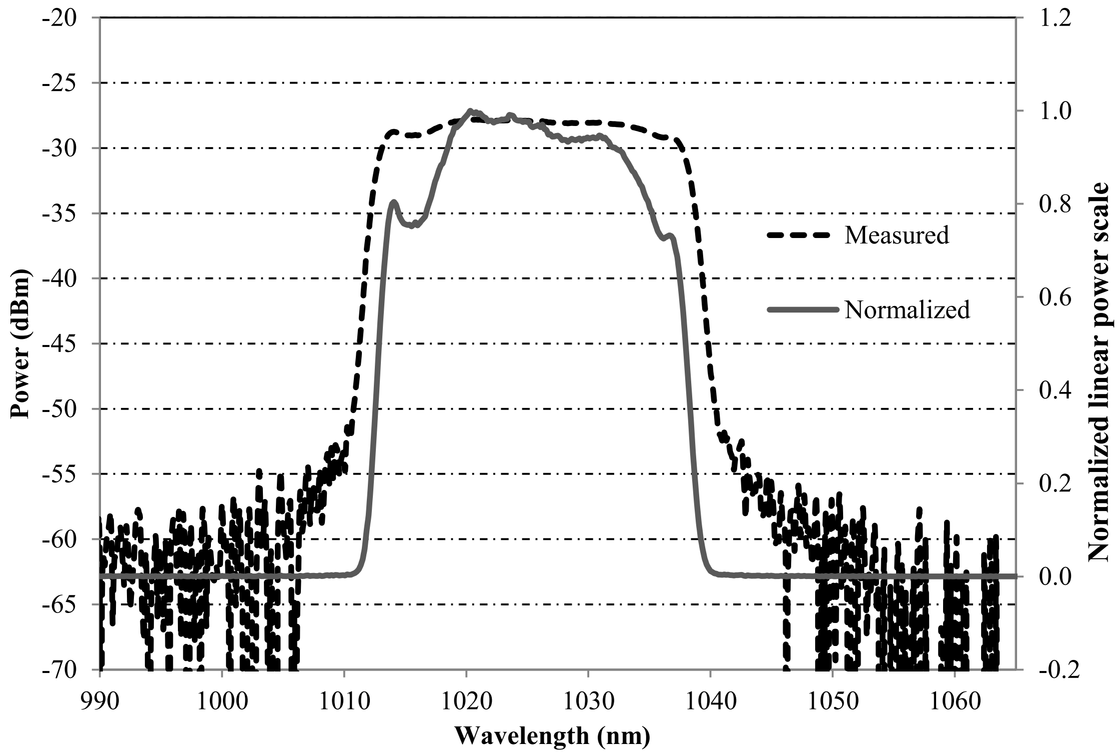

Figure 4-6: Self-similar pulse mode spectral shape at 24000 fs^2 in dBm (measured) and in a linear scale (normalized)

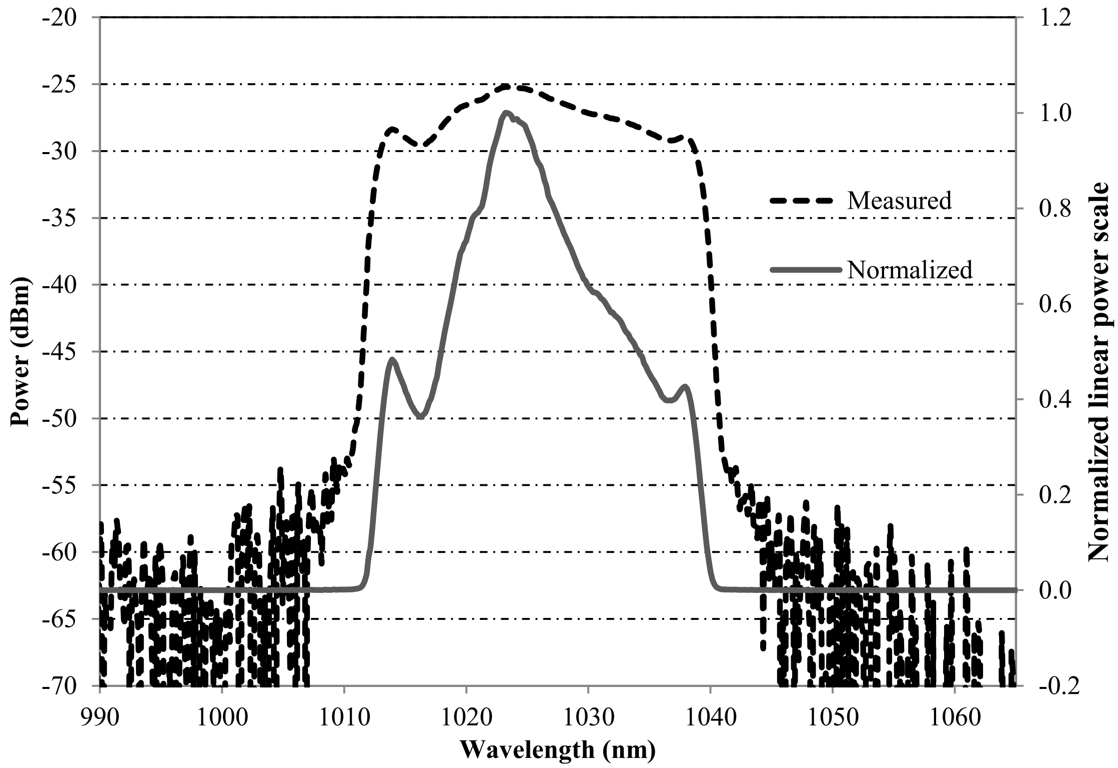

Figure 4-7: Dissipative soliton mode spectral shape at 24000 fs^2 in dBm (measured) and in a linear scale (normalized)

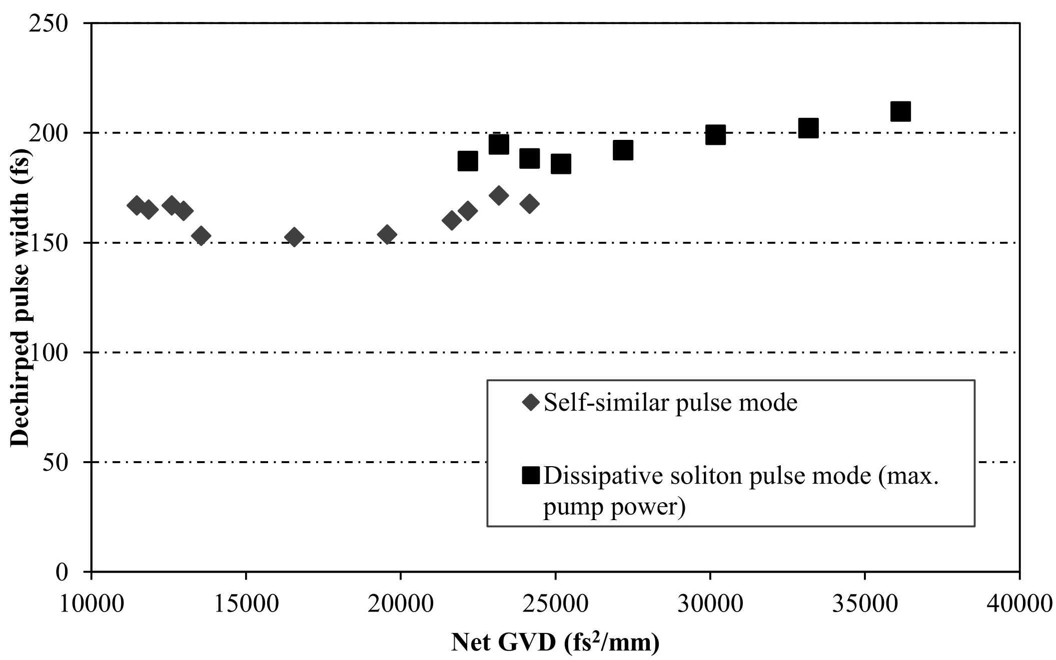

Figure 4-8: Dechirped pulse widths for both observed modes

The dechirped pulse widths for both modes are also different. As shown in Figure 4-8, the dissipative solitons cannot be compressed as much as the self-similar pulses. Both could probably be shortened if the TOD were compensated as well.

4.3.2 Incident angle of 2°

The measurements from section 4.3.1 were repeated for an incident angle of 2° onto the diffraction gratings. Figure 4-9 shows the same trends for the energy of single pulses vs. net cavity GVD. Figure 4-10 shows the total nonlinear phase shift. Figure 4-11 displays the same change in required dispersion compensation for compressing the pulse for the two modes as in the previous section. And, finally Figure 4-12 shows the difference in pulse width for the two modes observed.

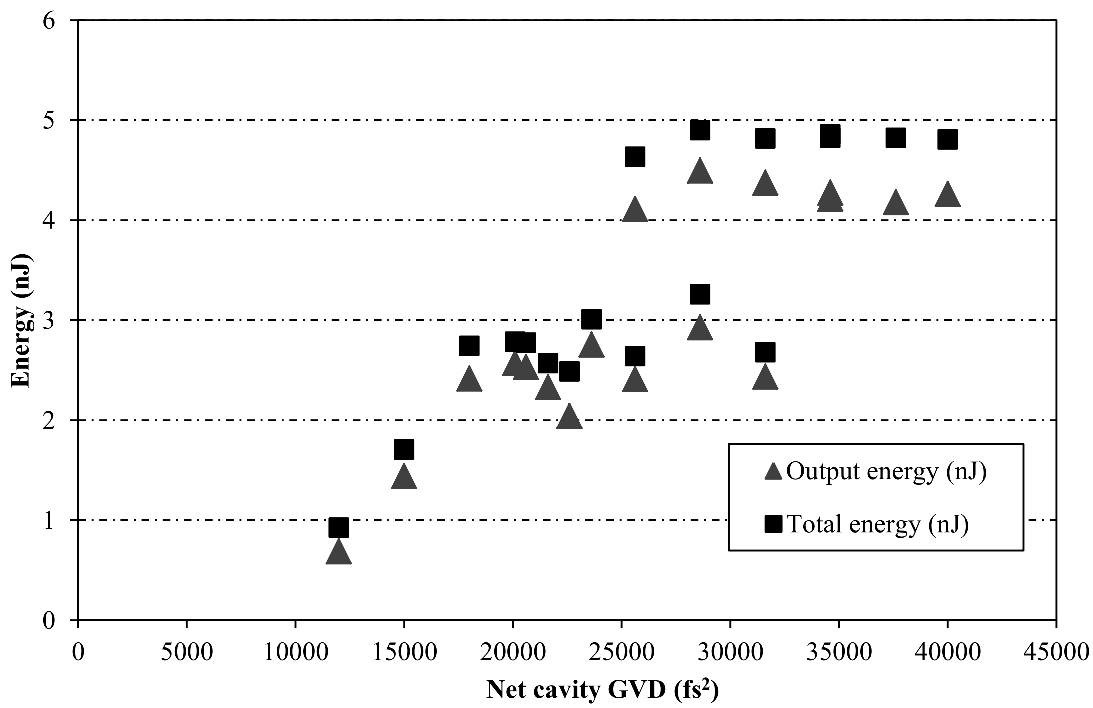

Figure 4-9: Energy for single pulses vs. net cavity GVD

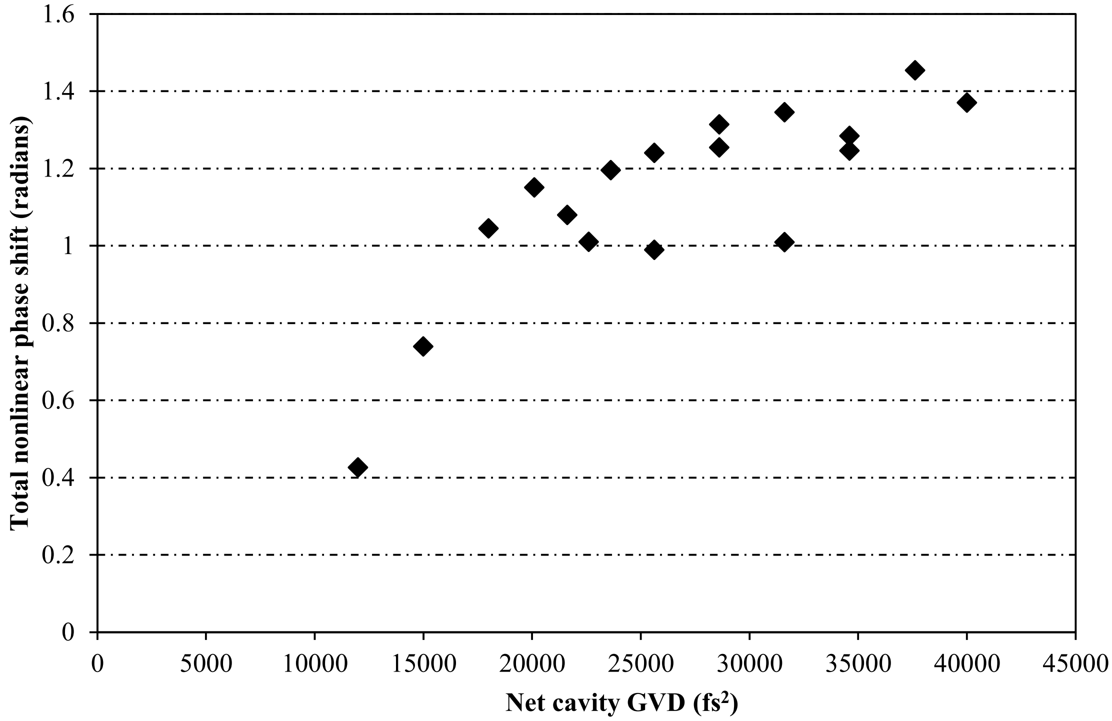

Figure 4-10: Total calculated nonlinear phase shift for each mode-locking

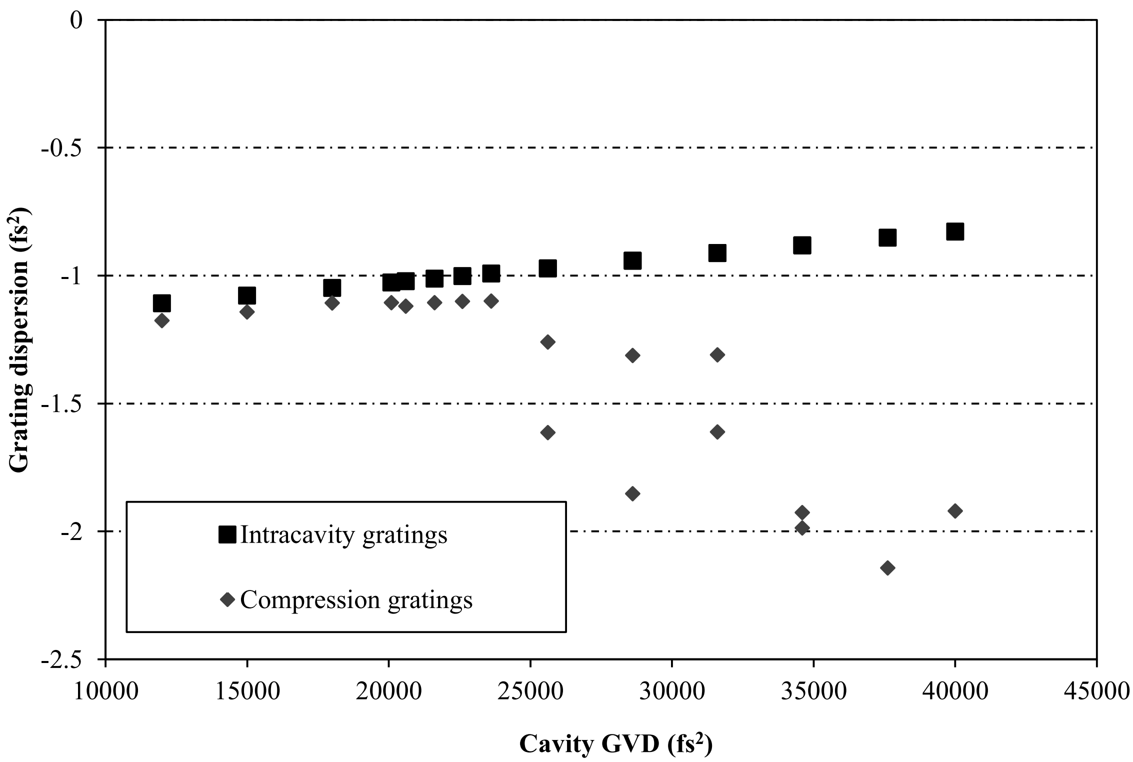

Figure 4-11: Comparison of dispersion contributed from intracavity gratings and dechirping gratings

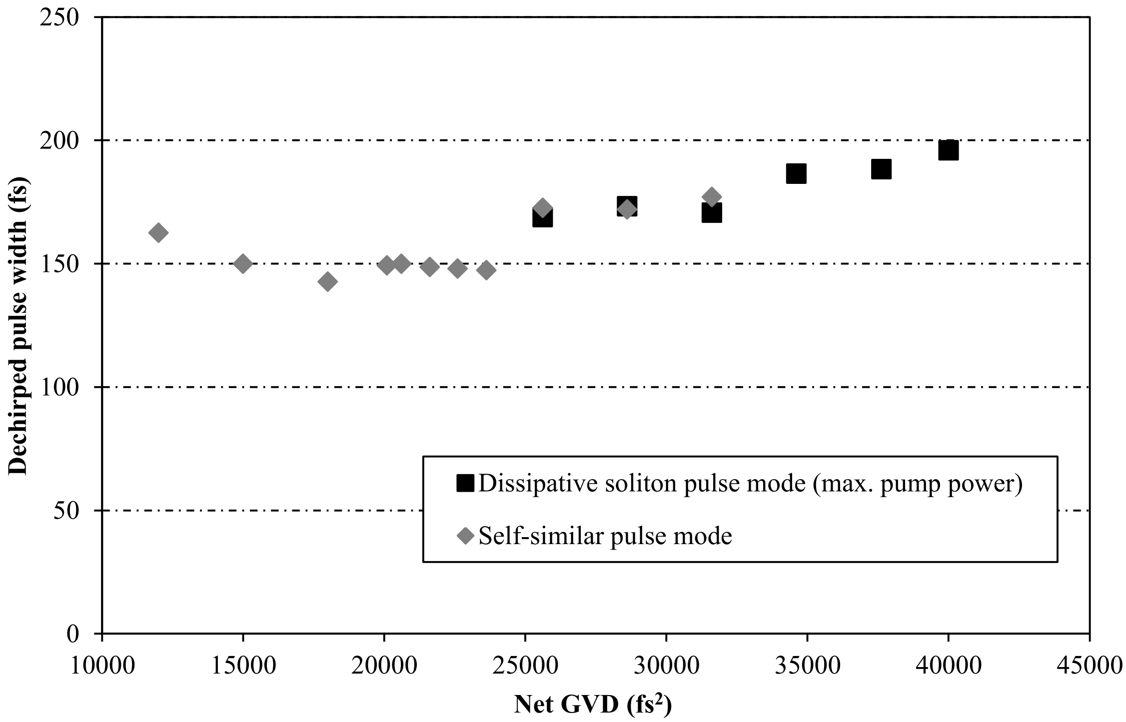

Figure 4-12: Dechirped pulse widths for two modes observed

In Figure 4-12, it should be noted that there is less of a difference in dechirped pulse width in this case than previously in Figure 4-8. With a smaller angle of incidence on the intracavity diffraction gratings, the overlapped region between the two modes has almost the same dechirped pulse width for both modes.

4.3.3 Comparison between 2° and 20° angle of incidence configurations in Yb214

The discovery of the additional dissipative soliton regime was unexpected in this work as it had not been seen in previous experiments. The focus of this thesis is heavily on self-similar pulses, as they are the highest energy pulses that could be mode-locked in most cases. However, data for both modes was measured out of interest and to see how the TOD affects both these regimes as the TOD was the motivation for these measurements. Figure 4-13 plots together the output energy of both cases from Figure 4-3 and Figure 4-9. It is evident that the change in TOD has no discernible effect on the output power measured. This was a truly unexpected result, based on the preliminary work that inspired these measurements. In this figure, the dissipative soliton points are circled.

Figure 4-13 does show that for a 2° incident angle there is a small shift towards higher values of GVD for the stable pulse region for both pulse types. This implies that perhaps a larger TOD can push the operating point to a higher GVD; however, this shift could also be a result of systematic error in calculating the GVD from the measured separation of the diffraction gratings.

Figure 4-14 instead plots the output energy of both trials against the TOD value. Here it can be seen that tilting the grating from 20° to 2° shifted the TOD range to higher values, as expected. Again, the circled data highlights the dissipative soliton mode. The overlapped region of the two modes is larger under the effects of higher TOD.

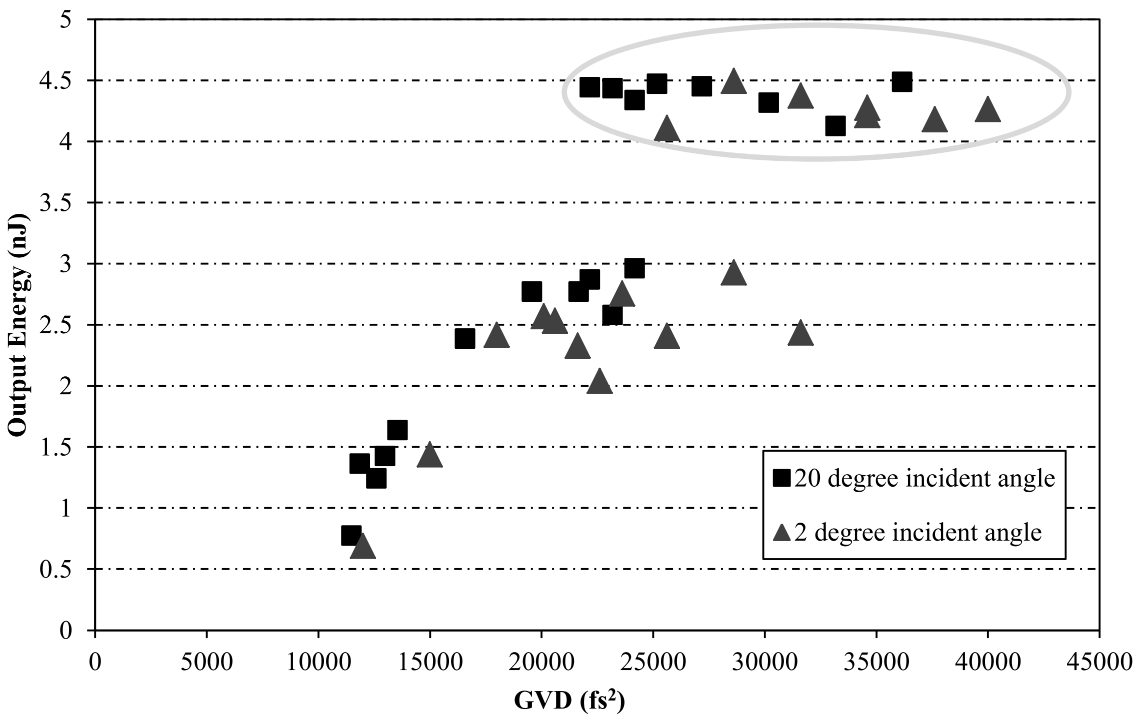

Figure 4-13: Comparing output energy for two different incident angles on the diffraction gratings in the cavity

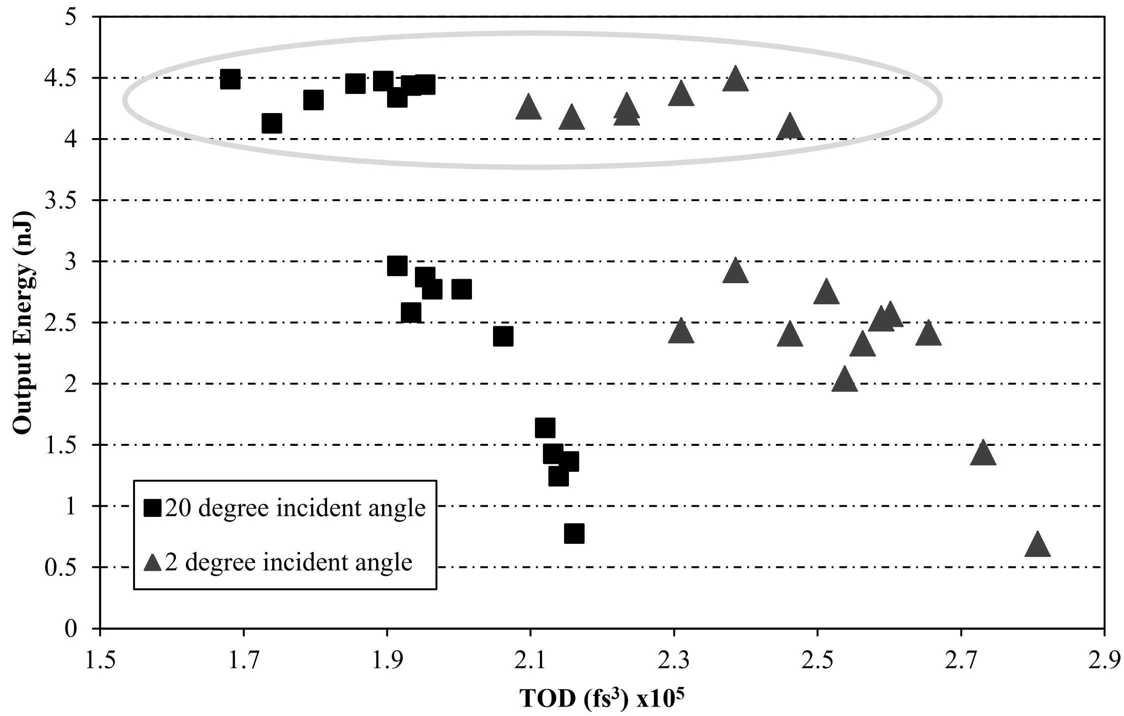

Figure 4-14: Comparing output energy for two different incident angles vs. TOD

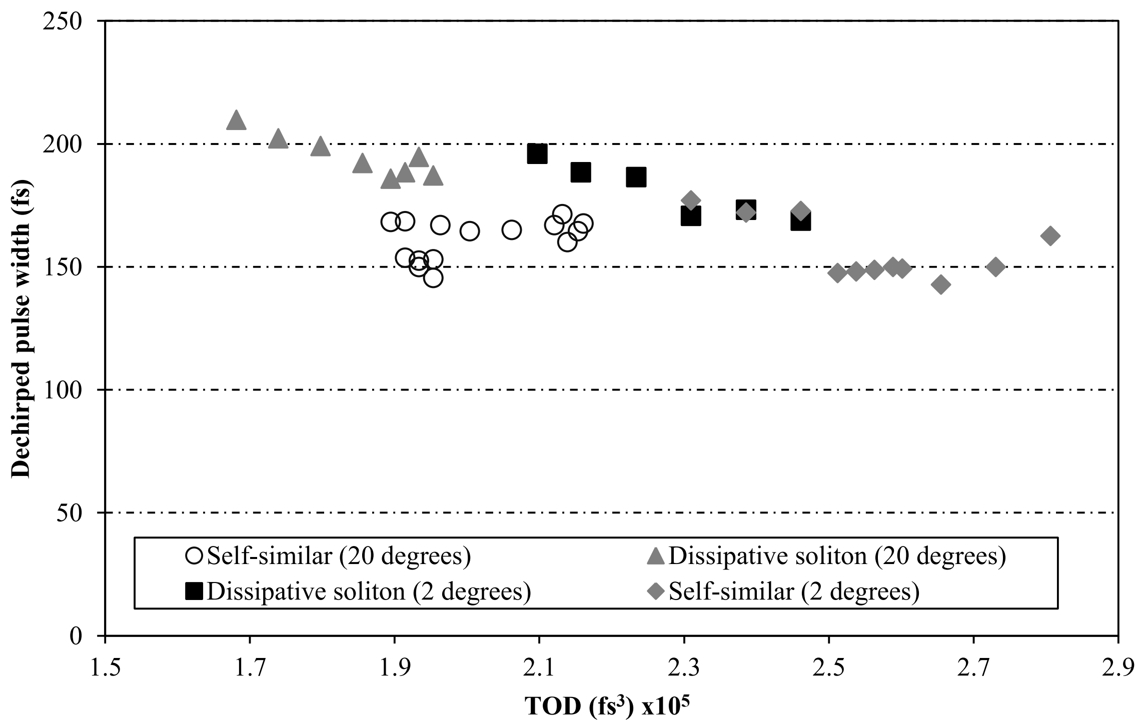

Figure 4-15: Dechirped pulse width vs. TOD

Figure 4-15 shows the dechirped pulse widths both incident angles and both pulse types observed. The narrowest pulses seem to be the self-similar pulses with higher TOD. This is counterintuitive because the accumulated TOD which is known to cause distortion in the pulse shape is not compensated with the pulse-compressor. However, this effect has been demonstrated in the stretched-pulse regime [54], and appears to hold for both of the pulse regimes in this study.

4.3.4 Discussion

There was no improvement in energy from changing tilt of the diffraction gratings, and effectively the TOD. Reasons for the inconsistency between the results and the predictions and expectations are two-fold. Firstly, the results in section 4.1 may have suffered from multi-pulsing since the measurement techniques were not robust enough to detect all multi-pulsing. The electrical channel of the oscilloscope was limited by the bandwidth of the photodetector, so it is possible that the measured single-pulses and their corresponding single-pulse energies were in fact unresolved multiple pulses. Secondly, the work was done with a longer gain fiber, pushing the operating point to a more unstable region due to higher nonlinearity.

The experiment from section 4.1 which motivated the investigation of TOD was repeated using a higher resolution technique of observing multipulsing; the high resolution technique was used for all the other measurements in this chapter. This resulted in having to lower the pump power drastically to achieve single pulsing, indicating that in section 4.1 there was undetected multipulsing. The energy values in Figure 4-1 are therefore not for single pulses. Figure 4-16 shows the results from repeating the experiment done in section 4.1. It can be seen from this figure that there was no impact of the TOD on the energy, indicating that the work that motivated the study of the TOD was misleading.

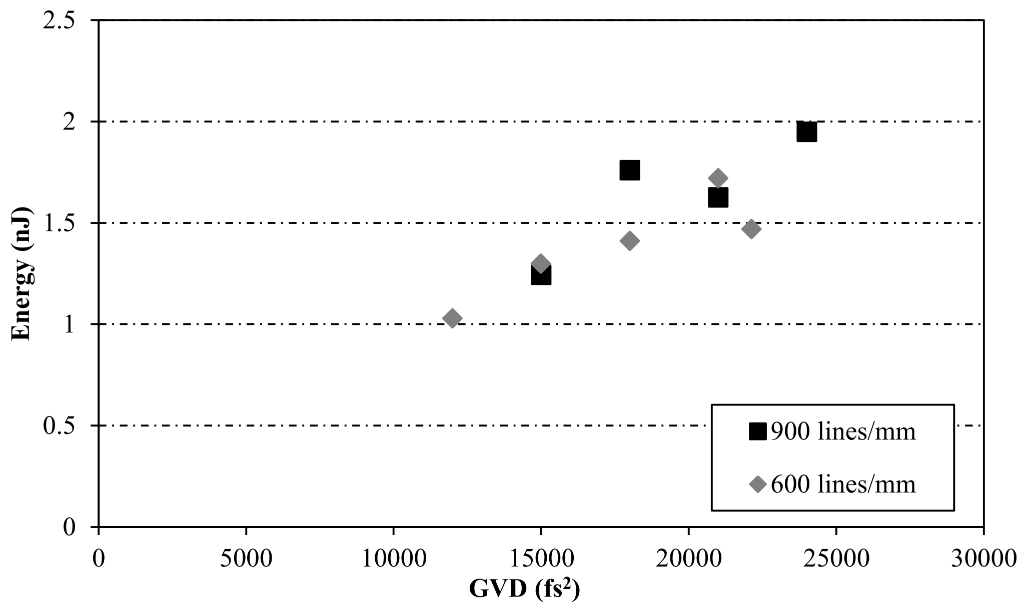

Figure 4-16: Single pulse output energy for two different pairs of gratings in the cavity vs. net cavity GVD, using the optical channel of the high-speed oscilloscope

The results are still useful. Firstly, it is important to know that the TOD contribution at this length is negligible to the pulse energy. This means that gratings with different values of line spacing can be used in the cavity based on what is most convenient for practically setting up given the available space. On the contrary, it becomes challenging to set-up the gratings experimentally when they are very close together, so gratings with a smaller β_2 can be used to increase the separation. The target GVD is typically known, so the value of anomalous dispersion required can be used to determine how far or how close the gratings must be.

The most important result, however, is the overlapped region of the self-similar and dissipative soliton modes. This change in regimes resulted from only changing the angles of the wave plates and nothing else, meaning that the operating points of NPE were shifted. It is believed that the wave plates change the transmittance curve of the NPE mode-locking, allowing for a lower energy regime to exist in part of the region of GVD values that the dissipative soliton pulse mode exists. This to my knowledge has not been observed for these two modes by other researchers. An over-lapped region has been seen in other modes (i.e. stretched pulse and self-similar) at lower GVD values, so it is not completely unexpected that it could be found in this higher GVD region as well [6] [40].

Chapter 5 - Increasing energy with low-doped gain fiber

5.1 Introduction

This chapter discusses the major objective of my studies, which was to show that by using a long length of low-doped ytterbium gain fiber instead of a traditional short length of highly doped gain fiber, more energetic pulses can be achieved out of the cavity. The increase in energy is due to the slower accumulation of the nonlinear phase shift, which limits the energy of the pulse before optical wave-breaking. Experimental results were published [55] and verify that an increase in length of gain medium with a lower doping results in an increase in the output pulse energy. This chapter is based on the results from [55] with additional information on selecting the lengths of fiber that were compared and verifying that the nonlinear phase shift was comparable in both cases that were studied.

This chapter first discusses the theory behind this experiment that led to the hypothesis that a longer length of low-doped gain fiber could generate higher peak power pulses than a short length of a more highly-doped gain fiber. Results from a preliminary experiment are discussed in Appendix D where the results support the hypothesis, but the details are not accurate since the measurement technique at the time could not detect multipulsing. The experiment was repeated in a more robust manner, which is presented in section 5.3 for not only NPE mode-locking, but also for a cavity using a SESAM. Here the experiment was performed with the same fiber lengths as in the preliminary work in Appendix D, and then again for fiber lengths chosen by a different and more accurate set of criteria.

5.2 Theory of method for generating higher energy pulses

Two ytterbium (Yb^{+3}) doped fibers with different doping parameters are selected for comparison in a femtosecond fiber laser cavity where one fiber is highly doped and the other is lightly doped; the ratio between the doping levels of the two fibers is 1.5. The total fiber length is fixed to have constant repetition rate by ensuring that the sum of the ytterbium-doped gain fiber and the subsequent SMF is the same for both cases, which also ensures that the nonlinearity in both cases is comparable. The two fibers were chosen such that their characteristics (such as core diameter, mode field diameter, and core numerical aperture) were all the same except for the doping and absorption (dB/m). All cavity parameters within reason are held constant while comparing the two cases with the exception of the gain fiber parameters previously mentioned and also ratio of gain fiber to SMF in the cavity. The repetition rate, pump power and range of group velocity dispersion (GVD) values of the cavity were all constants between the two sets of measurements.

The basic principle of the experiment is that lowering the doping of the gain fiber will increase the energy per pulse output for an otherwise identical laser cavity by reducing the rate at which the nonlinear phase shift is accumulated. Figure 5-1 shows a simplified depiction of the evolution of the peak power through the Yb^{+3} gain fiber and the nonlinearly-acting SMF that the light passes through after amplification; this figure shows the change in peak power for both a highly-doped gain fiber cavity and a low-doped gain fiber cavity. The short Yb fiber with length *LYb1_HighDoped* has higher gain per unit length, indicated by its slope, than the long Yb fiber with length *LYb2_LowDoped*. The long, low-doped case can reach higher peak powers due to the slower accumulation of nonlinear phase shift. As an approximation, the base area is neglected to simplify the qualitative depiction. The peak power in the cavity is shown to drop off at the PBS in the cavity since that acts as the rejection port.

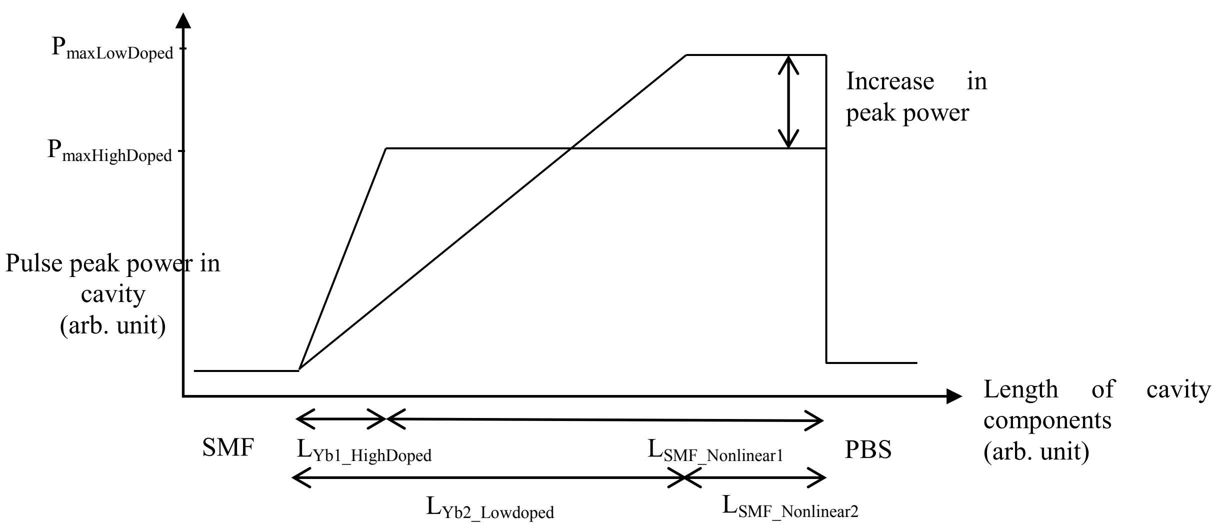

Figure 5-1: Sketch of peak power evolution through the gain and high power regions of the cavity for two cases of varied ytterbium and single mode fibers.

The total nonlinear phase shift must be constant to compare only the rate of accumulation of the nonlinear phase shift resulting from varying the length and doping of the gain fiber; as a result the area under the peak power (P_{peak}) vs. length (L) curve in Figure 5-1 must be the same for both cases for this condition to be met. The integration of both curves in Figure 5-1 must be equal for the two cases given the relationship [18]:

$$\Phi_{\max} = \sum \gamma P_{Peak} L$$

Eq. 6

In Eq. 6, Φ_{max} is the maximum excessive nonlinear phase shift, γ is the nonlinear coefficient, P_{peak} is the peak power and L is the length of each section of the cavity. The limiting factor of the peak power according to this relationship is the maximal nonlinear phase shift, which is equal to the area under the curve in Figure 5-1. By keeping this area constant between two cases and using a lower doped gain fiber with a lower gain per unit length, P_{peak} is allowed to increase further than a higher doped gain fiber while still avoiding optical wave breaking. It is clear from the figure that the peak power for the case of low doped fiber is much higher at the location of the polarization beam splitter in the cavity, which is where the output is coupled. In turn, it is predicted that using lower doped, longer lengths of ytterbium gain fiber will achieve higher energy per pulse outputs for a self-similar femtosecond fiber laser by avoiding the optical wave breaking.

5.3 Experimental work

The preliminary work in Appendix D seemingly proved the hypothesis that a long length of a lower-doped gain fiber is able to provide higher energy per pulse than the more highly-doped gain fiber when mode-locked before the threshold of multi-pulsing. However, my colleagues and I later determined that this work would need to be revised as the data was taken using the electrical channel of the oscilloscope using a photodetector of only 1.2 GHz (similarly to section 4.1) which indicates that it is possible that there was multi-pulsing in all of the data taken. The comparison of the total energy circulating for the low and high doped cases is still valid because the nonlinear phase shift in both cases was comparable, although it is not a rigorous enough to make a statement about the improvement in single pulse energy or peak power. Using the optical channel of the high-speed oscilloscope which has an embedded detector with a bandwidth of 30 GHz the experiment could be repeated, having full confidence that single-pulse data would be recorded.

5.3.1 Experimental procedure

The process of measuring the single pulse energy for various values of net cavity GVD for two differently doped gain fibers was repeated using the standard laser set-up used previously in the rest of this thesis. The comparison of the two fibers was also done using a SESAM for mode-locking instead of NPE. The transmittance curve of NPE is a challenging factor in trying to compare two identical cavities as it changes with the orientation of the wave-plates and can result in changing the maximum attainable energy. Using a SESAM as a saturable absorber avoids the issues resulting from the variable and periodic NPE transmittance curve [16].

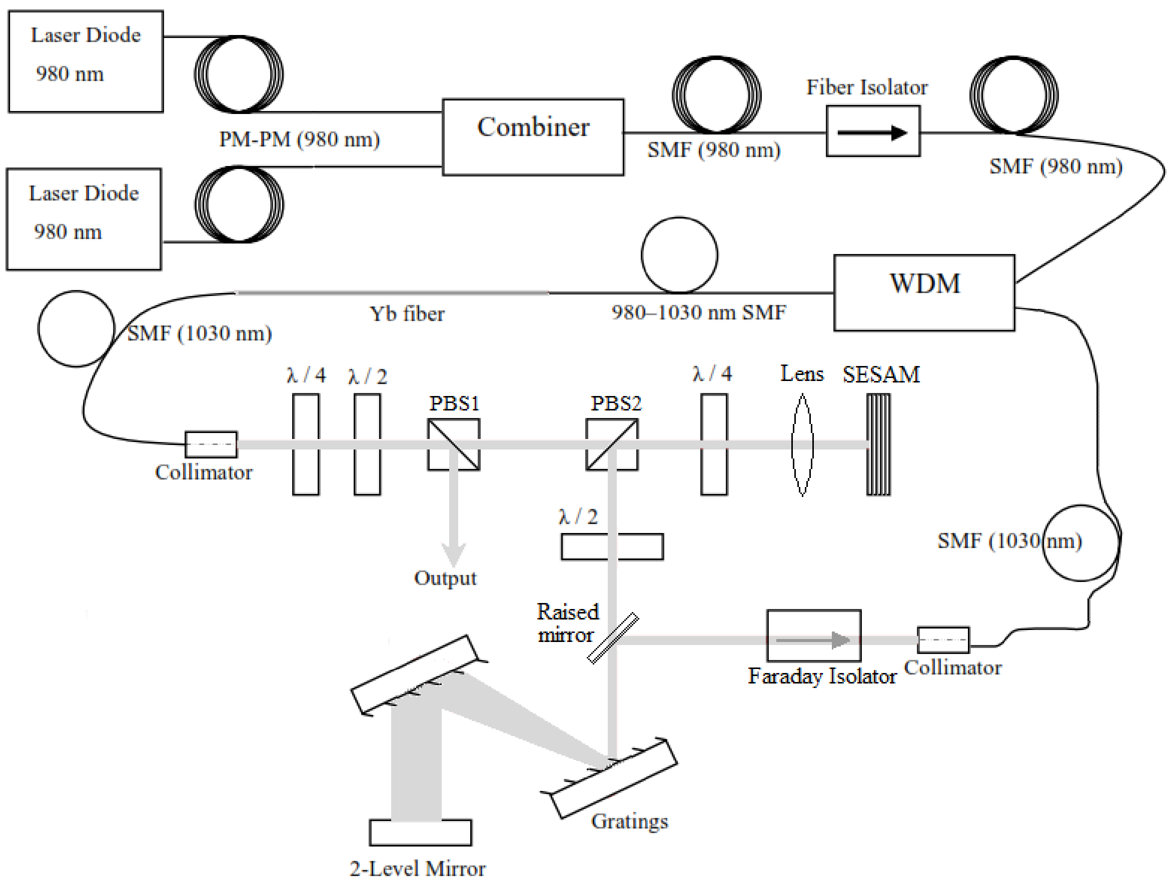

Figure 5-2: Modified set-up for mode-locking with SESAM

Figure 5-2 shows the modified cavity set-up which includes a SESAM (*Batop optoelectronics*, SAM-1040-30-500fs) used for mode-locking. The output beam is taken from PBS1. The half-wave plate between PBS2 and the gratings is to set the polarization into gratings for maximum efficiency of the diffraction gratings. The quarter-wave plate between PBS2 and SESAM acts like a half-wave plate after two passes and effectively acts like a switch in combination with PBS2, which changes the beam path. The half-wave and quarter-wave plates between the collimator and PBS1 add extra degrees of freedom for tuning the mode-locking.

5.3.2 Fiber length criteria: calculating nonlinear phase shift

To make a fair comparison between the two cases with differently doped gain fibers, the nonlinear phase shift must be the same. Experimentally, the nonlinear phase shift was presumed to be the same at the threshold for multipulsing, determined by the value of pumping power. Mode-locking was achieved for the highest pump power at which multipulsing would not occur for both fibers, indicating that the nonlinear phase shift should be equal in both cases, since it is the trigger for multipulsing.

However, the technique used to choose the optimal fiber lengths in the preliminary work from Appendix D is not necessarily valid as it was also skewed by undetected multipulsing. An improved method of determining comparable lengths of highly doped and low doped gain fibers is to calculate the nonlinear phase shift for one case and to use that value to find the length of the other fiber needed to achieve that.

The nonlinear phase shift can be calculated as the area under the curve in Figure 3-1 for both the high and low-doped gain fiber cases. The gain (*g*) cannot truly be approximated linearly as shown in the sketched graph in Figure 3-1. Instead, at low powers an effective small signal length of the gain fiber is defined where the small signal gain e^{gL} can be used instead. The effective small signal length is where e^{gL} is equal to the measured large signal gain. The gain parameters of the fibers used are g_{Yb214} = 41.953= m^{-1} and g_{Yb501} = 20.23 m^{-1}. The nonlinear parameter γ for the ytterbium used is 4.7 km^{-1} W^{-1}.

The total nonlinear phase shift can be calculated as the sum of the contributions from each segment. The only segments that contribute non-trivially to the nonlinear phase shift are the gain fiber and the length of SMF following it:

$$\Phi_{NL} = \Phi_{Yb} + \Phi_{SMF_{NL}}$$

Eq. 7

The nonlinear phase shift contribution of the nonlinear segment of SMF (length L_2) is simply derived from Eq. 6 :

$$\Phi_{SMF_{NL}} = \gamma P_2 L_2$$

Eq. 8

L_1 and L_2 are the lengths of the segments of gain fiber and nonlinearly-acting SMF, respectively, and P_1 and P_2 are the peak power leaving each corresponding segment. The large signal gain is approximated by measuring the total output power and dividing by the power inside the cavity factored by the known losses of bulk components following it (i.e. diffraction gratings, isolator losses).

For the length of ytterbium-doped gain fiber, only a part of the fiber undergoes gain. To find the area under the curve of the small signal length, the integral is taken over the length of the fiber:

$$P_1 = P_{in} e^{gL}$$

$$Area = P_{in} \int_0^{L_{SS}} e^{gL} dL$$

$$= P_{in} \frac{e^{gL_{SS}} - 1}{g}$$

$$\approx \frac{P_1}{g}$$

The gain fiber segment must be split into small signal and large signal components. So adding the small signal gain section to the rest of the fiber (length L_1- L_{SS}), the nonlinear phase shift for the entire length of ytterbium-doped fiber can be expressed roughly as:

$$\Phi_{Yb} = \gamma P_1 (L_1 - L_{SS}) + P_1/g$$

Eq. 9

For both the low-doped and highly-doped cases in this section, the fiber lengths used in the preliminary work is repeated (section Appendix D) to be able to compare then directly to see if the masked multipulsing inflated the observed energy values. Then the nonlinear phase shift for the highly-doped case was calculated and the length of low-doped fiber and SMF needed to match the nonlinear phase shift was determined by a PhD student. These new lengths were used to repeat the measurements (section 5.3) such that the two cavity arrangements could indeed be compared.

5.3.3 Results with preliminary lengths of fibers

Using the lengths of fiber determined in section Appendix B, measurements were taken with both types of gain fiber for both the NPE mode-locking cavity and the SESAM cavity to see if the results from work in Appendix D hold true. These measurements included pulse width, spectral width, output power, repetition rate for single-pulse operation, as before.

For the highly-doped case (Yb214), the length of gain fiber was 25.5 cm and the length of nonlinearly acting SMF was 143.5 cm. The repetition rate was 32 MHz. For all the measurements, the pump power was reduced to attain single-pulsing. For the low-doped case (Yb501), the length of gain fiber was 97.5 cm, and the length of nonlinearly acting SMF was 71 cm, such that the repetition rate was also 32 MHz.

The single pulse energy vs. net cavity GVD using NPE mode-locking is shown in Figure 5-3. Although the output energy is larger for the low-doped fiber, the downward trend is concerning. At higher values of GVD, mode-locking the low-doped fiber was not possible, so it is unclear if the trend reverses. The corresponding peak power for single pulses circulating the cavity is shown in Figure 5-4. It is presumed that the NPE masks higher GVD values and causes the negative slope of the low-doped fiber results in Figure 5-3.

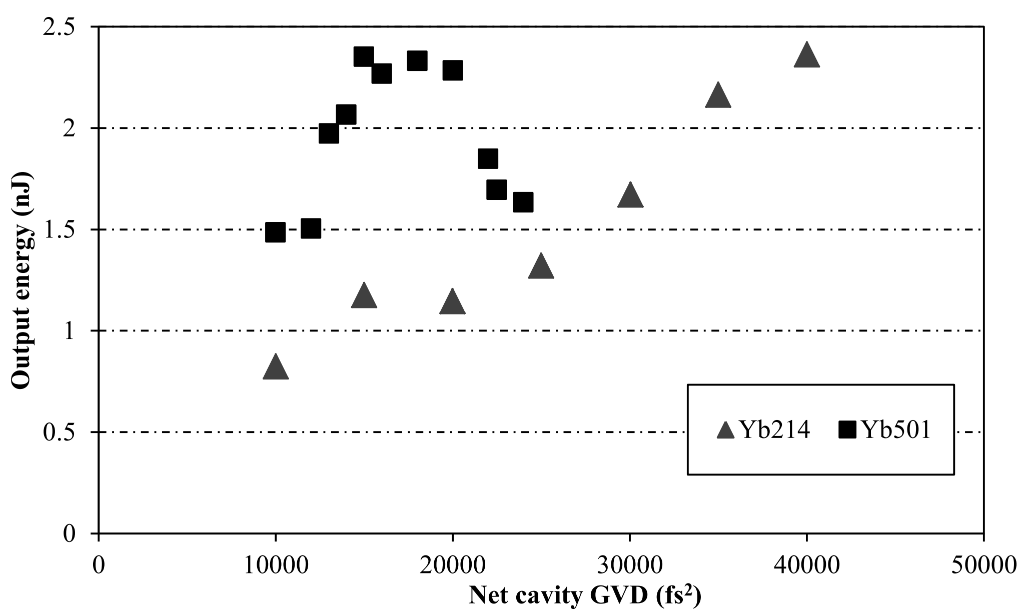

Figure 5-3: Comparison of output energy using NPE mode-locking, with 97.5 cm Yb501 (71 cm nonlinear SMF), and 25.5 cm Yb214 (143.5 cm nonlinear SMF)

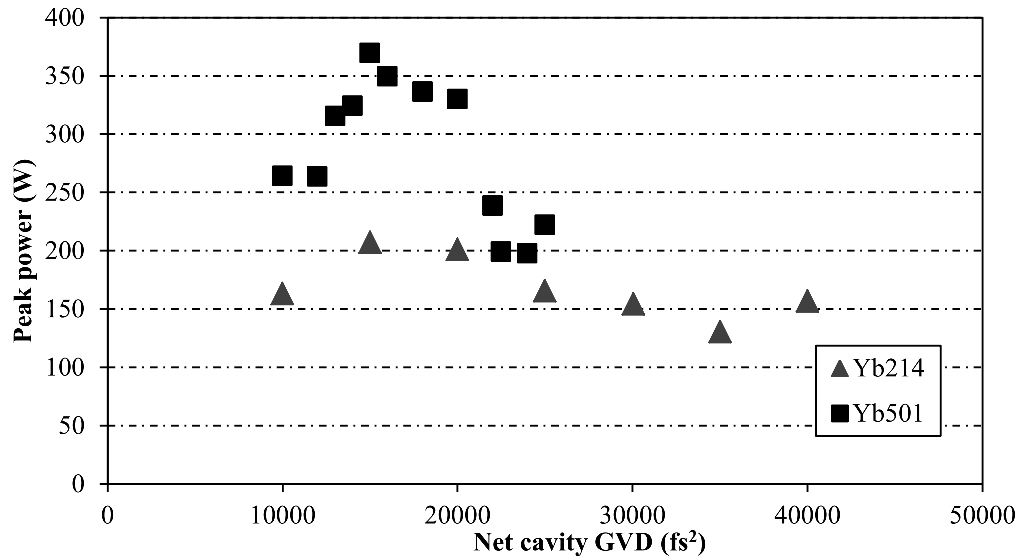

Figure 5-4: Peak power of output pulse width vs. GVD using NPE for cavities with 97.5 cm Yb501 and 25.5 cm Yb214

Using the same fiber lengths, the same measurements were taken with the cavity mode-locked using a SESAM. Figure 5-5 demonstrates that the low-doped Yb-fiber appears to have a higher energy, over a broader range of GVD values, avoiding the sharp decrease in energy observed with the NPE mode-locking. However, Figure 5-6 demonstrates that only for the lowest GVD values is there actually an improvement in peak power. This indicates that the apparent increase in energy is simply caused by an increase in pulse width. To prove the idea from section 5.2 it is necessary that the peak power is shown to increase in the low-doped gain fiber scenario.

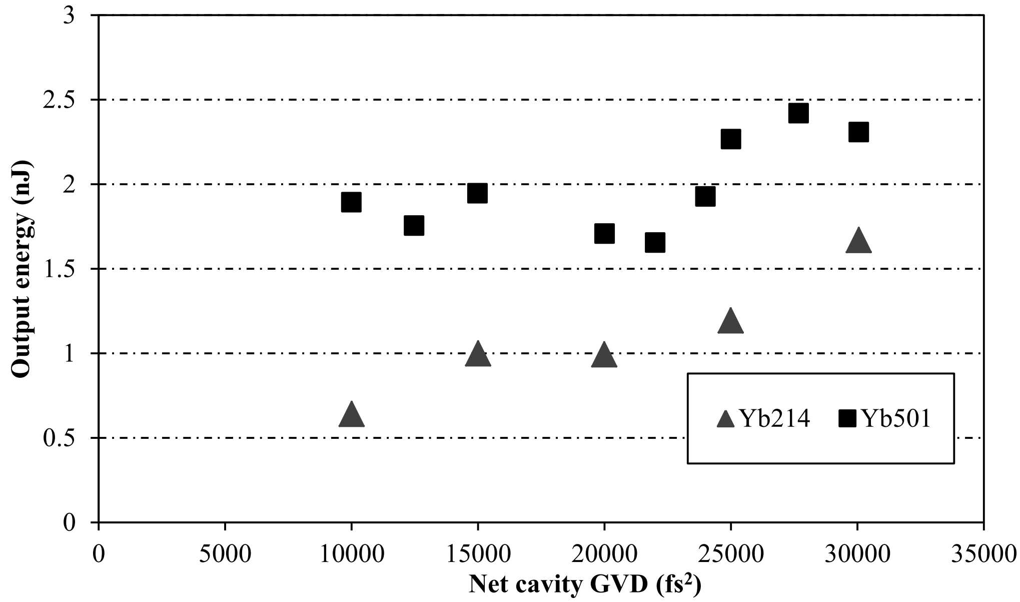

Figure 5-5: Output pulse energy using SESAM mode-locking and 97.5 cm of Yb501 and 25.5 cm Yb214

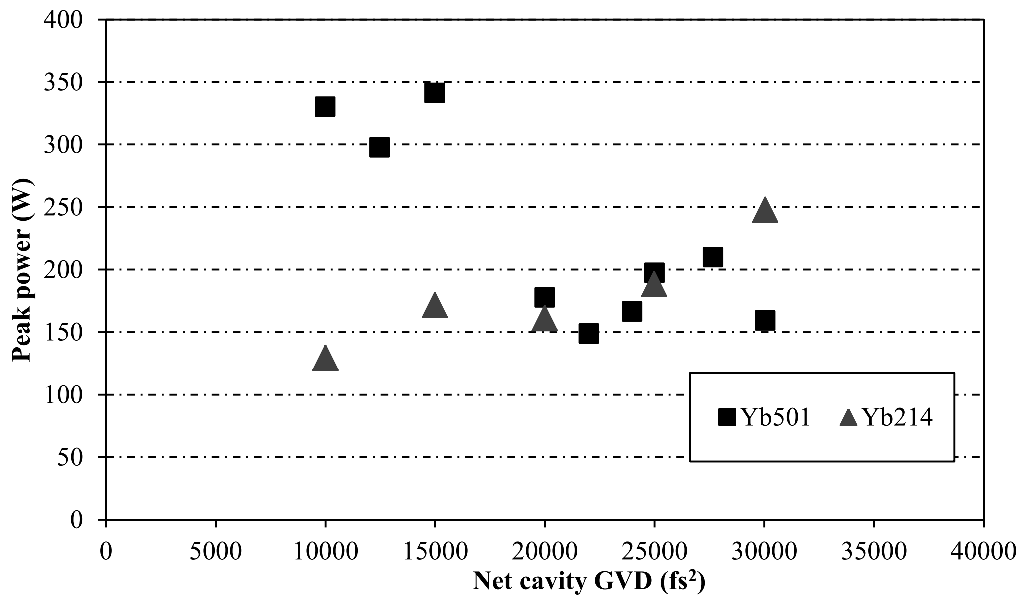

Figure 5-6: Output peak power using SESAM mode-locking and 97.5 cm of Yb501 and 25.5 cm Yb214

The idea was verified for values of net GVD only below 15 000 fs^2. The major problem with these results was found to be that in reality, the calculated nonlinear phase shift in the higher GVD region was not equal for both gain fiber cases.

5.3.4 Modified lengths of fibers

To ensure the condition that the nonlinear phase shift is equal in both cases under comparison, the nonlinear phase shift from the highly-doped case was used to determine what length of low-doped ytterbium would produce the same result. A colleague and I found that 72.5 cm of low-doped Yb501 would produce the same nonlinear phase shift as 25.5 cm of highly-doped Yb214.

The low-doped fiber results are repeated for both the NPE and the SESAM cavities and are plotted with the previous results for the highly-doped gain fiber. The length of low-doped Yb is 72.5 cm, and the nonlinear SMF length is changed to 98 cm to preserve the cavity length.

Figure 5-7 shows the comparison of the two fibers with NPE mode-locking. It is clear that this does not support the hypothesis for all values of GVD. At low GVD the results are what were expected, but then at higher GVD values, the trend reverses until a point at which the highly-doped fiber has higher output energy. This is likely due to the transmittance curve for NPE and is expected to not be a problem in the SESAM case. Figure 5-8 shows that only for low GVD is there a significant improvement in the output peak power for the low-doped gain fiber.

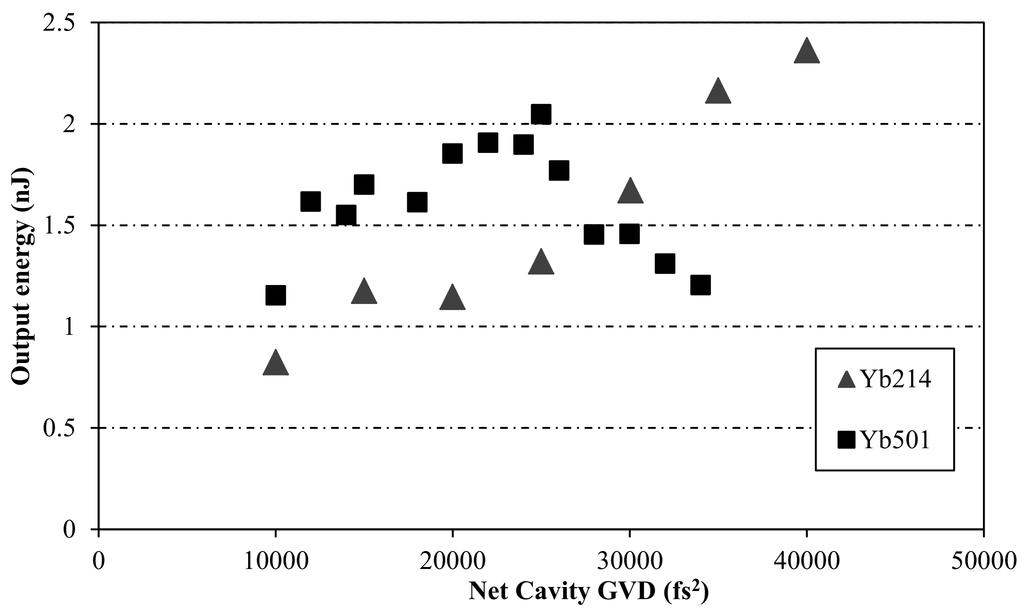

Figure 5-7: Comparison of output energy using NPE mode-locking, with 72.5 cm Yb501 (98 cm nonlinear SMF), and 25.5 cm Yb214 (143.5 cm nonlinear SMF)

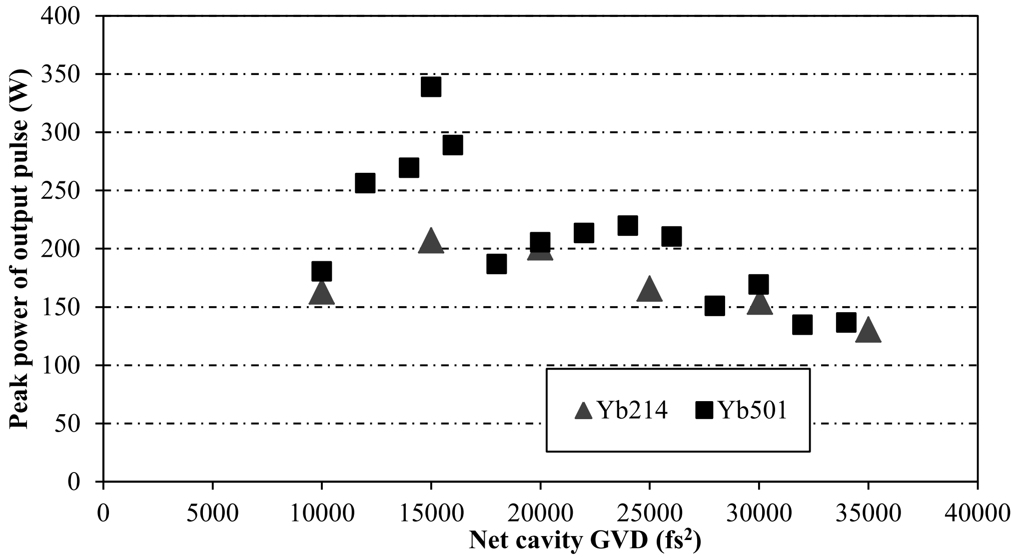

Figure 5-8: Peak power of output pulse width vs. GVD using NPE for cavities with 72.5 cm Yb501 and 25.5 cm Yb214

The measurement was repeated for the SESAM and the new fiber lengths for the low-doped case. Figure 5-9 shows clearly that the low-doped case does retain higher energy values before the limit of wave breaking across the GVD range which could be mode-locked when not limited by the NPE. The slopes are nearly parallel and won't intersect until the negative GVD region, which is not the same pulse regime. Figure 5-10 shows the consistency of the dechirped pulse widths and Figure 5-11 shows that indeed the peak power is higher for the low-doped case. It is clearly shown that with SESAM mode-locking, a low-doped, longer length of gain fiber allows for higher peak power, and higher energy pulses.

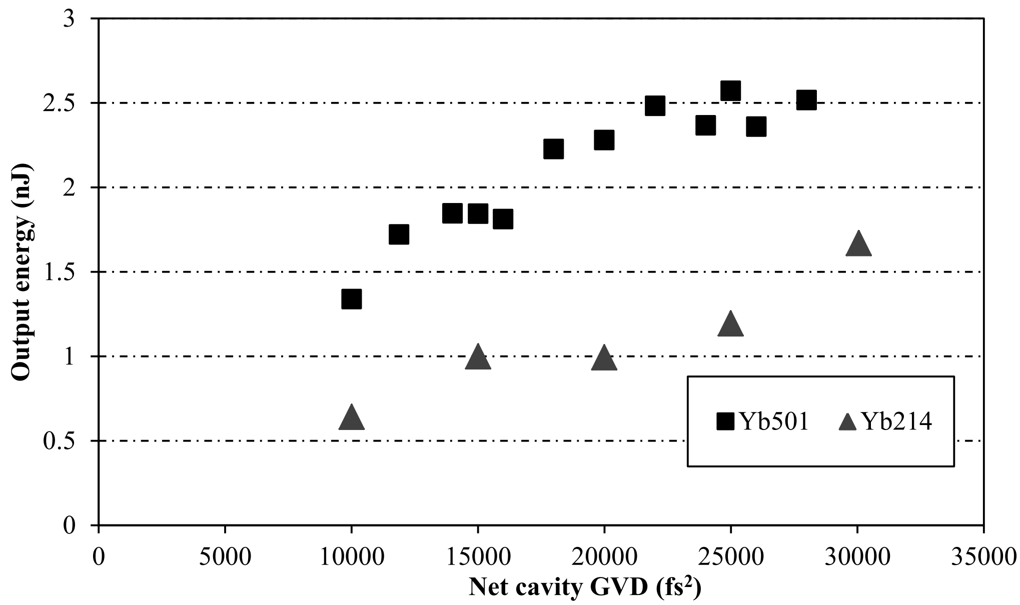

Figure 5-9: Output pulse energy vs. net cavity GVD using a SESAM cavities using 25.5 cm Yb214 and 72.5 cm Yb501

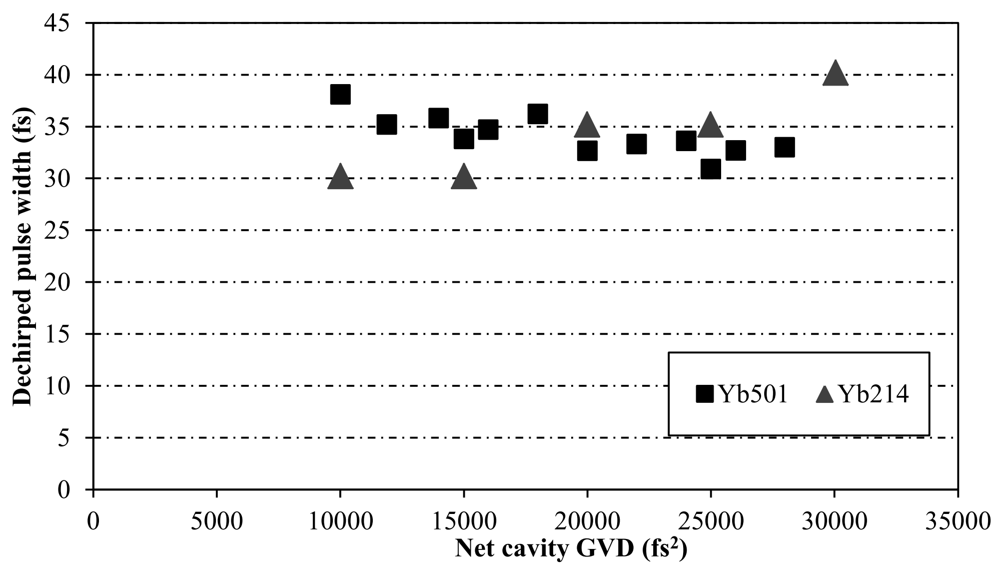

Figure 5-10: Dechirped pulse widths using SESAM cavity

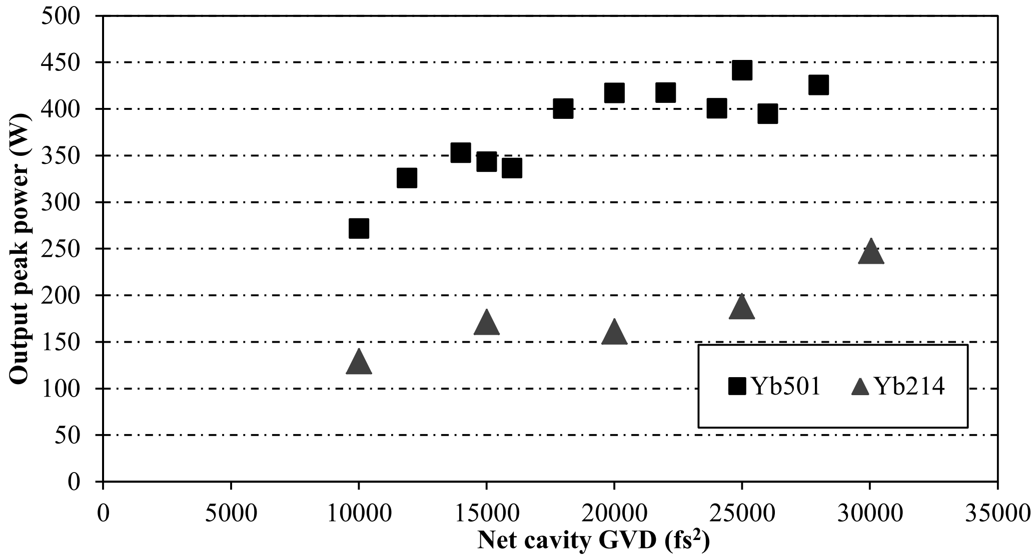

Figure 5-11: Output peak power using SESAM cavity

5.4 Conclusions

The most important and original finding of this part of my work is that the lower-doped gain fiber is able to provide higher peak power pulses than the more highly-doped gain fiber when mode-locked before the threshold of multi-pulsing. The low doped gain fiber allows for the nonlinear phase shift in the nonlinear region of the cavity to accumulate more slowly than in the cavity with a higher-doped gain fiber; the slow accumulation of nonlinear phase shift allows the cavity to generate a higher output energy (and thus operate at a higher energy circulating in the cavity) before approaching the optical wave-breaking limit. The low-doped case is shown to provide better output peak power and energy, which proves that the slow accumulation of nonlinear phase shift is advantageous in a self-similar (similariton) femtosecond fiber laser. The nonlinear phase was first estimated to be the same in both cases since both were mode-locked to operate at the highest energy circulating in the cavity just before the limit of wave breaking, given that wave breaking occurs at the same threshold value of nonlinear phase shift in both cases; later it was calculated and the fiber lengths were adjusted to ensure constant nonlinear phase shift.

The SESAM cavity shows a clear improvement in attainable peak power for a longer length of low doped gain fiber which was previously masked by the NPE action. NPE can be overdriven and its saturable absorber (i.e. transmittance) curve causes problems depending on where the bias point is. It was also expected that the SESAM would be able to sustain higher values of energy than the NPE mode-locking since NPE can be overdriven into a state where higher intensities are attenuated; there is an improvement of 0.5 nJ that can be seen at 25 000 fs^2 in Figure 5-9 using the SESAM compared to Figure 5-7.

This is the first work to our knowledge to do a direct, non-trivial comparison of high doped versus low doped gain fiber in two fiber-laser cavities with the same repetition rate, nonlinear phase shift, net GVD and nonlinear length that generate femtosecond regime similariton pulses. Furthermore, it demonstrates the negative energy-limiting effects of NPE mode-locking.

Chapter 6 - Conclusion

The original intent for this thesis was to develop an all-fiber laser to be used as a source for confocal microscopy. However, working on the laser led my research down different roads, such as multipulsing and TOD. The work that was done was necessary for establishing the fundamentals and paving the way to make an all-fiber laser. The results showing that a long length of low doped gain fiber is advantageous are aiding the development of the high power all-fiber laser. The work done in this thesis opened the doors for a wide variety of future work, but most importantly the development of the all-fiber prototype.

In this chapter, I summarize the work done in each chapter and suggest future directions that the femtosecond fiber laser project can take as a result of this work. The work central to this thesis investigated the femtosecond fiber laser experimentally and then optimized it, as the project has been predominantly theoretical previously. The major motivation was increasing the single pulse energy per period for the purpose of optimizing the output before making an all-fiber prototype for confocal microscopy applications.

6.1 Summary

Multipulsing was the first problem to investigate and address as it limits the single pulse energy by requiring that the pump power be reduced until there is only one pulse. Certain aspects of the cavity were investigated to ensure that they were not contributing to the damaging effect of multipulsing in the cavity. Bound pulses and rare harmonic mode-locked were observed in the cavity and recorded out of interest.

Third order dispersion became a topic of interest after some preliminary results suggested that it may be an interesting avenue of study. Although the experiments showed no energy dependence on the TOD, an interesting region was observed where two types of mode-locking could be achieved by simply tuning the nonlinear polarization evolution by means of the waveplates. This has been observed previously at low GVD values between the stretched-pulse and self-similar modes [6], but not at higher GVD values for overlap of self-similar and dissipative soliton pulse modes.

The goal of the final chapter was to show that a longer length of low-doped gain fiber could help produce higher energy pulses than a shorter length of highly-doped gain fiber. It took a number of iterations of work to finally prove the hypothesis. In the end, it was necessary to use a SESAM for mode-locking because the NPE was masking the data at higher values of net cavity GVD. This chapter shows an interesting comparison of the limitations of NPE directly against the SESAM technique. In the end, the idea was verified thoroughly.

6.2 Future work

The principal work to be done with this experiment is to move towards an all-fiber high power set-up which can be used with a confocal microscope. There are still many steps that can be taken before reaching this end. The cavity can be improved upon significantly to increase the magnitude of the energy of single pulses. The environment affects the laser set-up, especially in the nonlinear length of SMF, which had to be wound and secured carefully to reduce the likelihood of disturbances. Stresses from nearby vibrations have upset the mode-locking during various experiments causing the pulses to collapse. Changing the mode-locking technique to a SESAM which is polarization independent is a first step towards improving mode-locking due to its constrained transmission curve compared to NPE; a SESAM allows for the adoption of polarization maintaining fibers to reduce the environment effects on the system.

It is possible that the stable instances of multipulsing that were observed, such as bound pulses and harmonic mode-locking, may be studied further in the future. There is interest in the literature of the physics of the interactions of these pulses. Controlling harmonic mode-locking in a cavity such as this would be an interesting way to control the repetition rate without changing the length of the cavity. It is important to keep mindful of the pump power threshold at which multipulsing begins to occur, as there is no explanation of why the energies I measured were lower than those seen elsewhere in the literature, such as in [6].

The TOD work could also be expanded in the future. As I showed, in some instances, higher TOD contributed to narrower pulses. This could be studied further to find an optimal value of TOD which can contribute to generating narrower pulses. This could be useful later in optimizing and controlling pulse specifications in this laser. More importantly, the region of overlap between the two modes should be studied in greater detail as it is novel and was only observed with one type of fiber. Understanding the conditions of this region would be interesting and even useful in designing a laser with two optional modes that can be toggled simply by changing the orientation of the wave plates.

After showing that the long length of low-doped gain fiber gives a relative improvement, the next steps for the project include replacing all the SMF in the cavity with only low-doped ytterbium. Thus, a new fiber with even lower doping needs to be characterized and investigated. This is the idea that motivated the work done comparing two different doping values. Doing this will, in theory, allow even more nonlinear phase shift accumulation to increase the pulse energy further.

Furthermore, in the future, the laser will be tested with a confocal microscope set-up. A primary concern that has kept this from being undertaken so far is that the average power is still too low to investigate modalities such as coherent anti-Stokes Raman scattering. Another reason is that the set-up that is available to test with is fiber-delivered and will require pre-compensation for the high dispersion that will be accumulated in the fiber delivery system. A study of how the prechirp (additional anomalous dispersion when compressing the pulse) will affect the pulse. Studies into other realms of biomedical applications will be worthwhile as well, since this laser can be optimized for various needs.

Appendix A Laser source current

The laser source used as a pump in this thesis is two 980 nm laser diodes which are combined and injected into the cavity through a WDM. The power supply drives each with a particular current, set by the user. The two sources are called Las1 and Las2 and can be tuned individually. To determine the pumping power entering the laser cavity, the SMF immediately after the WDM (before the Yb-doped fiber) was cut and focused with a lens onto a power meter. Four cases where characterized, as shown in Figure A-1:

1) Las1 turned off, varying Las2,

2) Las1 set to 1000 mA (the maximum), varying Las2,

3) Las1 varied, Las2 off,

4) Laser 1 varied, Las2 set to 1000 mA.

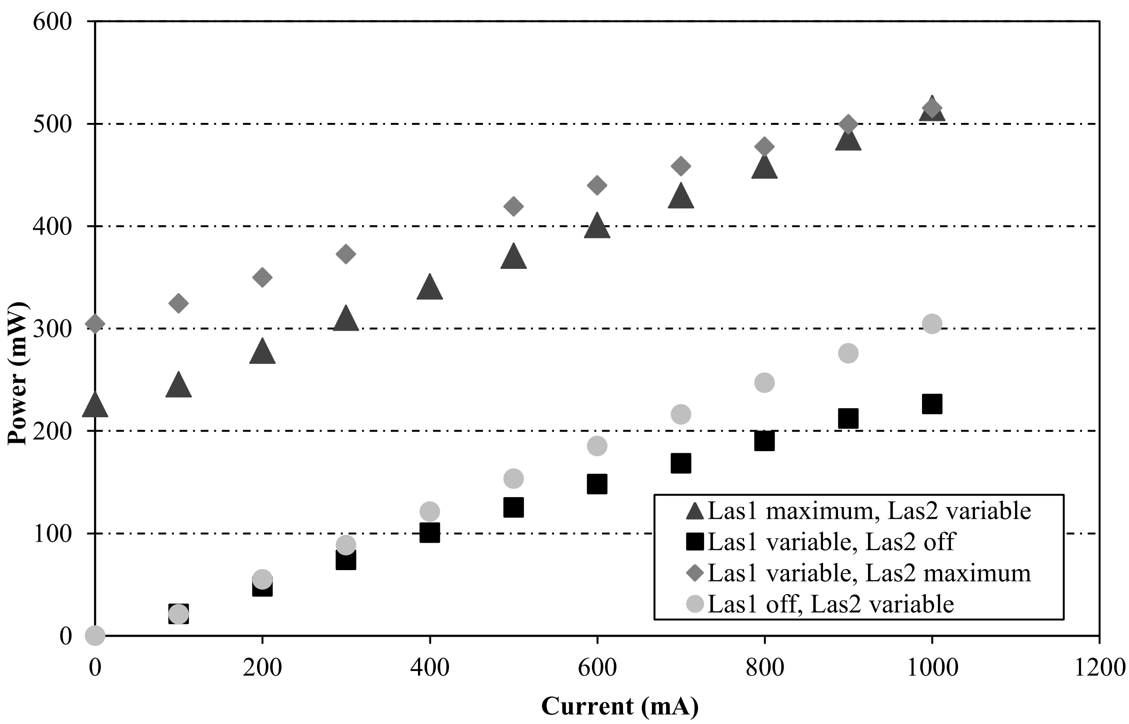

Figure A-1: Pump power into the cavity vs. current

Experimentally, the laser sources were always tuned such that one of these four cases was always true. That is to say, when recording data both lasers were never varied at the same time. Each set of data was fit with a linear model to get an equation of best fit, from which the pump power could be determined for any experiment.

The equations for each case are as follows:

1) Las1 = 0 mA, Las2 = I_2 [mA]:

$$P_{pump}[mW] = 0.3125I_2 - 4.5636$$

$R^2 = 0.9992$

2) Las1 = 1000 mA, Las2 = I_2 [mA],

$$P_{pump}[mW] = 0.2956I_2 - 221.73$$

$R^2 = 0.9992$

3) Las1 = I_1 [mA], Las2 = 0 mA

$$P_{pump}[mW] = 0.2303I_1 + 4.8333$$

$R^2 = 0.9954$

4) Las1 = I_1 [mA], Las2 = 1000 mA

$$P_{pump}[mW] = 0.2140I_1 + 307.02$$

$R^2 = 0.9979$

Appendix B Fiber types

Two different types of ytterbium-doped fibers are used in the experimental set-up for this thesis. They are both single-clad fibers, designed by *CorActive* to be used with single-mode pumping. The two ytterbium-doped gain fibers are called Yb214 and Yb501, which were selected based on their similar physical characteristics and different values of doping. Yb214 has a higher level of doping level of 1.85×10^{26} ion/m^3, while the Yb501 has a doping level of of 1.26×10^{26} ion/m^3. The parameters of the fiber as given by *CorActive* are listed below in Table B-1 for the Yb214 and in Table B-2 for the Yb501.

Finally, the single mode fiber used in the cavity was *Corning Hi 1060 Specialty fiber*. Its specifications are listed in Table B-3.

Table B-1: Yb214 optical and physical properties

Optical and physical properties	Specification	Measurement
Numerical aperture	0.14 ± 0.02	0.14
Peak absorption at 915 nm	350 ± 70 dB/m	350 dB/m
Mode field diameter at 1060 nm	6.0 ± 1.0 μm	6.1 μm
Attenuation at 1200 nm	≤ 30 dB/km	22 dB/km
Low-pass cut-off wavelength	800 – 900 nm	838 nm
Cladding diameter	124.7 ± 1.0 μm	125.0 ± 0.8 μm
Coating diameter	250.0 ± 10.0 μm	250.0 ± 10.0 μm
Screen proof tested	≥ 100 kpsi	110 kpsi

Table B-2: Yb501 optical and physical properties

Optical and physical properties	Specification	Measurement
Numerical aperture	0.14 ± 0.02	0.13
Peak absorption at 915 nm	150 ± 30 dB/m	139 dB/m
Mode field diameter at 1060 nm	6.0 ± 1.0 μm	6.0 μm
Attenuation at 1200 nm	≤ 30 dB/km	21 dB/km
Low-pass cut-off wavelength	850 – 950 nm	930 nm
Cladding diameter	124.7 ± 1.0 μm	125.0 ± 0.3 μm
Coating diameter	250.0 ± 10.0 μm	252.0 ± 0.6 μm
Screen proof tested	≥ 100 kpsi	100 kpsi

Table B-3: SMF optical and physical properties

Optical and physical properties	Specification
Numerical aperture	0.14
Mode field diameter at 1060 nm	6.2 ± 0.3 μm
Mode field diameter at 980 nm	5.9 ± 0.3 μm
Maximum attenuation at 1060 nm	1.5 dB/km
Maximum attenuation at 980 nm	2.1 dB/km
Low-pass cut-off wavelength	920 ± 50 nm
Cladding diameter	125 ± 0.5 μm
Coating diameter	245 ± 10 μm
Screen proof tested	100, 200 kpsi

Appendix C Diffraction gratings

Diffraction gratings are commonly used in ultrafast optics to provide anomalous dispersion to compress pulses of light temporally. Diffraction gratings are known to generate spatial dispersion. The blue-shifted light off the diffraction grating acquires a smaller angle of diffraction than the red-shifted components. By placing a second diffraction grating in the path of the dispersed light, one can recombine the frequencies into a parallel ray of light, where the red-shifted light has acquired more delay as a result of a longer path length, translating into effectively increasing the phase velocity of the blue-shifted light.

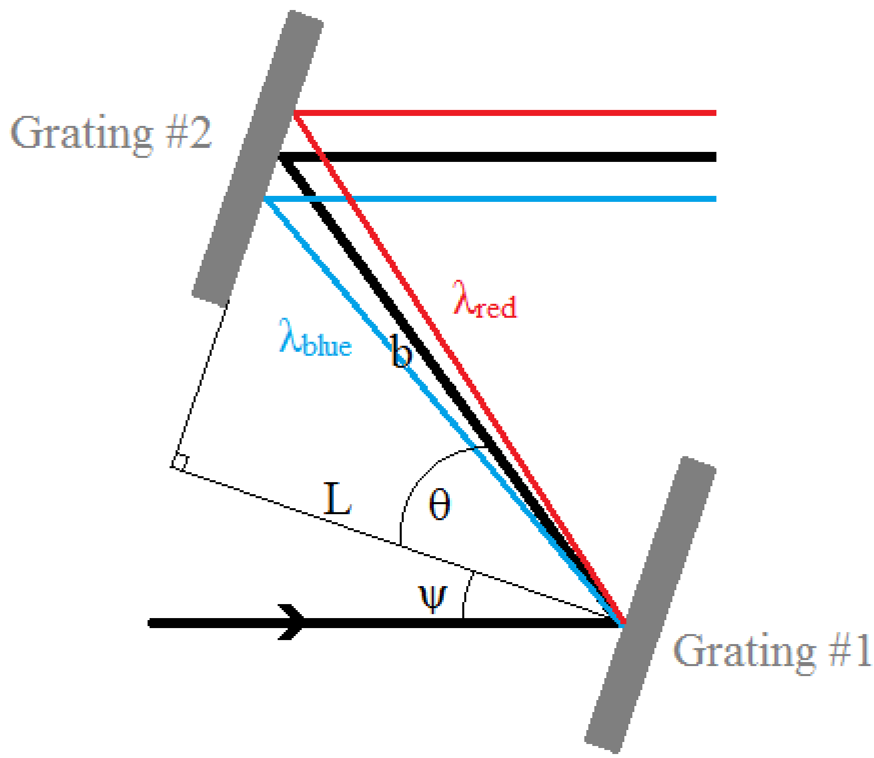

Figure C-1: Diffraction grating pair geometry

In Figure C-1, *b* is the slant length between the diffraction gratings, *L* is the normal separation, ψ is the incident angle and θ is the diffracted angle (which is actually a function of wavelength, λ). The number of lines/mm of the gratings is characterized by the variable *d*. The central wavelength and central frequency are λ_0 and ω_0 respectively.

In 1969, Treacy found the relationship for the phase-shift off of a grating as a function of frequency, which came out to [56]:

$$\phi(\omega) = \phi_0 + bc^{-1}(1+\cos\theta)(\omega-\omega_0) - \frac{b\lambda_0^3}{4\pi c^2 d^2}\frac{(\omega-\omega_0)^2}{[1-(\lambda/_d - \sin\psi)^2]}$$

Eq. 10

In Eq. 10, ϕ_0 represents the initial phase shift.

The group velocity dispersion is simply the second derivative of the phase shift with respect to angular frequency. One can put equation Eq. 10 in terms of θ to simplify the derivation. In combination with trigonometric laws to simplify the denominator in Eq. 10, one can use the grating equation [18]:

$$\sin\psi + \sin\theta = \frac{m\lambda}{d}$$

Eq. 11

In the grating equation, m is the order of diffraction, which is equal to -1 since the first order is the most powerful, and the negative sign indicates the direction.

The simplified equation is:

$$\phi(\omega) = \phi_0 + bc^{-1}(1+\cos\theta)(\omega-\omega_0) - \frac{b\lambda_0^3}{4\pi c^2 d^2}\frac{(\omega-\omega_0)^2}{(\cos\theta)^2}$$

Eq. 12

The derivative then becomes:

$$\left.\frac{\partial^2\phi(\omega)}{\partial\omega^2}\right|_{\omega=\omega_0} = \frac{-b\lambda_0^3}{2\pi c^2 d^2 (\cos\theta)^2}$$

Eq. 13

The second order dispersion, β_2, that is to say, the GVD per unit length (actually GDD/path length), accumulated across the light's path length b is simply:

$$\beta_2 = \frac{1}{b}\left.\frac{\partial^2\phi(\omega)}{\partial\omega^2}\right|_{\omega=\omega_0}$$

Eq. 14

Substituting the GVD equation and returning back to incident angle since it is more useful experimentally, the equation for anomalous dispersion between two diffraction gratings is:

$$\beta_2 = \frac{\lambda_0^3}{2\pi c^2 d^2 [1 - (\lambda/_d - \sin\psi)^2]}$$

Eq. 15

A mirror is used at the output of the diffraction grating pair to pass the light back through the two gratings. This not only doubles the temporal dispersion attained, but also undoes for the spatial dispersion by making the blue and red-shifted light return along their prior paths [26].

So for a grating pair using a retro-reflecting mirror to pass the light back through the compressor, the equation becomes:

$$\beta_2 = \frac{\lambda_0^3}{\pi c^2 d^2 [1 - (\lambda/_d - \sin\psi)^2]}$$

Eq. 16

Appendix D Preliminary experiment for increasing energy with low-doped gain fiber

N.B. *The work in this appendix was done using the electrical channel of the oscilloscope with a photodetector of only 1.2 GHz, so it is likely that undetected multipulsing is occurring. The results are still qualitatively useful, even though they do not prove the theory in section 5.2*

The experimental set-up is similar to section 3.2 . The laser cavity was built of the same components, with some of the fiber parameters changed; the fiber parameters are determined in section D.1. The zero-order output of the intra-cavity diffraction gratings was used to capture the chirped pulse on the autocorrelator and to watch for multiple pulses circulating the cavity with a small temporal separation using an autocorrelator with 120 ps scanning range. The average power at this port was also used to estimate the power inside the cavity entering the diffraction gratings; this was calculated using the fixed power efficiency of the diffraction grating pair and the measured ratio, at a fixed incident angle, of the zero order reflection to the first order which remains in the cavity.

The level of doping of the gain medium was varied by using lengths of differently doped ytterbium fiber. The fibers' characteristics are shown in Appendix B.

As mentioned previously, the average power measured at the zero order output port during mode-locking was used to estimate the power inside the cavity entering the diffraction gratings in addition to being the port at which the chirped pulse measurement was taken with an autocorrelator. The pulse energy circulating inside the cavity was calculated given the measured ratio, at a fixed incident angle, of the zero order reflection to the power of light incident on the diffraction grating. The ratio of zero order to incident power was measured on the 600 line/mm gratings (Edmund Optics, NT49-573) with CW light and was found to be 0.0386. To determine the energy per pulse inside the cavity (for pulses entering the PBS), the output energy per pulse was added to the pulse energy remaining in the cavity. The pulse energy remaining in the cavity was determined from the measured average power in the zero-order reflection, which was divided by 0.0386 and by the pulse repetition rate to get the energy.

D.1 Determining optimal fiber length

Before being able to begin comparing the effects of the length and doping of the gain fiber within the laser cavity, the optimal lengths of ytterbium fibers to be used for comparison need to be selected. The optimal lengths of ytterbium gain fibers occur at the lengths at which there is complete population inversion in the fiber causing the maximal gain; this can be determined empirically based on the detection of the pump wavelength of 980 nm inside the cavity. If the gain fiber is too short, 980 nm pump breakthrough can be measured on the optical spectrum analyzer. If the gain fiber is too long, the gain will be reduced due to reabsorption of the amplified wavelength. It should be noted that the optimal length of gain fiber is hypothesized to be different under pulsed operation than in CW (due to the high peak power and slow transition time) and should be shorter than the predicted lengths from CW simulations.

Initially, simulations were attempted using VPI software using the Giles parameters of the fibers (i.e. wavelength-dependent absorption and gain coefficients) to try to determine the optimal lengths of gain fiber for both cases. These simulations predicted that the optimal gain in CW operation for a fixed pump power would be found at 29 cm of highly doped Yb214 and at 95 cm for the low-doped fiber, Yb501. No one to our knowledge has studied determining the optimal length of gain fiber under mode-locking conditions. Using these values as a starting point, a series of measurements were done for each fiber to determine the approximate optimal length of operation.

The length of ytterbium fiber was varied by cleaving the fiber and splicing it again to close the cavity. The mode-locked output energy and energy inside the cavity were measured and calculated respectively, and this was repeated for a series of lengths for both ytterbium fibers. The highest energy inside the cavity was taken as an indicator of the optimal length instead of the actual output energy (though for most cases, they were the same). This highest energy circulating in the cavity before wave-breaking was used as the indicator for the optimal length of gain fiber since it is the highest energy per pulse that can be sustained in the cavity before the limit at which multipulsing occurs. It was determined that the lengths of ytterbium that produce the highest energy mode-locked pulses inside the cavity can be compared since they are both optimized; it should be noted that the gain in the optimal length of Yb214 and Yb501 are not the same. The difference in total gain is not a problem as the different rate of gain/length (slope in Figure 5-1) for the two fibers changes the rate of accumulation of nonlinear phase shift, which in turn changes the energy that can circulate in the cavity before reaching mode-locking.

While performing the cut-back measurements to determine the optimal lengths of both fibers, the amplified stimulated emission (ASE) power was measured in CW operation at both fiber collimators inside the cavity in the forward and backward directions of light propagation. It was hypothesized that at optimal gain, the ASE power would be equal in both directions since, but under pumping conditions any noise can be amplified and the results were unstable. This approach could be improved with a systematic study using a 1030 nm seed pump in addition to the 980 nm pump laser.

It has been convention in fiber laser experiments to simply use a short gain fiber since it works well and provides ample gain. For this work, it was important to compare laser cavities that are as close to being the same as possible with the exception of the length and doping of the gain fiber; this is why it was significant to compare optimal lengths of both of the gain fibers.

D.1.1 Yb214 - Highly-doped gain fiber length

To determine the optimal length of gain fiber for the fixed pump power of 530 mW, a series of measurements is taken for three different lengths of Yb214: 25 cm, 29.5 cm, and 40 cm. The repetition rate was held constant by compensating for the change in length of gain fiber by adding SMF. Figure D-1 shows the output energy for each length at several values of GVD to feel confident in the measurements. Figure D-2 shows the total maximal energy per pulse inside the cavity (before the output port and after the gain section). It is clear that the 25 cm length of gain fiber provides the lowest output power for most values of GVD, but also the largest total power. For this reason, 25 cm was selected as the optimal length. It should be noted that at 25 cm there was a small amount of 980 nm breakthrough detected, which implies that this length is in fact very close to the length of perfect pump absorption at the maximum pump power of 530 mW.

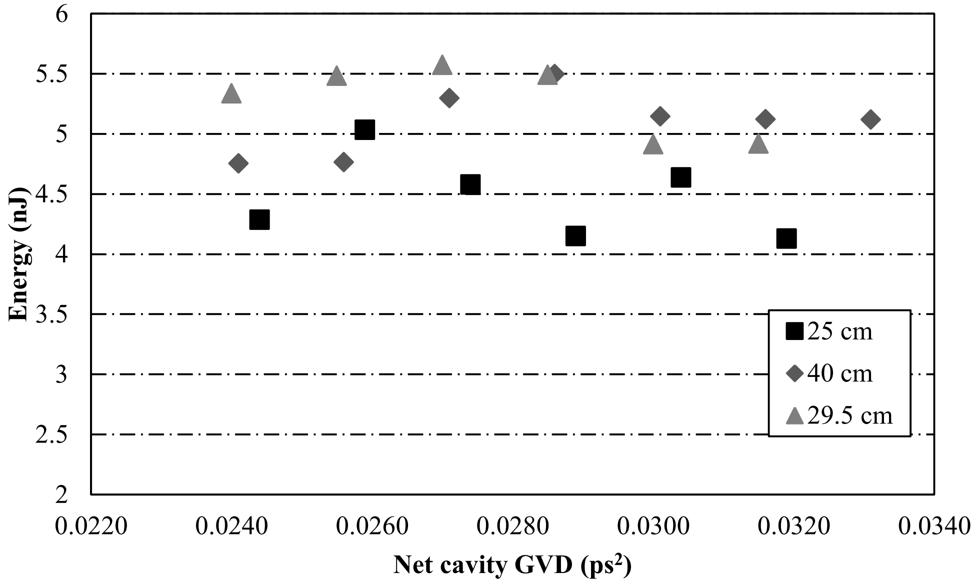

Figure D-1: Output energy vs. GVD for various lengths of Yb214 highly-doped gain fiber

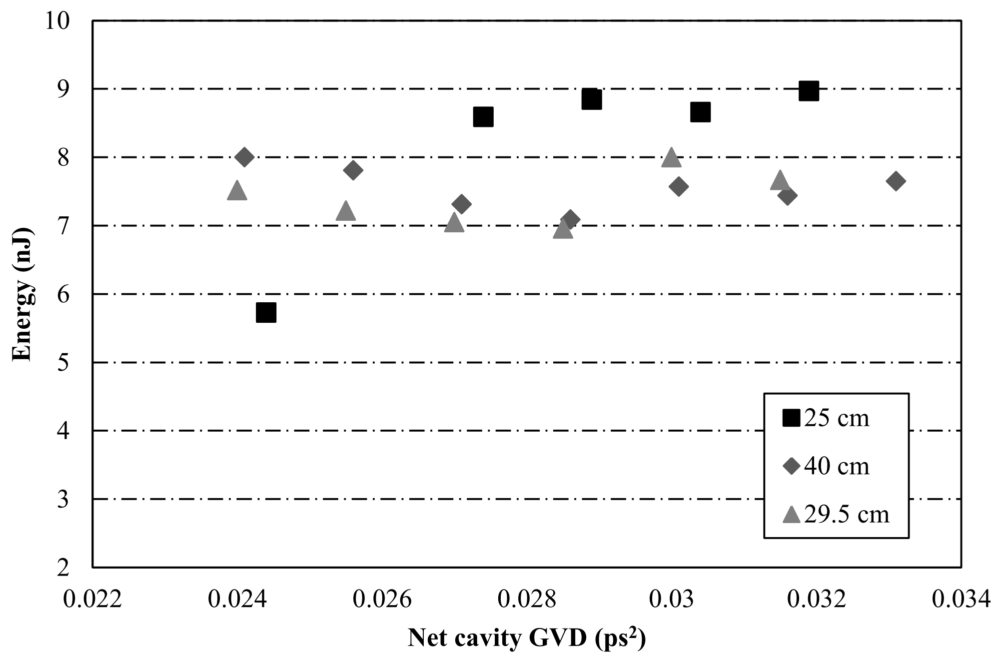

Figure D-2: Energy inside the cavity after the output port vs. GVD for Yb214 highly-doped gain fiber

D.1.2 Yb501 - Low-doped gain fiber length

The same set of measurements was repeated for several lengths of low-doped gain fiber, Yb501. The lengths investigated were: 55.5 cm, 65 cm, 82.5 cm, and 102.5 cm. The core absorption of the highly doped fiber was nearly 3 times that of the Yb501, so it was expected that the optimal length will be much longer than the length of Yb214. Figure D-3 shows the output energy, which was highest at 65 cm, and then 102.5 cm. Figure D-4 similarly shows that 65 cm is highest total energy followed again by 102.5 cm. However, all of the total energy values are confined to a range of 2 nJ. 102.5 cm was chosen as the optimal length for comparison due to it having a more stable operating point and that it has a very high total energy per pulse. Furthermore, since I am trying to prove that the long, low-doped case provides higher energy, it was more critical to carefully optimize the highly doped case than the low-doped. If the hypothesis is proven with a low-doped gain fiber length that is not quite optimal, it would only be proven more convincingly with an ideal case.

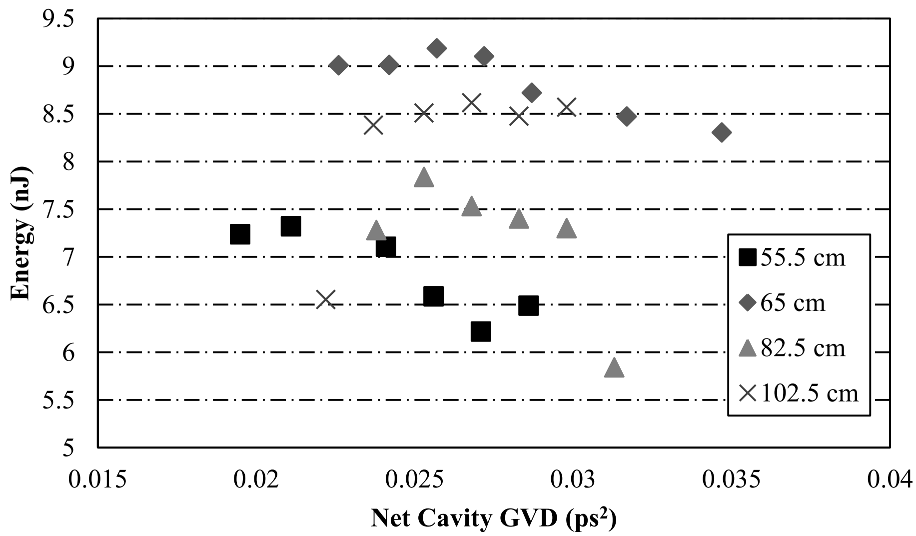

Figure D-3: Output energy vs. GVD for various lengths of Yb501 low-doped gain fiber

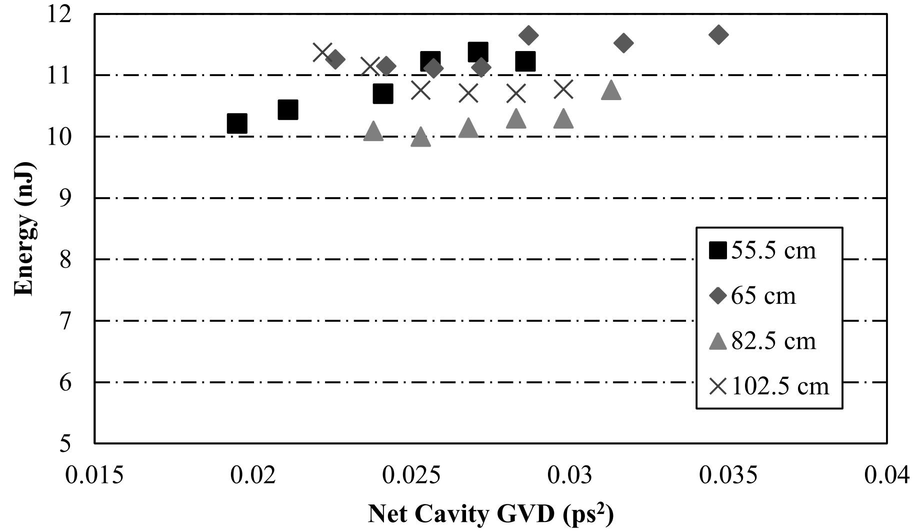

Figure D-4: Energy inside the cavity after the output port vs. GVD for Yb501 low-doped gain fiber

D.2 Results

For the optimal length of gain fiber for both cases, a set of measurements was taken to determine if the slow accumulation of nonlinear phase shift helps to increase the total energy generated before wave breaking. For a series of intracavity GVD values, average power is measured at the output port and at the zero order reflection off of the intracavity diffraction gratings. The repetition rate, pulse train, spectral width, chirped and dechirped pulse widths are recorded for each point. The repetition rate is held constant by compensating the change in length of gain fiber with SMF in the nonlinear region of the cavity. This keeps the repetition rate the same and also the effective nonlinear length the same for the sake of the consistency of the NPE mode-locking.

D.2.1 Yb214 - Highly-doped gain fiber results

The optimal length of the highly doped ytterbium gain fiber (CorActive, *Yb214*) for the laser cavity for a fixed set of cavity conditions was found to be 25 cm (with a doping level of 1.85×10^{26} ion/m^3 and a 6 µm core diameter) as this was where the highest total energy was found circulating the cavity. This length of gain fiber gives 4.1 nJ of mode-locked output energy with a net normal GVD of 0.0289 ps^2 at the point of maximal energy inside the cavity as shown in Figure D-5. It was necessary to optimize the total energy inside the cavity to ensure that the nonlinear phase shift is the same in both the high and low doped gain fibers. It should be noted that the theory suggests that output energy must increase with increasing total cavity GVD [17]; however it can be seen in Figure D-5 that the energy is a monotonic function with changing GVD. This may be due to the saturation of the NPE, since its sinusoidal transmission function may be blocking energies at certain values of power [57]. This pulse is recognized as a similariton pulse due to the parabolic spectrum inside and outside the cavity and also from the relationship between the anomalous dispersion required to dechirp the parabolic pulse compared to the intracavity grating dispersion as shown in Figure D-6.

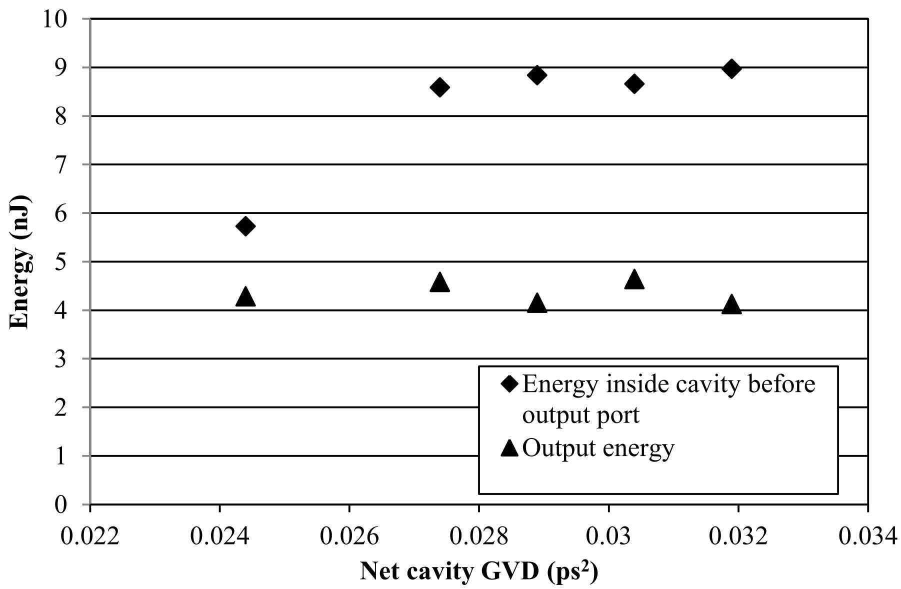

Figure D-5: Total energy inside cavity per pulse after nonlinear SMF and output energy at rejection port, versus net cavity GVD for 25 cm of highly doped Yb (149.5 cm SMF after the gain length)

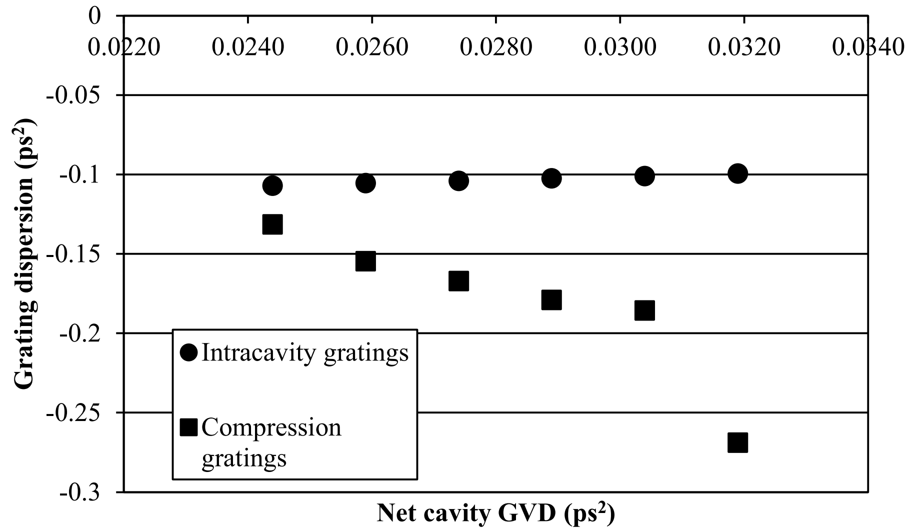

Figure D-6: Comparison of dispersion contributed from intracavity gratings and dechirping gratings

Figure D-6 shows that the pulse is always positively chirped inside the cavity since the magnitude of the anomalous dispersion required for optimal compression is larger than the intracavity anomalous dispersion, which indicates that the pulse is highly positively chirped before being injected into the normal dispersion SMF after the intracavity gratings; the positive chirp throughout the cavity in combination with the parabolic spectral shape support that this is in fact a self-similar mode of operation [40].

Since it is known that the pulses are parabolic, the measured pulse width from the autocorrelator was compensated by a factor of 0.875 to account for the shape [30]. As mentioned, the maximal energy inside the cavity occurs at a net GVD of 0.0289 ps^2, which generates 4.1 nJ at the output port. Figure D-7 shows the chirped pulse (5.8 ps FWHM), the dechirped (compressed) pulse (170 fs FWHM), the waveform with a repetition rate of 30.29 MHz, and the spectrum with a bandwidth of 19.92 nm.

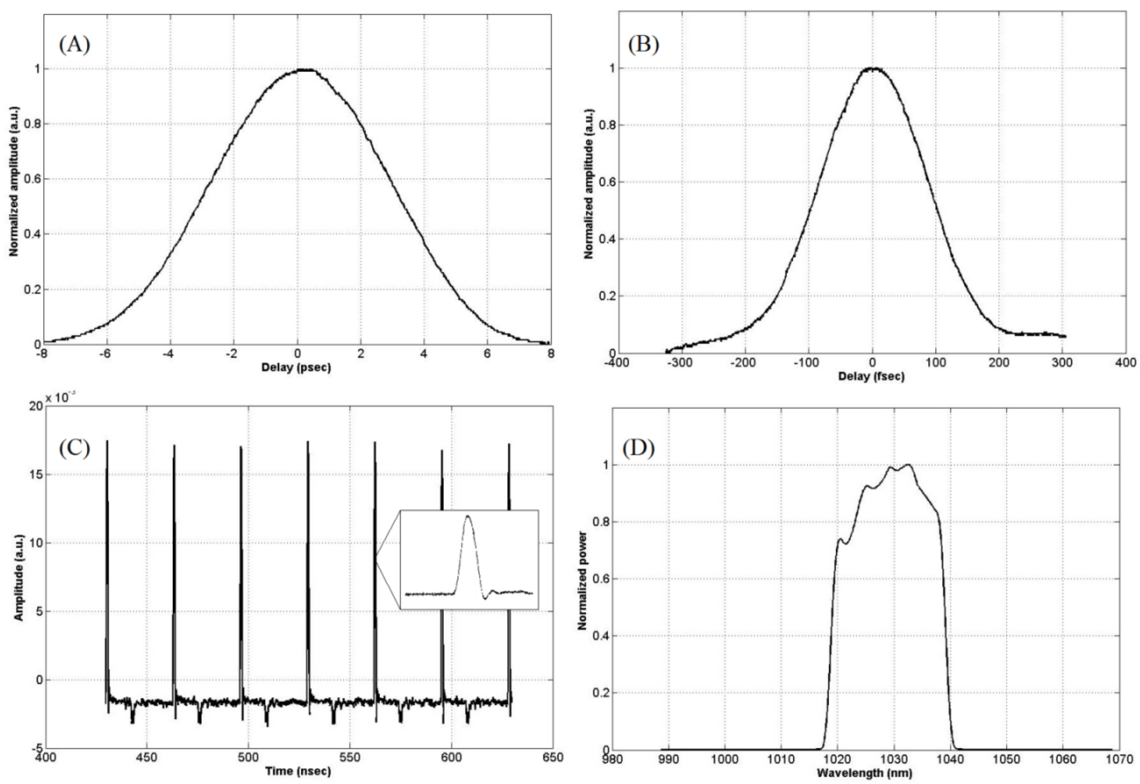

Figure D-7: Output pulse characteristics for 25 cm of highly doped Yb fiber with a net GVD of 0.0289 ps^2 (A) Chirped pulse with actual width 5.8 ps, (B) Dechirped pulse with actual width 170 fs, (C) waveform at 30.29 MHz on oscilloscope showing no multiple pulsing on the zoomed-in pulse envelop shown in the inset, (D) parabolic spectral bandwidth (19.92 nm).

D.2.2 Yb501 - Low-doped gain fiber results

The maximum total energy circulating the cavity was found to occur at 102.5 cm using the lower doped gain fiber (CorActive *Yb501*), which has a doping level of 1.26×10^{26} ion/m^3 and also a 6 µm core diameter. After replacing the highly doped gain fiber with the longer, lower doped fiber, the nonlinearly acting SMF after the gain fiber was shortened to keep the effective nonlinear length the same in both cases and also to maintain the repetition rate at 30.3 MHz. The maximal energy inside the cavity appeared at the extreme point at 0.0222 ps^2; however, this value has uncharacteristically low output energy. To maintain a constant net GVD to compare with the highly-doped case, the next highest total cavity energy point was used for the comparison, which occurs at 0.0237 ps^2. The output energy for this point is 8.4 nJ, as shown in Figure D-8, and Figure D-9 supports that this is in fact a self-similar mode of operation. Figure D-10 shows the chirped pulse (4.4 ps), the dechirped pulse (146 fs), the waveform with repetition rate of 30.33 MHz, and the parabolic spectrum with a bandwidth of 24.72 nm for the optimal length of low-doped Yb gain fiber for these cavity conditions based on maximal total energy circulating in the cavity.

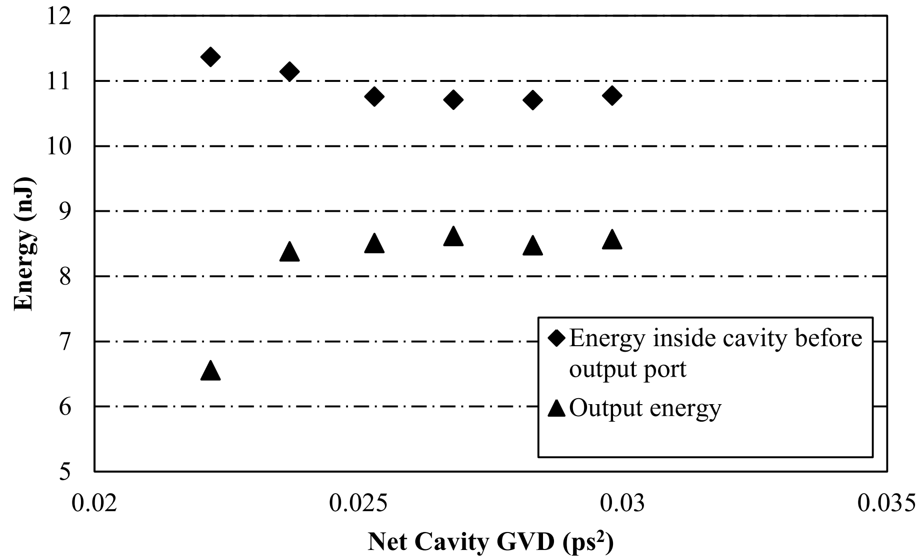

Figure D-8: Total energy inside cavity per pulse after nonlinear single mode fiber, and output energy at rejection port, versus net cavity GVD for 102.5 cm of highly doped Yb (72cm SMF after the gain length)

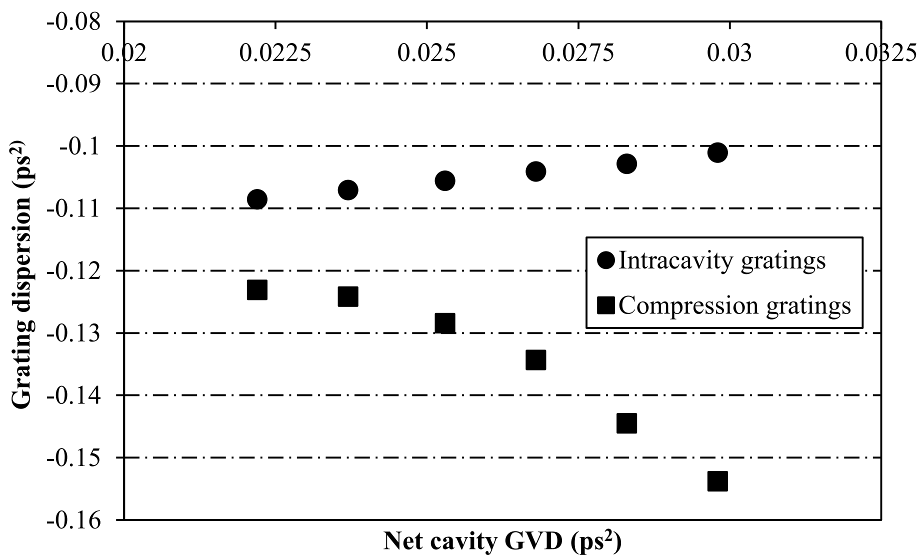

Figure D-9: Comparison of dispersion contributed from intracavity gratings and dechirping gratings

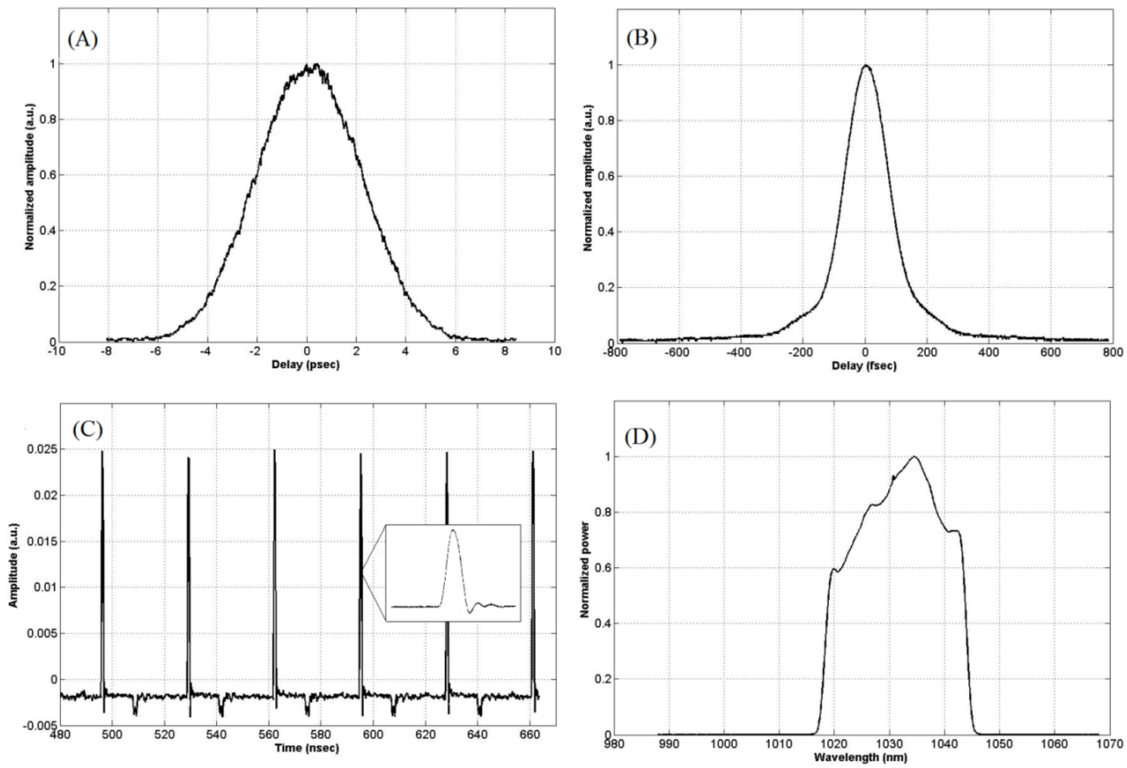

Figure D-10: Output pulse characteristics for 102.5 cm of low doped Yb fiber with a net GVD of 0.0237 ps^2 (A) Chirped pulse with actual width 4.4 ps, (B) Dechirped pulse with actual width 146 fs, (C) waveform at 30.33 MHz on oscilloscope showing no multiple pulsing on the zoomed-in pulse envelop shown in the inset, (D) parabolic spectral bandwidth (24.72 nm)

D.3 Comparison

The application of the low-doped gain fiber produced a higher output energy (8.4 nJ) compared to the highly-doped gain fiber (4.1 nJ) under the same cavity conditions (i.e. repetition rate, effective nonlinear length and nonlinear phase shift) which supports the theory for generating more energetic pulses. The spectrum is broader and the compressed pulse width is shorter for the low-doped case (24.72 nm and 146 fs for the low-doped; 19.92 nm and 170 fs for the highly-doped).

The resulting peak power of the low-doped case is also higher (23.5 kW compared to 10.0 kW for the highly doped case) as expected after the set of compression gratings, which have a total efficiency of 0.8^4 since each grating degrades the power by 20%. It should be noted that the amplified stimulated emission (ASE) output after the gain fiber for both cases showed only small amounts of pump wavelength (980 nm) breakthrough. This indicated ideal population inversion before re-absorption of pump, which further supports that the lengths of fiber used were correct.

Chapter 7 - Bibliography

[1] V. Venugopalan, "Tutorial on Tissue Optics," OSA Biomedical Topical Meeting, 2004.

[2] Q. Peng, A. Juzeniene, C. Jiyao, S. O. Lars , T. Warloe, K.-E. Giercksky and J. Moan, "Lasers in medicine," *Reports on Progress in Physics,* vol. 71, no. 5, 2008.

[3] H. Anis, *Femtosecond Fiber Lasers and Applications,* Ottawa: Extreme Photonics Workshop, University of Ottawa, 2011.

[4] B. E. A. Saleh and M. C. Teich, Fundamentals of Photonics, 2nd ed., Hoboken, New Jersey: Wiley-Interscience, 2007.

[5] J.-C. Diels and W. Rudolph, Ultrafast Laser Pulse Phenomena, New York: Academic Press, 2006.

[6] J. Buckley, "Dissertation on High-energy ultrafast ytterbium fiber lasers," Cornell University, 2006.

[7] J. P. Cranska, "Do all dentists use lasers?," 1 May 2006. [Online]. Available: http://www.dentistrytoday.com/technology/lasers/1371. [Accessed April 2012].

[8] I. Arons, "AAO Highlights: Lasers for Cataract Surgery, Laser Vision Correction Trends, and More," 10 November 2009. [Online]. Available: http://eyedocnews.com/002583-aao-highlights-lasers-for-cataract-surgery-laser-vision-correction-trends-and-more/. [Accessed April 2012].

[9] F. Hupston, "How to Find the Best Tattoo Removal Methods," 23 September 2009. [Online]. Available: http://www.suite101.com/content/how-to-find-the-best-tattoo-removal-methods-a151671. [Accessed April 2012].

[10] P. N. Prasad, Introduction to Biophotonics, Hoboken, New Jersey: John Wiley & Sons, Inc., 2003.

[11] H. Haus, "Mode-locking of lasers," *IEEE Journal of Selected Topics in Quantum Electronics,* vol. 6, no. 6, pp. 1173 - 1185, 2000.

[12] M. Piché and M. Olivier, *Nonlinear Dynamics in Fiber Lasers,* Ottawa: Extreme Photonics Workshop, University of Ottawa, 2011.

[13] G. Agrawal, Applications of Nonlinear Fiber Optics, New York: Academic Press, 2001.

[14] N. Duling III, Compact Sources of Ultrashort Pulses, New York: Cambridge University Press, 1995.

[15] R. Trebino, "Pulse Generation," [Online]. Available: http://frog.gatech.edu/lectures/lectures/UltrafastOptics/lectures/UFO02Generation.zip. [Accessed April 2012].

[16] F. Li, P. K. A. Wai and J. N. Kutz, "Geometrical description of the onset of multipulsing in mode-locked laser cavities," *J. Opt. Soc. Am. B,* vol. 27, no. 10, pp. 2068 -2077, 2010.

[17] F. Ö. Ilday, J. R. Buckley, W. G. Clark and F. W. Wise, "Self-similar evolution of parabolic pulses in a laser," *Physical Review Letters,* vol. 92, no. 21, pp. 213902-1 - 213902-4, 2004.

[18] M. A. A. Abou seif, *Dissertation on Generation of High Energy Ultra-fast Laser Pulse Using Laser Fiber,* Cairo: Electronics Research Institute, 2010.

[19] "How does a SAM™ work?," Batop optoelectronics, [Online]. Available: http://www.batop.de/information/SAM_infos.html. [Accessed 22 July 2012].

[20] U. Keller, K. J. Weingarten, F. X. Kartner, D. Kopf, B. Braun, I. D. Jung, R. Fluck, C. Hönniger, N. Matuschek and J. Aus der Au, "Semiconductor saturable absorber mirros (SESAM's) for femtosecond to nanosecond pulse generation in solid-state lasers," *IEEE Journal of Selected Topics in Quantum Electronics,* vol. 2, no. 3, pp. 435 - 453, 1996.

[21] K. Kieu and F. W. Wise, "All-fiber normal-dispersion femtosecond laser," *Optics Express,* vol. 16, no. 15, pp. 11453 - 11458, 2008.

[22] W. H. Renninger, A. Chong and F. W. Wise, "Self-similar pulse evolution in an all-normal-disperion laser," *Physical review,* vol. 82, no. 2, pp. 3 - 6, 2010.

[23] M. E. Fermann and I. Hartl, "Ultrafast fiber laser technology," *IEEE Journal of Selected Topics in Quantum Electronics,* vol. 15, no. 1, pp. 191 - 206, 2009.

[24] B. Ortaç, M. Plötner, J. Limpert and A. Tünnermann, "Self-starting passively mode-locked chirped pulse fiber laser," *Optics Express,* vol. 15, no. 25, pp. 16794 - 16799, 2007.

[25] L. F. Mollenauer and R. H. Stolen, "The soliton laser," *Optics letters,* vol. 9, no. 1, pp. 13 - 15, 1984.

[26] A. M. Weiner, Ultrafast Optics, Hoboken: Wiley, 2009.

[27] M. E. Fermann, A. Galvanauskas and G. Sucha, Ultrafast Lasers: Technology and Applications, New York: Marcel Dekker, Inc., 2003.

[28] M. E. Fermann and M. Hoffer, "Mode-Locked Fiber Lasers," in *Rare Earth Fiber Lasers and Amplifiers*, New York, Marcel Dekker Inc., 1993.

[29] H. Lim, F. Ö. Ilday and F. W. Wise, "Femtosecond ytterbium fiber laser with photonic crystal fiber for dispersion control," *Optics Express,* vol. 10, no. 25, pp. 1497 - 1502, 2002.

[30] K. Tamura, E. P. Ippen, H. A. Haus and I. E. Nelson, "77-fs pulse generation from a stretched-pulse mode-locked all-fiber ring laser," *Optics letters,* vol. 18, no. 13, pp. 1080 - 1082, 1993.

[31] D. Anderson, M. Desaix, M. Karlsson, M. Lisak and M. L. Quiroga-Teixeiro, "Wave-breaking-free pulses in nonlinear-optical fibers," *J. Opt. Soc. Am. B,* vol. 10, pp. 1185 - 1190, 1993.

[32] D. Anderson, M. Desaix, M. Lisak and K. L. Quiroga-Teixeiro, "Wave breaking in nonlinear-optical fibers," *J. Opt. Soc. Am. B,* vol. 9, no. 8, pp. 1358 - 1361, 1992.

[33] W. J. Tomlinson, R. H. Stolen and A. M. Johnson, "Optical wave breaking of pulses in nonlinear optical fibers," *Optics letters,* vol. 10, no. 9, pp. 457 - 459, 1985.

[34] H. Zhou, W. X. Li and H. P. Zeng, "Yb-doped fiber oscillator generating 41 fs wave-breaking-free pulses," *Laser Physics,* vol. 21, no. 2, pp. 399 - 403, 2011.

[35] A. C. Peacock, R. J. Kruhlak, J. D. Harvey and J. M. Dudley, "Solitary pulse propagation in high gain optical fiber amplifiers with normal group velocity disperion," *Optics communications,* vol. 206, pp. 171 - 177, 2002.

[36] B. Ortaç, A. Hideur, C. Chedot, M. Brunel, G. Martel and J. Limpert, "Self-similar low-noise femtosecond ytterbium-doped double-clad fiber laser," *Appl. Phys. B.,* vol. 85, pp. 63 - 67, 2006.

[37] Y. Logvin and H. Anis, "Similariton pulse instability in mode-locked Yb-doped fiber laser in the vicinity of zero-cavity dispersion," *Optics express,* vol. 15, no. 21, pp. 13607 - 13612, 2007.

[38] J. R. Buckley, F. W. Wise, F. Ö. Ilday and T. Sosnowski, "Femtosecond fiber lasers with pulse energies above 10 nJ," *Optics Letters,* vol. 30, pp. 1888 - 1890, 2005.

[39] P. K. Mukhopadhyay, "Femtosecond pulse generation and amplification in Yb-doped fibre oscillator-amplifier system," *Pramana - journal of physics,* vol. 75, no. 5, pp. 787 - 805, 2010.

[40] B. Ortaç, A. Hideur, C. Chédot, J. Limpert, A. Tünnermann and F. Ö. Ilday, "Generation of parabolic bound pulses from a Yb-fiber laser," *Optics Express,* vol. 14, pp. 6075 - 6083, 2006.

[41] G. Martel, C. Chédot, V. Réglier, A. Hideur, B. Ortaç and P. Grelu, "On the possibility of observing bound soliton pairs in a wave-breaking-free mode-locked fiber laser," *Optics letters,* vol. 32, pp. 343 - 345, 2007.

[42] W. H. Renniger, A. Chong and F. W. Wise, "Dissipative solitons in normal-dispersion fiber lasers," *Physical Review A,* vol. 77, no. 2, pp. 023814-1 - 023814-4, 2008.

[43] X. Liu, L. Wang, X. Li, H. Sun, A. Lin, K. Lu, Y. Wang and W. Zhao, "Multistability evolution and hysteresis phenomena of dissipative solitons in a passively mode-locked fiber laser with large normal cavity dispersion," *Optics express,* vol. 17, no. 10, pp. 8506 - 8512, 2009.

[44] A. Chong, J. R. Buckley, W. Renniger and F. W. Wise, "All-normal-disperion femtosecond fiber laser," *Optics Express,* vol. 14, no. 21, pp. 660 - 662, 2006.

[45] F. W. Wise, *Dissipative solitons in femtosecond fiber lasers,* Ottawa: Extreme Photonics Workshop, University of Ottawa, 2011.

[46] K. Kieu, W. H. Renniger, A. Chong and F. W. Wise, "Sub-100 fs pulses at watt-level power from a dissipative soliton fiber laser," *Optics letters,* vol. 34, no. 5, pp. 593 - 595, 2009.

[47] F. Ö. Ilday, H. Lim, J. R. Buckley and F. W. Wise, "Practical all-fiber source of high-power, 120-fs pulses at 1 um," *Optics letters,* vol. 28, no. 15, pp. 1362 - 1364, 2003.

[48] D. Strickland and G. Mourou, "Compression of amplified chirped optical pulses," *Opt. Comm.,* vol. 56, no. 219, 1985.

[49] A. Komarov, H. Leblond and F. Sanchez, "Multistability and hysteresis phenomena in passively mode-lockd fiber lasers," *Physical review A,* vol. 71, no. 5, pp. 053809-1 - 053809-4, 2005.

[50] A. Haboucha, A. Komarov, H. Leblond, F. Sanchez and M. Gilles, "Mechanism of multiple pulse formation in the normal dispersion regime of passively mode-locked fiber ring lasers," *Optical Fiber Technology,* vol. 14, pp. 261-267, 2008.

[51] A. Hideau, B. Ortaç, T. Chartier, M. Brunel, H. Leblond and F. Sanchez, "Ultra-short bound states generation with a passively mode-locked high-power Yb-doped double-clad fiber laser," *Optics Communications,* vol. 225, pp. 71-78, 2003.

[52] Y. Deng and W. H. Knox, "Self-starting passive harmonic mode-locked femtosecond Yb3+-doped fiber laser at 1030 nm," *Optics Letters,* vol. 29, no. 18, pp. 2121-2123, 2004.

[53] G. Agrawal, Nonlinear fiber optics, Burlington, MA: Academic Press, 2007.

[54] Y. Logvin, V. P. Kalosha and H. Anis, "Third-order dispersion impact on mode-locking regimes of Yb-doped fiber laser with photonic bandgap dispersion compensation," *Optics Express,* vol. 15, no. 3, pp. 985 - 991, 2007.

[55] K. J. Bock, H. E. Kotb, M. A. Abdelalim and H. Anis, "Increasing energy in an ytterbium femtosecond fiber laser with a longer gain medium and lower doping," in *Fiber Lasers IX: Technology, Systems, and Applications (Proceedings of SPIE Volume: 8237)*, San Francisco, 2012.

[56] E. B. Treacy, "Optical pulse compression with diffraction gratings," *IEEE Journal of Quantum Electronics,* Vols. QE-5, no. 9, pp. 454 - 458, 1969.

[57] E. Ding, E. Shlizerman and J. N. Kutz, "Generalized master equation for high-energy passive mode-locking: the sinusoidal Ginzburg-Landau equation," *IEEE Journal of Quantum Electronics,* vol. 47, pp. 705 - 714, 2011.

[58] F. Ö. Ilday, J. R. Buckley, H. Lim, F. W. Wise and W. G. Clark, "Generation of 50-fs, 5 nJ pulses at 1.03 um from a wave-breaking-free fiber laser," *Optics letters,* vol. 28, no. 15, pp. 1365 - 1367, 2003.

[59] F. Jie, X. WenCheng, L. ShuXian and L. SongHao, "Analytic solutions of self-similar pulse based on Ginzburg-Landau equation with constant coefficients," *Science in China Series G: Physics, Mechanics & Astronomy,* vol. 51, no. 3, pp. 299 - 306, 2008.

[60] A. Chong, W. H. Renniger and F. W. Wise, "Properties of normal-dispersion femtosecond fiber lasers".